

**STUDY ON THE DEGRADATION CHARACTERISTICS OF LI-ION  
BATTERIES UNDER DIFFERENT CHARGING AND DISCHARGING  
CURRENT PROFILE**

**CHONG ZHENG WEN**

**A project report submitted in partial fulfilment of the  
requirements for the award of Bachelor of Electrical and Electronics with  
Honours Engineering**

**Lee Kong Chian Faculty of Engineering and Science  
Universiti Tunku Abdul Rahman**

**May 2024**

**DECLARATION**

I hereby declare that this project report is based on my original work except for citations and quotations which have been duly acknowledged. I also declare that it has not been previously and concurrently submitted for any other degree or award at UTAR or other institutions.

Signature :   
\_\_\_\_\_

Name : Chong Zheng Wen  
\_\_\_\_\_

ID No. : 1901105  
\_\_\_\_\_

Date : 15/5/2024  
\_\_\_\_\_

**APPROVAL FOR SUBMISSION**

I certify that this project report entitled “**STUDY ON THE DEGRADATION CHARACTERISTICS OF LI-ION BATTERIES UNDER DIFFERENT CHARGING AND DISCHARGING CURRENT PROFILE**” was prepared by **CHONG ZHENG WEN** has met the required standard for submission in partial fulfilment of the requirements for the award of Bachelor of Electrical and Electronics with Honours Engineering at Universiti Tunku Abdul Rahman.

Approved by,

Signature :   
\_\_\_\_\_

Supervisor : Prof Lim Yun Seng  
\_\_\_\_\_

Date : 17 May 2024  
\_\_\_\_\_

Signature : \_\_\_\_\_

Co-Supervisor : \_\_\_\_\_

Date : \_\_\_\_\_

The copyright of this report belongs to the author under the terms of the copyright Act 1987 as qualified by Intellectual Property Policy of Universiti Tunku Abdul Rahman. Due acknowledgement shall always be made of the use of any material contained in, or derived from, this report.

© 2024, CHONG ZHENG WEN. All right reserved.

## ABSTRACT

Li-ion batteries are extensively used because of their high density and longer cycles life, which make them important for powering anything from electric vehicles to cell phones. But over time, degradation lowers their capability and effectiveness. It is essential to understand degradation elements in order to maximise battery management and prolong battery life. Through the analysis of degradation characteristics, this research seeks to improve battery performance and longevity, thereby improving the sustainability of energy storage systems. In the research a real lithium-ion batteries with 15 cells are used. It also has a Battery Monitoring System which monitoring condition of the 15 cells. A Sunny Island Inverter is used to charge and discharge the batteries. The node-red software is implemented to retrieve the data from the batteries. The State of Health (SOH) estimation is based on the Incremental Current Analysis is used to determine the SOH from the cell voltage. The SOH, degradation rate and optimal charging and discharging profiles is determine which the best profiles is around 18A to 19A which is 1kW power. This is because it has the lowest degradation rate and good SOH compared to 2kW and 1.5kW. Therefore, this research gives an insight of information in developing Li-ion battery solution. The correct charging and discharging can maximise the battery longevity and performance. In future work recommendations, a consistency charging and discharging in longer or more cycles to provide a better accuracy of the results.

## TABLE OF CONTENTS

<b>DECLARATION</b>		<b>i</b>
<b>APPROVAL FOR SUBMISSION</b>		<b>ii</b>
<b>ABSTRACT</b>		<b>iv</b>
<b>TABLE OF CONTENTS</b>		<b>v</b>
<b>LIST OF TABLES</b>		<b>viii</b>
<b>LIST OF FIGURES</b>		<b>ix</b>
<b>LIST OF SYMBOLS / ABBREVIATIONS</b>		<b>xi</b>
<b>LIST OF APPENDICES</b>		<b>xii</b>
<b>CHAPTER</b>		
<b>1</b>	<b>INTRODUCTION</b>	<b>1</b>
1.1	General Introduction	1
1.2	Importance of the Study	2
1.3	Problem Statement	2
1.4	Aim and Objectives	3
1.5	Scope and Limitation of the Study	3
<b>2</b>	<b>LITERATURE REVIEW</b>	<b>5</b>
2.1	Introduction	5
2.2	Causes of Battery Degradation	6
2.3	Battery Degradation Processes and Mechanisms	7
2.4	Factors Affecting Battery Degradation	10
2.5	Optimum Charging and Discharging Current Profiles for Minimum Battery Degradation	13
2.6	State of Health Estimation	16
2.7	Limitations and Recommendation	17
2.8	Summary	18
<b>3</b>	<b>METHODOLOGY AND WORK PLAN</b>	<b>19</b>
3.1	Introduction	19

3.2	Battery Monitoring System Setup Architecture	19
3.3	Battery Management System (Batrium)	21
3.3.1	WatchMon CORE	21
3.3.2	Cell Monitors	22
3.3.3	ShuntMon2	23
3.3.4	IsoMon	24
3.3.5	Expansion Board	25
3.3.6	WatchMon Toolkit	25
3.4	Sunny Island Inverter	25
3.5	Node-red	26
3.5.1	Modbus	27
3.5.2	Wi-Fi Transmission Control Protocol/Internet Protocol (TCP/IP)	27
3.5.3	UDP Listener (WIFI)	28
3.5.4	Node-red Dashboard	28
3.5.5	Excel	29
3.6	Node-red Setup in Inverter and Batrium BMS	29
3.6.1	Node-red Inverter	29
3.6.2	Node-red Batrium BMS	31
3.7	State of Health (SOH) Estimation	32
3.8	Summary	34
<b>4</b>	<b>RESULTS AND DISCUSSION</b>	<b>36</b>
4.1	Introduction	36
4.2	Characteristics during Charging and Discharging	36
4.2.1	Part A: Capacity vs Shunt Current during Charging	36
4.2.2	Part B: Shunt Voltage vs Capacity under Charging	38
4.2.3	Part C: Capacity vs Shunt Current under Discharging	41
4.3	Part D: Voltage vs Capacity under Discharging	43
4.3.1	Charging and Discharging for Temperature Characteristics	45

<b>5</b>	<b>ESTIMATED RESULTS OF SOH USING ICA METHOD</b>	<b>50</b>
5.1	Incremental capacity analysis (ICA-based) SOC estimation of batteries (SOH Estimation)	50
5.1.1	dQ/dV Graph (Three Peaks Voltage)	50
5.1.2	Voltage vs Capacity Curve of Measured and Analytical	54
<b>6</b>	<b>STATE OF HEATH (SOH), DEGRDADATION RATE AND OPTIMAL CURRENT PROFILES ANALYSIS</b>	<b>60</b>
6.1	Comparison of Analytical and Measured Results	60
6.2	SOH, Degradation rate and Optimal Current Profiles Evaluation	61
6.2.1	Analysis of State of Health	61
6.2.2	Comparative Analysis of Battery Degradation and State of Health (SOH) under Different Charging Profiles	63
6.3	Summary	64
<b>7</b>	<b>CONCLUSION AND RECCOMENDATIONS</b>	<b>65</b>
7.1	Conclusions	65
7.2	Recommended of Future Work	66
	<b>REFERENCES</b>	<b>67</b>
	<b>APPENDICES</b>	<b>71</b>



## LIST OF TABLES

Table 2.1: Experimental settings triggering particular degradation processes (Edge et al., 2021)	12
Table 5.1: Table with Graph of $dQ/dV$ vs voltage points (0.8kW Charging)	51
Table 5.2: Table of Voltage vs Capacity Curve with Calculated Maximum Capacity (0.8kW Charging)	54
Table 6.1: Comparison of Analytical vs Measured Results	60
Table 7.1: Table with Graph of $dQ/dV$ vs voltage points (2kW Charging)	74
Table 7.2: Table with Graph of $dQ/dV$ vs voltage points (1kW Charging after 2 cycles)	77
Table 7.3: Table with Graph $dQ/dV$ vs voltage points (1 <sup>st</sup> 1.5kW Charging)	80
Table 7.4: Table with Graph $dQ/dV$ vs voltage points (2 <sup>nd</sup> 1.5kW Charging)	83
Table 7.5: Table with Graph $dQ/dV$ vs voltage points (1 <sup>st</sup> 1kW Charging)	86
Table 7.6: Table with Graph $dQ/dV$ vs voltage points (2 <sup>nd</sup> 1kW Charging)	89
Table 7.1: Table of Voltage vs Capacity Curve with Calculated Maximum Capacity (2kW Charging after 2 cycles)	92
Table 7.2: Table of Voltage vs Capacity Curve with Calculated Maximum Capacity (1kW Charging after 2 cycles)	97
Table 7.3: Table of Voltage vs Capacity Curve with Calculated Maximum Capacity (1 <sup>st</sup> 1.5kW Charging)	103
Table 7.4: Table of Voltage vs Capacity Curve with Calculated Maximum Capacity (2 <sup>nd</sup> 1.5kW Charging)	108
Table 7.5: Table of Voltage vs Capacity Curve with Calculated Maximum Capacity (1 <sup>st</sup> 1kW Charging)	115
Table 7.6: Table of Voltage vs Capacity Curve with Calculated Maximum Capacity (2 <sup>nd</sup> 1kW Charging)	121

## LIST OF FIGURES

Figure 2.1: Figure 2: Flowchart degradation in lithium-ion batteries. (Birkl et al., 2017)	8
Figure 2.2: Flowchart degradation in lithium-ion batteries. (Birkl et al., 2017)	12
Figure 3.1: Set up for Monitoring Li-ion Batteries in Hardware	20
Figure 3.2: System Architecture of Set Up	20
Figure 3.3: Structure of WatchMon CORE (Batrium Knowledge / Wiki, n.d.) <sup>22</sup>	
Figure 3.4: BlackMon M8 Cell Monitor	23
Figure 3.5: WatchMon CORE with ShuntMon2 (Batrium Knowledge / Wiki, n.d.)	24
Figure 3.6: IsoMon Connection with WatchMon CORE with cell Monitor (Batrium Knowledge / Wiki, n.d.)	24
Figure 3.7: Expansion Board (Batrium Knowledge / Wiki, n.d.)	25
Figure 3.8: Sunny Island Inverter	26
Figure 3.9: Inverter Node-red Whole Function	30
Figure 3.10: Inverter's Information Display	30
Figure 3.11: WatchMon 14 Batteries Cell	31
Figure 3.12: Retrieve Information of Battery from Watchmon4 Batrium	32
Figure 3.13: Protection for stop Charging and discharging when the voltage above the level or lower the level respectively.	32
Figure 3.14: Graph of $dQ/dV$ vs Cell Voltage	33
Figure 3.15: Graph of Voltage vs Capacity (Measured and Calculated)	34
Figure 4.1: Graph of Shunt Measured Capacity against Shunt Current (1kW Charging)	37
Figure 4.2: Graph of Shunt Measured Capacity against Shunt Current (1.5kW Charging)	37

Figure 4.3: Graph of Shunt Measured Capacity against Shunt Current (2kW Charging)	38
Figure 4.4: Graph of Total Voltage against Measured Capacity (1kW Charging)	39
Figure 4.5: Graph of Total Voltage against Measured Capacity (1.5kW Charging)	39
Figure 4.6: Graph of Total Voltage against Measured Capacity (2kW Charging)	40
Figure 4.7: Graph of Shunt Measured Capacity against Shunt Current (1kW Discharging)	41
Figure 4.8: Graph of Shunt Measured Capacity against Shunt Current (2kW Discharging)	42
Figure 4.9: Graph of Shunt Measured Capacity against Shunt Current (2kW Discharging)	42
Figure 4.10: Graph of Total Voltage against Measured Capacity (1kW Discharging)	43
Figure 4.11: Graph of Total Voltage against Measured Capacity (1.5kW Discharging)	44
Figure 4.12: Graph of Total Voltage against Measured Capacity (2kW Discharging)	44
Figure 4.13: Graph of Temperature for 1kW Charging.	46
Figure 4.14: Graph of Temperature for 1.5kW Charging	46
Figure 4.15: Graph of Temperature for 2kW Charging.	47
Figure 4.16: Graph of Temperature for 1kW Discharging.	47
Figure 4.17: Graph of Temperature for 1.5 kW Discharging.	48
Figure 4.18: Graph of Temperature for 2kW Discharging.	48
Figure 6.1: Analytical Graphs for Maximum Capacity	61
Figure 6.2: Analytical Graphs for State of Health (SOH)	62
Figure 6.3: Analytical Graphs with SOH and Maximum Capacity	62

**LIST OF SYMBOLS / ABBREVIATIONS**

$c_p$	specific heat capacity, J/(kg·K)
$h$	height, m
$K_d$	discharge coefficient
$M$	mass flow rate, kg/s
$P$	pressure, kPa
$P_b$	back pressure, kPa
$R$	mass flow rate ratio
$T$	temperature, K
$v$	specific volume, m <sup>3</sup>
$\alpha$	homogeneous void fraction
$\eta$	pressure ratio
$V_{0i}$	peak voltage, V
$\omega_i$	peak width
$C$	Constant produced by integral
$Q$	Capacity, Ah
$Q_{max}$	Maximum Capacity, Ah
$A_i$	area below <i>i</i> th peak
$n$	number of peaks

**LIST OF APPENDICES**

Appendix A: BMS UDP	71
Appendix B: Modbus Address of Sunny Island Inverter	72
Appendix C: dQ/dV Graphs for 1kW,1.5kW and 2kW	74
Appendix D: Voltage vs Measured and Calculated capacity of individual Cell	92

## CHAPTER 1

### INTRODUCTION

#### 1.1 General Introduction

Li-ion batteries are increasingly popular nowadays because of the electrification in transport sector. Li-ion batteries (LIBs) have experienced remarkable advancements and widespread adoption in multiple applications including, grid energy storage, consumer gadgets, and electric vehicles (EVs). The success of LIBs can be attributed to the availability of diverse electrode materials that cater to the specific performance demands of different application scenarios. Notably, EVs have emerged as a significant market for LIBs, with multiple countries intending to switch from internal combustion engines (ICEVs) to electric cars (EVs) gradually to align with net-zero carbon emission goals in the coming decades. (Yang et al., 2022)

The rapid expansion of the market for portable electronic gadgets in the 1990s necessitated the development of a lightweight rechargeable cell, which led to the development of lithium-ion batteries. The technology, which first appeared in cameras and cell phones, has developed into the go-to power source for everything from cordless power tools to massive energy storage systems and automotive applications. High energy density and a large number of discharge cycles are the two most important characteristics that make lithium-ion batteries necessary in mobile phones and electric vehicles (Introduction to Lithium-Ion Batteries - Yuasa UK, n.d.) But as time passes, these batteries lose their effectiveness and endurance. To optimise intake and reduce degradation rates, it is essential to understand the Li-ion battery's deterioration characteristics.

Battery degradation is the slow loss of a battery's ability to store and transfer power, which over time results in diminished performance. All batteries go through this process differently because of various reasons, which makes it a challenging task with many different facets. For instance, battery deterioration in electric cars reduces energy capacity, hence reducing the vehicle's range. As a result, the mileage on a full charge is reduced as compared to beginning usage. Similar to this, battery energy storage systems (BESS) suffer from deterioration,

which reduces the amount of energy they can store and deliver, which has an effect on how efficient the system is overall (Battery Degradation: Maximizing Battery Life & Performance, n.d.). Battery temperature, depth of discharge (DOD), charging current, and discharging current are the four key variables that affect the pace of deterioration (Xiong, 2019).

## **1.2 Importance of the Study**

It is important to study degradation of Li-ion batteries under different charging and discharging currents is of paramount importance as it enables us to implement effective measures to minimize degradation rates. By understanding how specific current profiles affect battery health, we can develop better battery management methods to optimize their performance. With the help of this research, we can better understand how particular current profiles affect state of health of battery, which will help us design better battery management strategies and optimise both the performance and longevity of batteries. We are able to forecast battery life and evaluate the cost-effectiveness of various energy storage devices by measuring the degradation rate. Additionally, we can increase battery longevity, improve efficiency, and foster sustainability in Li-ion battery technology applications by establishing optimised charging and discharging patterns that slow down the degradation of batteries. This thorough knowledge of battery degradation is crucial for improving the effectiveness and sustainability of energy storage devices.

## **1.3 Problem Statement**

The transportation sector has undergone a transformation due to the increasing use of lithium-ion batteries in Electrical Vehicles (EVs). Battery degradation is still a major scientific obstacle in battery research too. Lithium-ion battery ageing affects the overall performance and cost-effectiveness of EVs over the course of their lives by reducing the capacity for energy storage and power output. (Han et al., 2019)

Battery degradation is a phenomenon that is influenced by a variety of variables factors, including temperature, charging and discharging currents, including (Curtis, 2023) Therefore, the Battery Management System (BMS) is responsible for estimating the battery's state of health (SOH) by considering the

aging mechanism and the battery degradation model. SOH stands for the estimation of battery health, which is affected by its history. This SOH estimation plays a crucial role as an essential input for other estimation algorithms within the BMS. By accurately estimating the battery's health, the BMS can effectively manage the battery's performance and optimize its overall efficiency during its operational life. (Han et al., 2019)

Understanding the effects of different charging and discharging current profiles on battery degradation is essential for optimizing battery management strategies and prolonging battery lifespan (Wang et al., 2011). However, there is a knowledge gap regarding how specific charging and discharging current profiles influence battery health and degradation rates (Appelman et al., 2022). The lack of comprehensive understanding hinders the implementation of effective measures to minimize degradation and optimize battery performance (de Mendonça et al., 2020). Therefore, the study of the degradation rate of Li-ion batteries in different charging and discharging profile is done to cover the lack of information or more precise studies to minimize the degradation rate of li-ion batteries to prolong the age of batteries.

#### **1.4 Aim and Objectives**

The proposed final year project aims to achieve the following objectives:

1. Measure the state of health (SoH) of Li-ion batteries under different charging and discharging current profiles.
2. Determine the degradation rate of the batteries with respect to the different charging and discharging current profiles.
3. Identify the charging and discharging current profiles that result in the slowest degradation rate of the batteries.

#### **1.5 Scope and Limitation of the Study**

This study focuses on thoroughly investigating the rate of Li-ion battery degradation under various charging and discharging current profiles. The main objective is to fully understand the battery's degradation characteristics, with a focus on determining the state of health (SoH) under different operating conditions. This study intends to give useful insights into how different current



profiles effect battery degradation, eventually resulting in greater battery performance and the optimisation of its lifespan, by performing thorough experiments and in-depth analysis.

It is important to recognise the research's some limitations. First of all, because the study only looked at Li-ion batteries, its conclusions might not be directly relevant to other battery chemistries. Although Li-ion batteries are often used, it is important to use it with caution. The research may not cover the full range of potential operating situations because it concentrates on a predetermined set of charging and discharging current profiles. Further research work is necessary to study the effects of other current profile on the battery degradation to understand the response and characteristics of the battery under different current profiles. The external factors such as temperature, and DoD will be considered in the later part of the project:-

Despite these limitations, this study is important because its findings provide useful information about the rate of degradation and hence the durability of the batteries for a particular grid application such as peak demand reductions or frequency regulations.

## CHAPTER 2

### LITERATURE REVIEW

#### 2.1 Introduction

The development of Li-ion batteries and the electrification of the transportation industry have revolutionised energy storage. Li-ion batteries are important in electric cars and portable electronic gadgets due to their many benefits, including high energy density and efficiency. These batteries' performance and longevity are endangered by degradation, though. To maximise their use and reduce degradation rates, Li-ion battery degradation characteristics must be understood.

Lithium-ion batteries have gained prominence as the primary energy storage choice across various applications like electric vehicles (EVs), consumer electronics, and grid energy storage systems. In this landscape, EVs have emerged as a pivotal player, playing a vital role in curbing greenhouse gas emissions and addressing climate change. As the world shifts towards sustainable energy solutions and decarbonization, EVs are instrumental in this transition. Numerous nations have outlined plans to gradually replace internal combustion engine vehicles (ICEVs) with electric counterparts, aligning with the objective of reducing carbon emissions and achieving net-zero carbon standards. The International Energy Agency (IEA) reports that over 20 countries, including emerging economies like Cabo Verde, Costa Rica, and Sri Lanka, have committed to completely phasing out internal combustion engine car sales in the coming 10-30 years. These countries are implementing various policies and initiatives to promote the adoption of EVs and support the transition away from ICEVs. (International Energy Agency, 2021)

However, the broad adoption of EVs and other Li-ion battery applications faces significant challenges due to battery degradation. The performance and cost-effectiveness of EVs and other devices are impacted as a result of the limited energy storage and power output capabilities of ageing Li-ion batteries. Therefore, developing effective battery management techniques requires an understanding of the elements that affect battery degradation, particularly under various charging and discharging current profiles. The

literature review aims to investigate the degradation rate of Li-ion batteries under various charging and discharging current profiles. The main objectives include reviewing Cause of Battery Degradation, Battery Degradation Processes and Mechanism, Factors on Influences Battery Degradation and Optimum Charging and Discharging Current Profiles for Minimum Battery Degradation

By focusing on these objectives, the literature review hopes to provide insightful contributions to the battery research community, supporting improvements in battery technology and the development of sustainable energy sources. Literature review is important in this research work because its findings can inform the existing techniques and their effectiveness of managing the degradation and aging of the batteries.

## **2.2 Causes of Battery Degradation**

The causes of the battery degradation are mainly due to three processes: i) loss of lithium inventory, ii) loss of active material in the positive electrode, and iii) loss of active material in the negative electrode:

According to Birkl et al., 2017, Loss of Lithium Inventory (LLI) is occurs when lithium ions are consumed by unwanted reactions, such as the formation of a surface film (e.g., SEI growth), decomposition reactions, or lithium plating. As a result, these lithium ions become unavailable for cycling between the positive and negative electrodes, leading to a decline in the battery's capacity. Additionally, lithium ions may get trapped within electrically isolated particles of the active materials, further contributing to the capacity and power fade. Surface films formed during these reactions can also cause a reduction in power output.

Secondly, Loss of Active Material of the Negative Electrode (LAMNE) is the active mass of the negative electrode (anode) diminishes, limiting its ability to accept lithium during the charging process. This reduction in active material can occur because of particle cracking, loss of electrical contact between particles, or the presence of resistive surface layers. As a consequence, the battery experiences both capacity and power fade, impacting its overall performance. (Birkl et al., 2017)

Thirdly, loss of Active Material of the Positive Electrode (LAMPE) involves the decline of the active mass in the positive electrode (cathode),

resulting in a reduced capacity to store lithium during discharge. Structural disordering, particle cracking, or loss of electrical contact between particles are the primary causes leading to this degradation. The reduced active material availability in the positive electrode contributes to both capacity and power fade, negatively affecting the battery's performance over time. (Birkl et al., 2017). It is crucial to comprehend and address these degradation modes to enhance the longevity and durability of lithium-ion batteries, particularly in applications like electric vehicles and portable electronics. Ongoing research and engineering efforts aim to develop strategies to mitigate these degradation processes and improve battery performance and lifespan.

### **2.3 Battery Degradation Processes and Mechanisms**

According to Edge et al., 2021, three tiers of characterization for battery degradation: the underlying mechanisms, the observable outcomes at the cell level referred to as "modes," and the operational impacts such as capacity or power fade. Degradation mechanisms elucidate the chemical and physical transformations occurring within the cell. While mechanisms offer the deepest insights into deterioration, they can often be the most challenging to observe when the battery is operating. Capacity fade and power fade represent two observable degradation phenomena. Power fade denotes a decrease in the cell's deliverable power as it degrades, whereas capacity fade signifies a reduction in the cell's usable capacity. These visible effects, though relatively easy to measure, provide the least detailed view of degradation. Consequently, capacity fade and power fade serve as widely employed practical indicators of cell degradation. Five main processes of degradation were found that are typically thought to be the root of battery degradation during regular usage. These factors encompass the formation of Solid Electrolyte Interphase (SEI) layers, the occurrence of lithium plating, structural alterations in the positive electrode (PE breakdown), and the particles breakage at both electrode surfaces. The interaction of the five primary degradation mechanisms leads to the emergence of thirteen secondary degradation mechanisms, as illustrated in Figure 2.1.

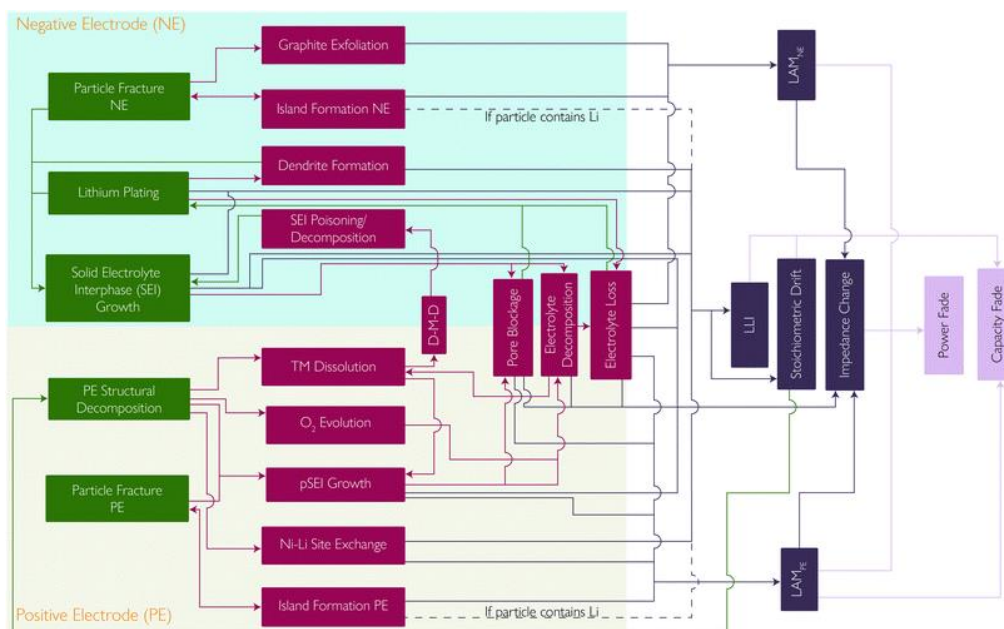


Figure 2.1:Figure 2: Flowchart degradation in lithium-ion batteries. (Birkel et al., 2017)

According to O’Kane et al., 2022, SEI growth occurs when lithiated graphite's equilibrium potential falls below a certain threshold, leading to electrolyte breakdown. This results in the formation of a Solid Electrolyte Interphase (SEI) layer on the graphite surface. The SEI layer contributes to battery degradation by trapping lithium ions, reducing their participation in charge storage (loss of lithium inventory), and increasing impedance due to higher ionic resistance compared to the electrolyte.

Furthermore, lithium plating is a side reaction that occurs on the negative electrode of a Li-ion battery. This occurs when lithium ions ( $\text{Li}^+$ ) from the electrolyte are deposited as metallic lithium (Li) on the graphite surface instead of being incorporated into the bulk of the graphite material. This phenomenon is more likely to take place under certain circumstances, such as low temperatures or when graphite surface is completely saturated with lithium, causing the lithium plating reaction to become more favourable than the primary intercalation reaction. (O’Kane et al., 2022) Fast charging or pore clogging, which elevates the electrolyte potential to unusually high levels, can also induce lithium plating. (Tomaszewska et al., 2019)

Besides that, particle fracture in Li-ion batteries occurs due to substantial volume changes in the electrode during cycling. As the electrode

particles experience mechanical stress caused by concentration gradients, cracks can develop. (Pistorio et al., 2022) This occurrence becomes more noticeable when higher currents are applied and when dealing with larger particle sizes. The resultant fractures expose additional surface area for the growth of SEI, which subsequently results in a greater reduction of lithium content (Ren et al., 2024) Moreover, conductive additives may detach during delithiation, resulting in reduced electronic conductivity. (Xu et al., 2019) A complete fracture or separation from the binder can isolate the particle, resulting in the loss of active material.

Breakdown of positive electrode (PE) typically refers to the degradation or failure of PE in a lithium-ion battery. PE deterioration is an ongoing area of research, but few studies investigate the mechanisms individually. One of the mechanisms under investigation is the phase change and oxygen evolution. Traditionally, the release of oxygen from the positive electrode (PE) is represented by modelling electrolyte oxidation on the PE side using a Tafel equation. (Marcias, 2023) In a recent study conducted by Ghosh et al., they have developed a model that incorporates physical principles to elucidate the process of oxygen evolution from the bulk and its subsequent diffusion through the rock salt layer. This model employs a shrinking core model to simulate the phenomena of loss of lithium inventory (LLI) and loss of active material (LAM), along with their implications on the deterioration of capacity and power.

Therefore, understanding the various battery degradation mechanisms is crucial for optimising the performance and longevity of lithium-ion batteries. This review has highlighted the significance of factors such as SEI growth, lithium plating, PE breakdown and particle fracture, which can contribute to the deterioration of battery health. By identifying these mechanisms and their interactions, researchers can develop more accurate and comprehensive models for predicting battery degradation. Such insights are invaluable for the global automotive, aviation, and energy storage industries, as they seek to enhance the efficiency and reliability of Li-ion batteries in various applications. Further research in this area is essential to continue advancing battery technology and promoting sustainable energy solutions.

## 2.4 Factors Affecting Battery Degradation

Factors that influence battery life may include design, production, and application-related aspects that influence battery health and longevity. In design factor like electrode material and electrolyte composition while like production factor like manufacturing quality will also affect the battery life. From the perspective of a user, three primary external factors or application-related aspects that can induce strain and contribute to the deterioration of a battery include temperature, state of charge (SoC), and load profile. The significance of each factor can vary depending on the battery's chemistry, form factor, and historical usage conditions, among other things. Birkl et al. have emphasized the impact of these stress factors on the fundamental physical degradation processes in Figure 2. According to Edge et al., 2021, Table 1 is provided to emphasise the experimental settings that are most likely triggering particular degradation processes.

According to Sui et al., 2021, this work examines the behaviour of lithium iron phosphate (LiFePO<sub>4</sub>/C) batteries during long-term calendar ageing, with particular attention to internal resistance rise and capacity decline. The effect of state-of-charge (SOC) level and storage temperature as stress factors on the calendar deterioration rate is investigated. A two-phase nonlinear regression technique is suggested to create an ageing model that reflects the connections between stressors and degradation. The rate of deterioration has a consistent downward trend with increasing age.

The rate at which resistance and capacity change is slowed down by low storage temperatures; at 25°C, rates rise exponentially. Degradation rates are influenced piecemeal by SOC level; greater SOC initially causes faster degradation up to a certain point, beyond which mid-SOC increases capacity loss. Similar behaviour is seen by the internal resistance, which has a cutoff point at 30% rise. Calendar lifespan may be approximated under various storage settings using the existing models. Lower temperatures reduce capacity loss but have less of an impact on resistance, while higher temperatures prolong capacity fading but moderate resistance growth. Optimising storage conditions requires careful consideration of resistance and capacity.

Cycling a battery induces additional aging caused by processes that are absent during calendar aging. Intercalation and de-intercalation lead to volume

changes in the material, which act as stress factors for the battery system. This may result in either a crack-and-repair phenomenon of the SEI, leading to lithium consumption and increased inner resistance, or a contact loss between active material particles. The suggested approach, which reflects piecewise variations in degradation during extremely long-term calendar ageing, forecasts battery lifespan more accurately when compared to a conventional semi-empirical model. In general, this research offers significant perspectives for enhancing storage circumstances to prolong battery lifespans in energy storage devices.

Oversizing the battery capacity is effective but costly. Understanding cycle depth dependency helps minimize oversizing. The studied cells show a non-exponential relationship with a more linear trend. Capacity loss exhibits a consistent linear dependency across all cycle depths, while resistance increase remains minimal at low cycle depths. Understanding cycle depth is essential for optimizing battery design and management strategies. At  $-20^{\circ}\text{C}$  compared to  $55^{\circ}\text{C}$ , there is a more noticeable levelling out of capacity fading in cells that have reached 100% Depth of Charge (DOD). Aged at  $-20^{\circ}\text{C}$  with 100% DOD, they show a noticeable early deterioration before levelling off. For both temperatures, capacity fading is greater at 50% DOD than at 100% DOD. At  $55^{\circ}\text{C}$ , there is little change in the ageing profiles of 50% and 100% DOD. While ageing at 100% DOD reveals a clear difference across procedures, ageing at 50% DOD at  $-20^{\circ}\text{C}$  displays comparable decrease rates with different methods. (Simolka et al., 2020) Therefore, to achieve lifetime-optimized charging strategies, it is essential to consider the dependency on average voltage.



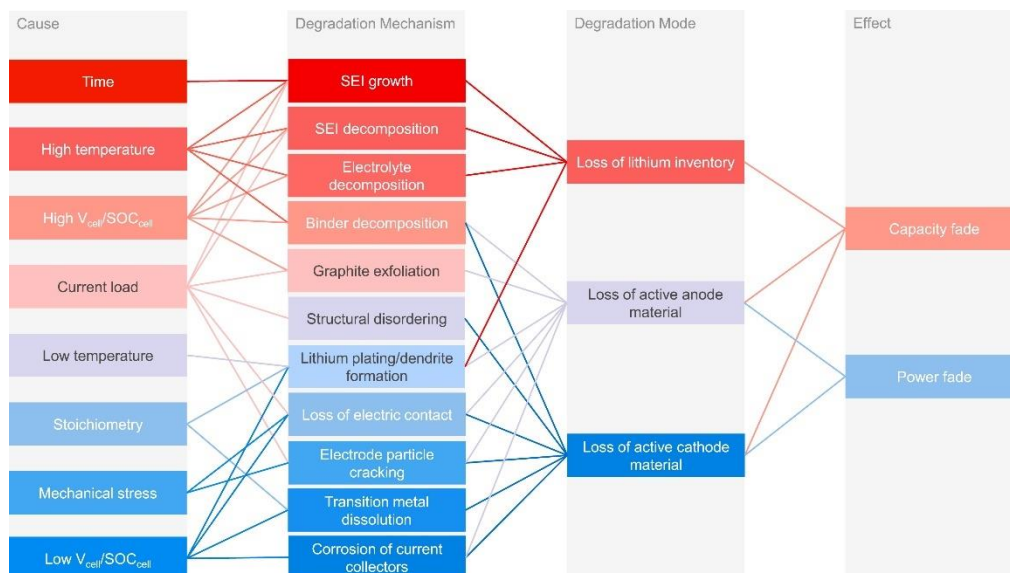


Figure 2.2: Flowchart degradation in lithium-ion batteries. (Birkl et al., 2017)

Table 2.1: Experimental settings triggering particular degradation processes (Edge et al., 2021)

Degradation Mechanism	Subsets	Tendency with Temperature	Voltage or State of Charge (SoC) Dependence	Current (I) Dependence
Lithium Plating	Reversible, irreversible, dendritic	Sensitive to Low Temperatures	Highly Dependent on Voltage	High Current Dependence
SEI Growth	Kinetic limited, diffusion limited	Temperature -Sensitive	Highly Dependent on Voltage	Not Applicable
Particle Fracture (Graphite)	Low Temperature Susceptible	Occurs Across Multiple SoC Ranges	High Current Dependence	

Particle Fracture (SiGr) Particle Fracture (NMC)	Low Temperature Susceptible	Occurs Across Multiple SoC Ranges	High Current Dependence	
	Low Temperature Susceptible	Highly Dependent on SoC	High Current Dependence	
PE Structural Change and Decomposition Phase Change (Layered to Spinel to Rock Salt) Electrochemical Decomposition (Oxidation of Lattice Oxygen) Ni-Li Site Exchange (LiNiO <sub>2</sub> ) Acid Attack	N/A	Temperature -Sensitive	Highly Dependent on Voltage	High Current Dependence
	Temperature -Sensitive	Highly Dependent on Voltage and SoC	High Current Dependence	
	Temperature -Sensitive	Highly Dependent on Voltage	High Current Dependence	
	Temperature -Sensitive	Highly Dependent on Voltage	Not Applicable	
	Temperature -Sensitive	Not Applicable	Not Applicable	

## 2.5 Optimum Charging and Discharging Current Profiles for Minimum Battery Degradation

In contemporary times, Lithium-ion batteries (LIBs) are typically recharged using either a Constant Current-Constant Voltage (CC-CV) strategy or a Constant Power-Constant Voltage (CP-CV) technique. According to Li et al., 2021, drawing from the preceding analysis and the data presented in the provided figures, our observations indicate that the energy patterns of signals,

particularly current and voltage, are notably more distinct during the Constant Current (CC) charging and discharging phases compared to other operational stages. This distinction implies that the Internal Charging Efficiency (ICE) and Voltage Charging Efficiency (VCE) exhibit a consistent reduction as the battery ages during the CC charging and discharging phases. While the Total Charging Efficiency (TCE) demonstrates a consistent trend across aging under each operational condition, its trajectory isn't uniform and showcases significant fluctuations.

According to Gao et al., 2022, The study investigated the impact of varying C-rates on the charging performance of Li-ion cells under low temperature charging, employing a two-tier modeling approach that combined COMSOL and MATLAB. The authors of this research examine the challenges faced by electric vehicles (EVs) in extremely cold environments, with a particular emphasis on the importance of quick charging in these conditions, since low temperatures can cause severe lithium plating and quick deterioration of lithium-ion batteries (LIBs). They build a porous pole-thermal coupling model that incorporates lithium plating and solid electrolyte interphase (SEI) development in order to examine the competing variables and primary causes of capacity degradation at different charging C-rates and ambient temperatures. Additionally, the paper suggests a lithium-free control strategy based on reaction overpotential at high charging C-rates. Furthermore, the study investigates the average cycle ageing rate of LIBs under various charging scenarios and finds an assessment index to strike a balance between charging efficiency and ageing rate. The ideal fast-charging method for LIBs under various ambient temperatures is explored using a chromaticity diagram, highlighting the significance of modifying the preheating temperature in accordance with battery capacity and charging C-rate in a low-temperature environment.

The conventional constant current-constant voltage (CC-CV) technique is widely employed for charging lithium-ion batteries. Yet, recent research highlights the potential benefits of utilizing pulse current charging strategies to enhance battery capacity retention rates. A study published in the

Ionics journal delved into the impact of pulse current charging-discharging strategies on lithium-ion battery capacity fade. The investigation employed a pseudo-two-dimensional model that considered thermal effects. The study revealed that pulse current-constant voltage (PC-CV) strategies, in contrast to the CC-CV approach, effectively mitigate capacity fade in lithium-ion batteries. This outcome is attributed to the relaxation process embedded within pulse charging, which curtails the current density of side reactions in the batteries. This reduction inside reactions aids in the recuperation of aged batteries and enhances their capacity retention rates. (Lv et al., 2020)

Enhancing the charging and discharging current profiles of lithium-ion batteries represents a crucial challenge for maximizing energy storage and efficient utilization. Researchers have applied dynamic optimization methods to determine the most effective charging current profile for lithium-ion batteries. In the study conducted by Chen et al., 2020, dynamic optimization was employed to determine the ideal current profile for charging a lithium-ion battery that takes into account the mechanical, thermal, and electrochemical stresses brought on by lithium-ion intercalation during charging. The primary objective of the study to use a dynamic optimization approach to an electrochemical-thermal battery model in order to design an effective fast-charging strategy that incorporates restrictions on intercalation-induced stresses and solid-liquid interface film formation, hence minimizing battery degradation. It compares the traditional constant current followed by constant voltage (CC–CV) approach with an optimized constant current value. The optimization goal is to reduce charging time as much as possible without increasing stress or film growth. This paper creating the ideal charging profile for lithium-ion batteries (LiBs) by controlling cell temperature and reducing the effects of ageing with the use of an electrochemical-thermal model. To avoid overheating, a backstepping technique for temperature management is suggested. Because they could accelerate ageing, intercalation-induced stress and film formation on particle surfaces are taken into consideration. According to the findings of the simulation, the ideal charging curve reduces film growth, which results in less lithium loss than alternative curves. Additionally, by efficiently controlling tangential and radial loads, the ideal profile lowers the possibility of electrode

fatigue fracture. The ideal charging duration provides an appropriate compromise between charging speed and battery ageing, taking only a little longer than conventional techniques.

These studies show that optimizing the charging and discharging current profiles for lithium-ion batteries can lead to more efficient use of the battery and can help to maximize its energy storage capacity.

## **2.6 State of Health Estimation**

State-of-health (SOH) of the li-ion batteries, is critical for maximum performance and longevity. There are two research publications that use charging profiles to estimate the state of health (SOH) of lithium-ion batteries. (Bian et al., 2019; Li et al., 2016)

According to Li et al. (2016) state that in order to produce a more understandable visualization of cell ageing, this work is converting the terminal voltage curve into an IC curve utilizing the incremental capacity analysis (ICA) technology. Based on the charging process, they proposed a charged capacity vs voltage model that accurately represented the voltage peaks and plateaus in the IC curve. With respect to nominal capacity, the proposed model's predicted charged capacity has an accuracy of less than 4%. The evaluation of this model's generality across several types of lithium-ion batteries (LIBs) with different electrode materials and ageing conditions suggests that it may find further application in SOH estimations.

A similar circuit model for battery energy storage systems (BESS) and battery management systems (BMS) was proposed in the paper by Bian et al. This model uses the capacity model of Li et al. to calculate the dependence of the state of charge (SOC) on the open circuit voltage (OCV). It was discovered that the ICA-based model, with parameters restricted to directly evaluating real capacity ( $Q_{max}$ ), required very little learning for a practical SOH estimate. Even in situations when temperatures changed dramatically, this method showed stable and closely matched actual data, although only providing an approximate approximation. On the other hand, an ICA-based model that necessitates

learning exhibited superior stability and accuracy, as evidenced by a percentage difference in SOH estimation of just 0.12%.

## **2.7 Limitations and Recommendation**

Despite the valuable insights provided by the aforementioned studies on optimizing charging and discharging current profiles for lithium-ion batteries, certain limitations and areas for future research need to be known.

Firstly, in studies above contribute knowledge under controlled laboratory or software which may not fully capture the complexities of real-world operational conditions. Future research should aim to bridge this gap by exploring a wider range of operating conditions and external influences, such as varying load profiles and temperature conditions. Another crucial consideration pertains to the validation of simulation models against actual experimental data. The accuracy and reliability of the optimization strategies proposed in these studies hinge upon comprehensive validation against real-world observations.

Moreover, while several studies focus on optimizing specific parameters like charge storage or stress reduction, a broader multi-objective optimization approach could yield more comprehensive results. Future research could delve into trade-offs between different factors such as energy storage capacity, cycle life, stress levels, and overall system efficiency. It's worth noting that some studies may be constrained by practical limitations, such as the availability of specific equipment or restricted testing timeframes. Addressing these constraints and expanding the experimental scope could yield a more holistic understanding of battery degradation and the performance of optimized profiles.

Furthermore, most of the discussed studies concentrate on short- to medium-term aging effects. Extending the investigation to encompass long-term aging effects give a clearer picture of how the optimized charging and discharging profiles fare over extended periods of battery operation. As battery technology evolves, it's crucial to consider the broader environmental impact of optimized charging strategies. Future research could explore in the environmental implications of different profiles and evaluate the overall sustainability of these approaches.

In summary, while the studies explored above present promising avenues for optimizing charging and discharging current profiles for lithium-ion batteries, by addressing these limitations and pursuing the recommended research directions will undoubtedly amplify the practical application and benefits of such optimization strategies.

## **2.8 Summary**

In conclusion, this literature review has illuminated the intricate degradation mechanisms within Li-ion batteries under varying charging and discharging current profiles. It emphasizes the significance of optimizing these profiles to mitigate degradation and enhance battery performance and lifespan. This optimization not only maximizes energy storage capacity but also ensures sustained battery health.

The reviewed studies highlight the need for further research to overcome limitations such as model validation and real-world applicability. Additionally, exploring multi-objective optimization and long-term aging effects will contribute to more robust battery systems. As Li-ion batteries remain pivotal in various industries, these findings underscore the importance of continued research for advancing battery technology and achieving a more sustainable energy future.

## CHAPTER 3

### METHODOLOGY AND WORK PLAN

#### 3.1 Introduction

In this section, a setup comprising an inverter, Batrium Battery Management System (BMS), and lithium-ion batteries was meticulously established to monitor li-ion battery. This integrated system was set up to give instantaneous information on the battery's functionality and state of health. Data interchange is facilitated by the inverter, which serves as an interface between the battery system and the monitoring device. A crucial part of this arrangement, the Batrium Battery Management System (BMS), provides continuous monitoring of numerous parameters like voltage, current, temperature, and state of charge. Additionally, the BMS actively balances cells and protects against overcharging or over discharging to guarantee the safe functioning and administration of the battery system.

The primary energy storage components are lithium-ion batteries, which were selected for their effectiveness and dependability. Each battery unit is tightly linked to the BMS, enabling administration and monitoring of individual cells. These batteries are arranged to mimic actual situations, giving precise information into various usage patterns.

#### 3.2 Battery Monitoring System Setup Architecture

In this Battery Monitoring System Setup, we use node-red software as our write and read data from inverter and Batrium BMS and logging the data to excel file per day. Figure 3.1 shows the set up for monitoring Li-ion batteries. Figure 3.2 explain more precise and clearly of the whole system architecture to write and retrieve the information in monitoring the batteries.



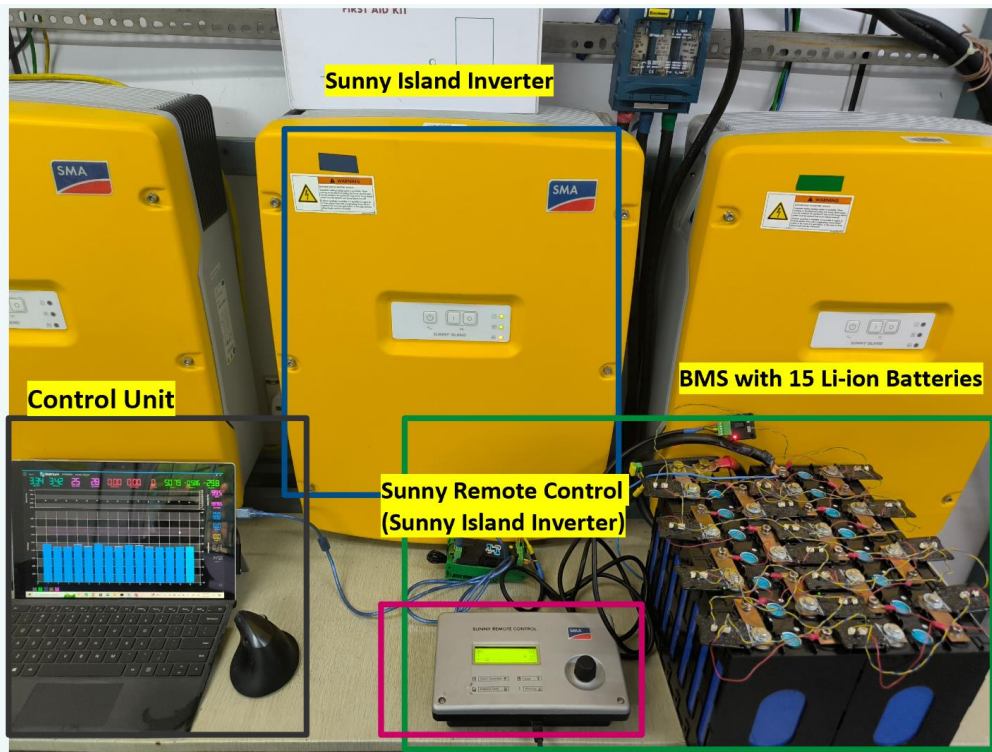


Figure 3.1: Set up for Monitoring Li-ion Batteries in Hardware

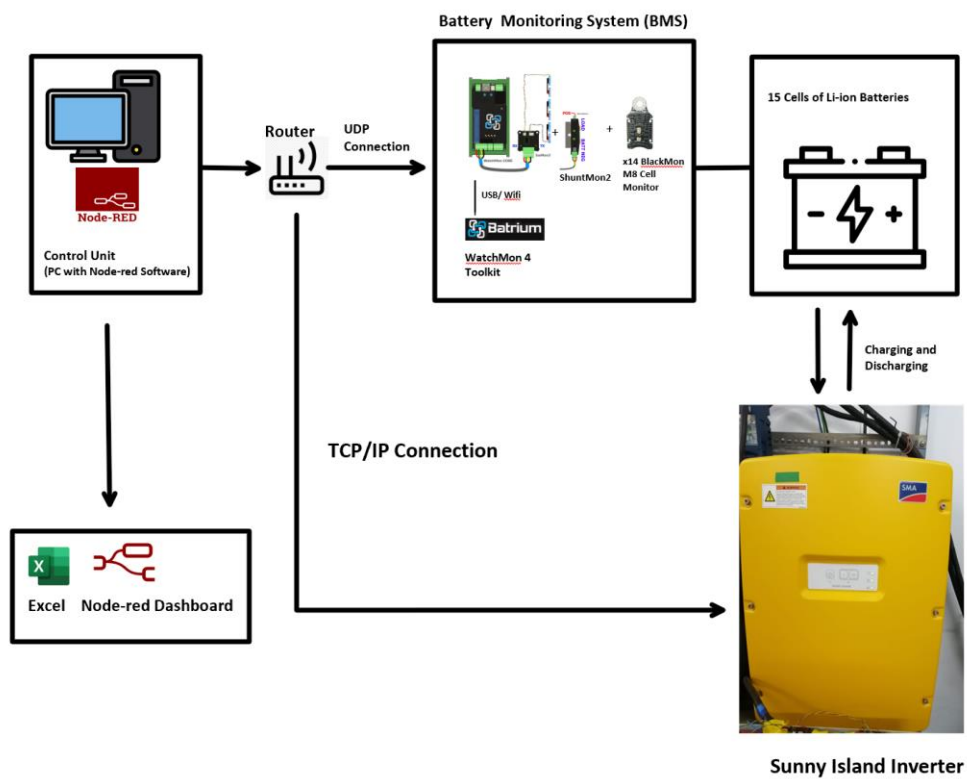


Figure 3.2: System Architecture of Set Up

In Figure 3.2 shows the system architecture which is built to monitor and give command to control the charging and discharging of Li-ion batteries. WatchMon 4 Toolkit software is used to show the information of the batteries through WatchMon Core. The WatchMon Core is connected with IsoMon3 and ShuntMon2. While For IsoMon3 and ShuntMon2 is connected to the BlackMon M8 Cell Monitor. Each of the 14 Cell Monitor is connected to each 14 Cells of the batteries. Sunny Island Inverter is to charge and discharge the 14 Li-ion batteries through write register in Node-RED. The information of Inverter will read by Node-red and display in Node-RED dashboard. The Node-red also will also log information of each cell voltage, State of Charge (SoC) and Shunt Current from WatchMon 4 Toolkit to excel file for further investigation. The Node-RED connected with Inverter through Wi-Fi with the correct TCP/IP. While to connect the WatchMon Core with WatchMon 4 toolkit through USB and connect with Node-RED with UDP Listener.

### **3.3 Battery Management System (Batrium)**

Battery Management Systems (BMS) play a crucial role within battery packs. They oversee the voltages and temperatures of individual cells, ensuring they remain within safe operational parameters. In the event of any deviations, BMS activates safeguards such as circuit breakers, fans, and contactors, or other connected components, using the collected data to maintain optimal conditions. Batrium BMS is made up of number of basic components which is WatchMon CORE, Cell Monitors, ShuntMon2 and Expansion board and IsoMon.

#### **3.3.1 WatchMon CORE**

WatchMon CORE is a supervisor and as a brain of the system. It can monitor based on your requirements between 1 to 250 cells. This BMS is suited for Lithium-ion battery (LiFePO<sub>4</sub>) or custom chemistry. Figure 3.3 shows the structure of WatchMon CORE.

The system offers a configurable 30V DC 5A relay, capable of functions like remote circuit breaker tripping, contactor control, or fan activation. Users can expand its capabilities through an additional Expansion Board and is compatible across all Expansion Board series (Series 1, 2, or 3). This system incorporates a clock with backup battery, ensuring data logging of

key metrics over a span of 10 years. Firmware upgrades are facilitated via a USB connection, ensuring continuous improvement. The USB connection is can to laptop. Notably, a 4-stage display effectively communicates State of Charge (SoC%) information. The setup further accommodates an external ambient temperature sensor, enhancing its environmental awareness. The inclusion of easy-to-use pluggable screw-terminal connectors simplifies installation. In addition, the system incorporates distributed cell monitors, offering precise 28 Ah/day balancing adjustments for each cell. Furthermore, it seamlessly integrates with ShuntMon, with power ratings of either 500A or 1000A. (Batrium Knowledge / Wiki, n.d.)

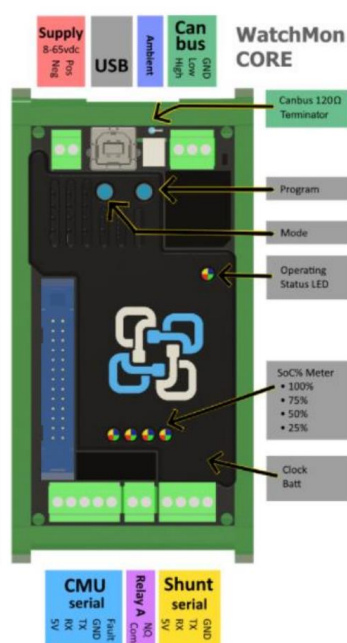


Figure 3.3: Structure of WatchMon CORE (Batrium Knowledge / Wiki, n.d.)

### 3.3.2 Cell Monitors

Cell monitor is to measures the voltage ad temperatures of the cells to ensure the battery system operates in a safe way. In this project, one of the types of cell monitor is used which is BlackMon M8. BlackMon are designed in the use with prismatic or brick-like cells. BlackMon M8 is choose rather than BlackMon M14 is because of the size of screws to each battery cells. BlockMon M8 allow up to 8mm hole. BlackMon M8 is choose is because it is suited for large format prismatic cells. Figure 3.4 shows a shape of BlackMon M8.



Figure 3.4: BlackMon M8 Cell Monitor

### 3.3.3 ShuntMon2

ShuntMon2 also known as State of Charge (SOC) % Sensor. Owing to the relatively uniform voltage pattern observed in most lithium batteries, voltage alone doesn't serve as an accurate gauge of the state of charge. The ShuntMon2 tackles this by effectively gauging parameters like voltage, current, and temperature. It accomplishes this by quantifying the Ampere-hours entering and exiting the battery bank, providing a more comprehensive assessment of the battery's state of charge.

The system comes in two models: the 500A model offers current measurement with a peak tolerance of  $\pm 500$  A (continuous at 400 A), while the 1000A model provides current measurement with a peak tolerance of  $\pm 1000$  A (continuous at 800 A). Both models accommodate a maximum voltage of 650V DC. Designed as a turnkey solution for on-field applications, the system consistently achieves remarkable precision with  $\pm 1.0\%$  accuracy in current measurement. It operates across a wide current range, capturing currents from 3 mA to 500 A, and features low power consumption. Additionally, the system includes built-in calibration mechanisms for both current and voltage measurements, along with inherent isolation for power and serial communication purposes. In this project, first model is chosen. Figure 3.5 shows how the ShuntMon2 connected with WatchMon CORE. (Batrium Knowledge / Wiki, n.d.)

## ShuntMon2

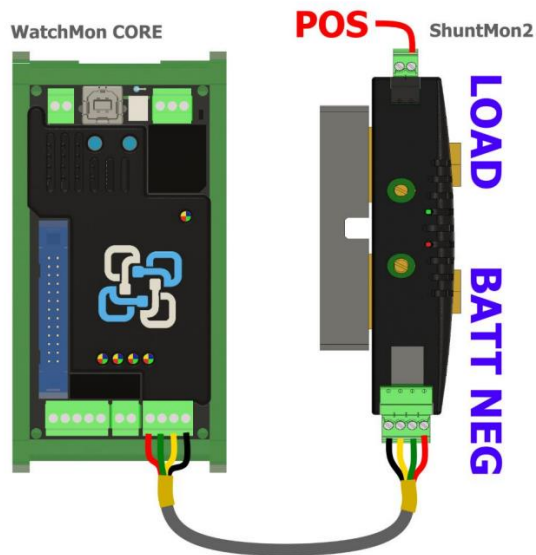


Figure 3.5: WatchMon CORE with ShuntMon2 (Batrium Knowledge / Wiki, n.d.)

### 3.3.4 IsoMon

IsoMon works with WatchMon Core to link and distribute cell monitors which is BlackMon M8 in this project. From Figure 3.6 it gives an evident in connection of WatchMon CORE with IsoMon and With the Cell monitors.

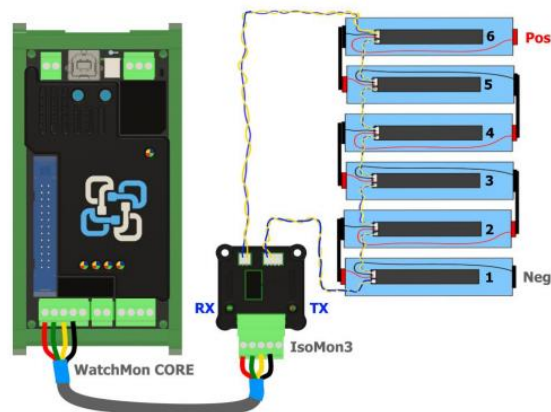


Figure 3.6: IsoMon Connection with WatchMon CORE with cell Monitor (Batrium Knowledge / Wiki, n.d.)

### 3.3.5 Expansion Board

Expansion Board is an onboard relay that is included on the WatchMon CORE intended for circuit breaker. Should there be a need to activate additional components like contactors, heaters, fans, alarms, and the like, the expansion board offers supplementary choices that can serve as triggers. (Batrium Knowledge / Wiki, n.d.) Figure 3.7 shows how Expansion Board looks like.

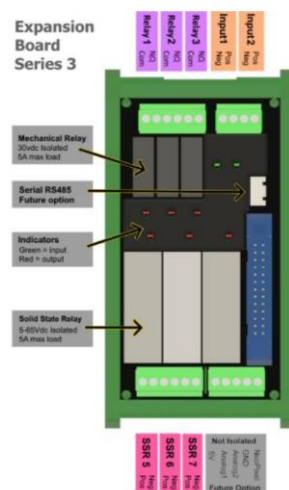


Figure 3.7: Expansion Board (Batrium Knowledge / Wiki, n.d.)

### 3.3.6 WatchMon Toolkit

WatchMon Toolkit is a custom-made software which allows to view and configure the WatchMon CORE or WatchMon Supervisor. It accesses through connection of USB port from WatchMon CORE to Laptop.

## 3.4 Sunny Island Inverter

The project utilizes the Sunny Island Inverter, a product manufactured by SMA Solar Technology. This inverter, bearing the Sunny Island brand, boasts a wide array of applications, catering to both on- and off-grid installations and offering a host of compelling features. Its versatility addresses a spectrum of needs, from powering off-grid regions to managing energy within homes. Drawing from SMA's extensive expertise, with a track record of over 100,000 Sunny Island inverters deployed worldwide, users can rely on consistent performance.

One of its standout features is the inclusion of an integrated user interface and standard WLAN and Ethernet interfaces, simplifying the commissioning and configuration processes. These functionalities can be

accessed conveniently via smartphones or tablets. Functioning as a cornerstone within the SMA Flexible Storage System, the Sunny Island excels at storing self-generated energy in batteries, enabling the uninterrupted utilization of solar power. The inverter exhibits robust attributes, including a high protection class, a broad operating temperature range, and exceptional overload capacity, ensuring its reliability across diverse applications. Additionally, its intelligent load and energy management mechanisms serve to sustain system functionality even during critical situations. (SMA,n.d.)

In this project inverter is used to charging and discharging using different current profiles to the lithium-ion batteries. Figure 3.8 gives a picture of how Sunny Island Inverter looks like.



Figure 3.8: Sunny Island Inverter

### 3.5 Node-red

Node-RED is an open-source visual programming tool designed for crafting and deploying applications geared toward data-driven projects, Internet of Things (IoT) applications, and home automation. This platform offers a web-based flow editor, enabling users to effortlessly create interconnected data flows between various devices and services by intuitively dragging and dropping nodes. (nodered.org, n.d.) Each node represents a specific function, such as a data source, data manipulation, or output destination, and can be connected to

other nodes to create a flow of data. The flows can be easily deployed and run on a variety of platforms, including desktop computers, servers, and Raspberry Pi devices.

Node-RED is crafted using JavaScript and is constructed atop Node.js, imbuing it with significant extensibility and seamless integration capabilities with various tools and services. Moreover, a robust and engaged community of users has actively contributed numerous nodes to the Node-RED library, simplifying connections to an extensive array of devices and services. Node-RED provides a simple and powerful way to create and deploy IoT applications and data-driven projects, even for users who are not experienced programmers.

In our project, data-driven projects from Inverter and BMS and also read and write command Inverter to charge and discharge is done in Node-red. The platform we used Node-red is laptop.

### **3.5.1 Modbus**

Modbus emerged as an industrial protocol in 1979, serving the purpose of enabling communication between automation devices. Initially conceived as an application-level protocol designed for data transfer across a serial layer, Modbus has since evolved to encompass applications spanning serial, TCP/IP, and the user datagram protocol (UDP) implementations. This document offers a comprehensive exploration of the protocol's implementation details.

Node-red can easily connect the Inverter using Modbus communication. Modbus is a master-slave type of communication. The master will issue read or write demands to the network slaves. After that, the slave will respond if the communication is sent to them. (accautomation.ca, n.d.) In this project, Modbus ethernet TCP/IP is used to connect with Inverter.

### **3.5.2 Wi-Fi Transmission Control Protocol/Internet Protocol (TCP/IP)**

TCP/IP, an abbreviation for Transmission Control Protocol/Internet Protocol, comprises a suite of communication protocols strategically employed for the linkage of network devices across the internet. Furthermore, TCP/IP serves as a communication protocol within private computer networks such as intranets or extranets. (Shacklett, 2021)



Collectively referred to as TCP/IP, the entire IP suite encompasses an assortment of rules and processes, with TCP and IP being the pivotal protocols, complemented by additional constituents within the suite. The TCP/IP protocol suite operates as an intermediary layer that exists between the routing and switching infrastructure and internet applications, providing a crucial abstraction layer.

TCP establishes the framework through which applications can establish communication pathways over a network. Additionally, it oversees the segmentation of messages into smaller packets, which are subsequently transmitted across the internet. Upon reaching their intended destination, these packets are reassembled in the correct sequence. On the other hand, IP prescribes the methodology for addressing and routing individual packets, ensuring their accurate delivery to the designated destination.

In this project, Inverter is used in TCP/IP connection. The IP address of the inverter that is used is “192.168.48.113” in the port of 502.

### **3.5.3 UDP Listener (WIFI)**

Utilize the UDP listener to initiate a UDP socket, directing incoming packets to a parser for further processing.

The UDP Listener offers compatibility with multiple parsers, provided these parsers are equipped with protocol detection capabilities. In this scenario, each parser associated with the listener is evaluated to determine its suitability for handling incoming packets. Once a parser accepts the packet, it assumes responsibility for parsing and dispatching the packet to its designated queue. Alternatively, if the listener designates a singular parser, the packet is directly channelled towards parsing without intermediary steps. (docs.opennms.com, n.d.)

In this project, UDP Port is used form retrieve information from WatchMon Core where the port number to be written in Node-red is “18542” using ipv4.

### **3.5.4 Node-red Dashboard**

The Node-RED Dashboard module introduces a collection of nodes within the Node-RED framework, facilitating the swift creation of dynamic data

dashboards. These nodes enable the rapid design of user interfaces featuring components like buttons, sliders, charts, and gauges. In this project dashboard is used to monitor the flow of Current, Voltage SOC and temperature in Inverter using chart function by time to time.

### **3.5.5 Excel**

In our project, Node-red will create file and data log information from Inverter and BMS to Excel file. It will be set interval each minutes log the information from Inverter and BMS to excel file. With the information of Excel, we can save the information easily from time to time. It also can insert line graph to see the trend form such as the fluctuating voltage, current, and SOC.

## **3.6 Node-red Setup in Inverter and Batrium BMS**

In this section, it will shows the full flows of node-red to command in Inverter and Batrium BMS.

### **3.6.1 Node-red Inverter**

In Figure 3.9, It use the function of the Node-red Palette. In this section of read inverter value shows how to read information through Wi-Fi and TCP/IP using Modbus Flex Getter and their specific address to read the inverter's Current, State of Charge (SOC), Battery Capacity, Temperature and Voltage which will be display in the Node-red Dashboard. In Figure 3.10 display the Inverter information with line chart over time. In Figure 3.9 section of Transfer Data to csv file is where log the data of Inverter to csv file with the interval time of 1 minute. To give instruction to inverter in charging and discharging, the inverter need to be in active mode and in Section of Charging/Discharging in Figure 3.9, can give a constant current charging.

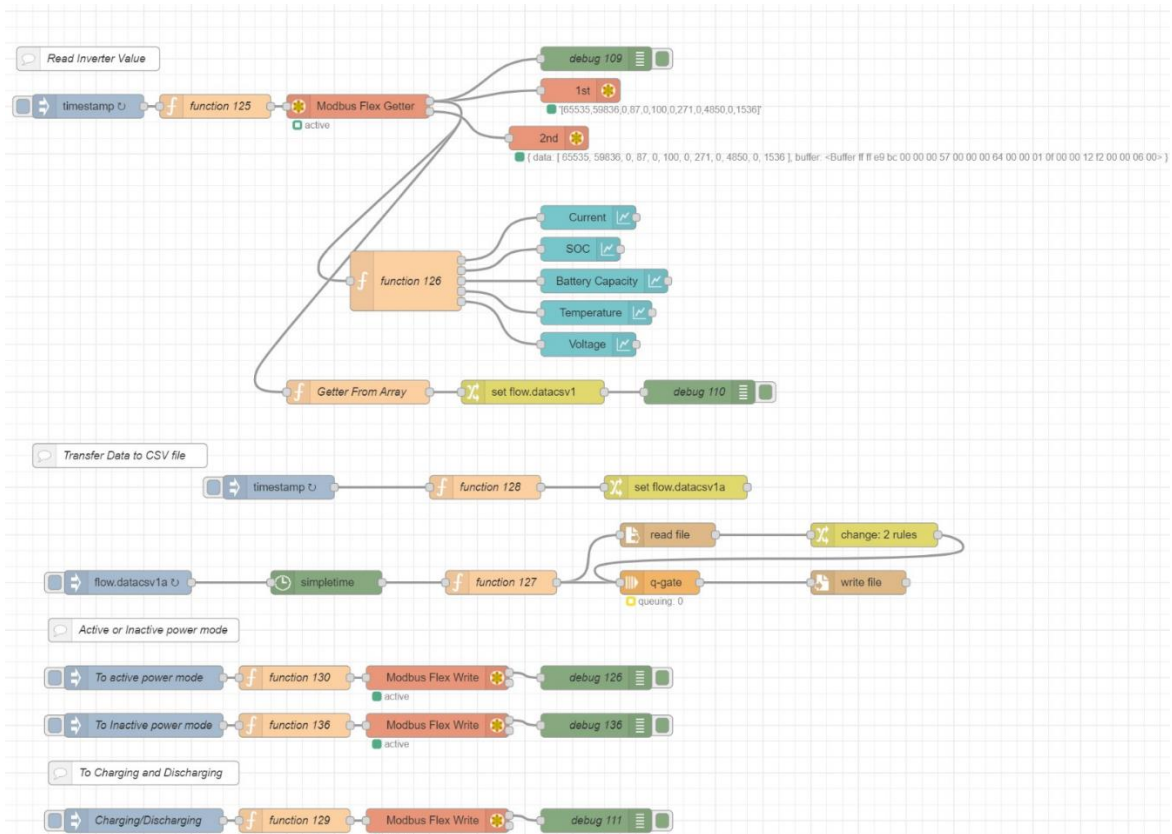


Figure 3.9: Inverter Node-red Whole Function

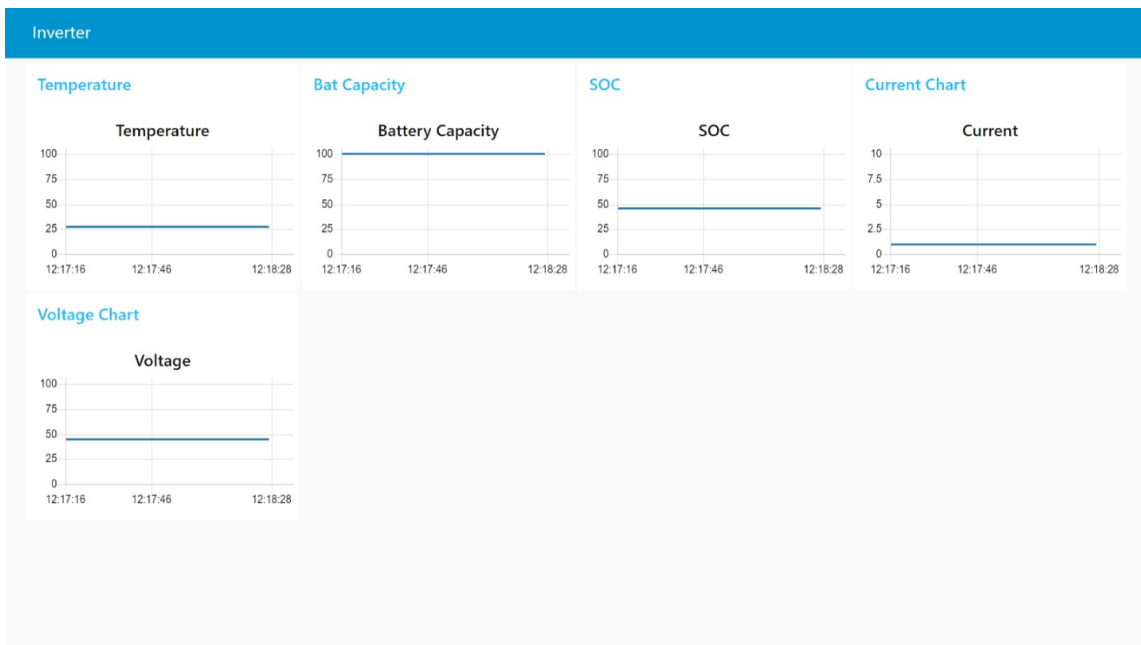


Figure 3.10: Inverter’s Information Display

### 3.6.2 Node-red Batrium BMS

In Batrium BMS, it can retrieve information from WatchMon4 where is shows in Figure 3.11. In Figure 3.12, it connects with UDP and with their special parser nodes, it can read each information from WatchMon 4. It then will log the data that collected to excel during charging and discharging the Li-ion Batteries. Figure 3.13 shows that the function where gives the protection to batteries which can be stop charging and discharging when above 3.6V and below 2.8V. In Figure 3.13, is the protection for stop charging and discharging when the cell voltage above 3.6V and under 2.8V respectively.

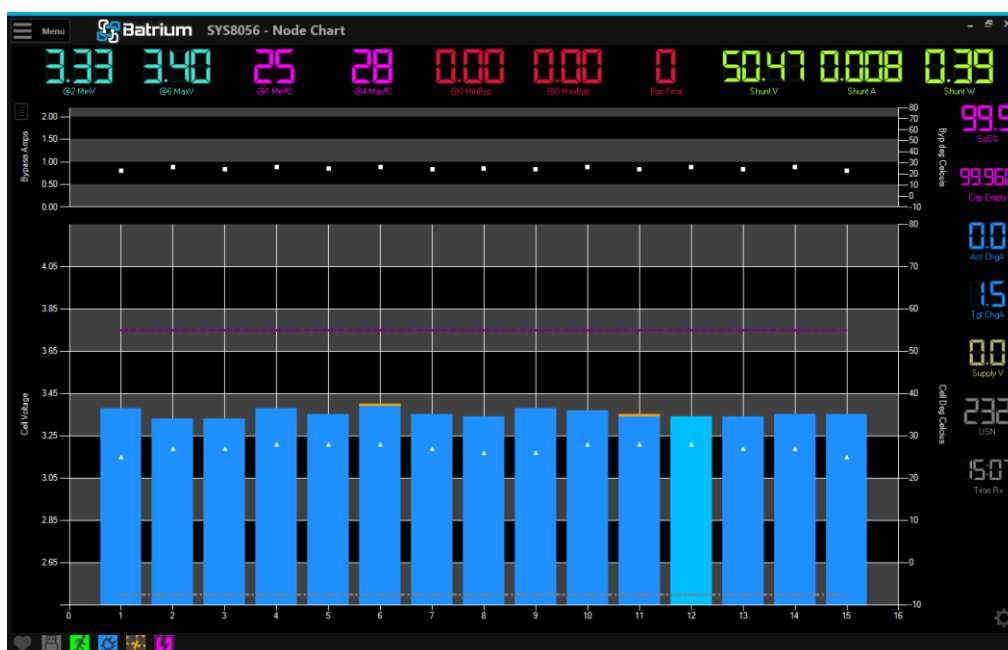


Figure 3.11: WatchMon 14 Batteries Cell

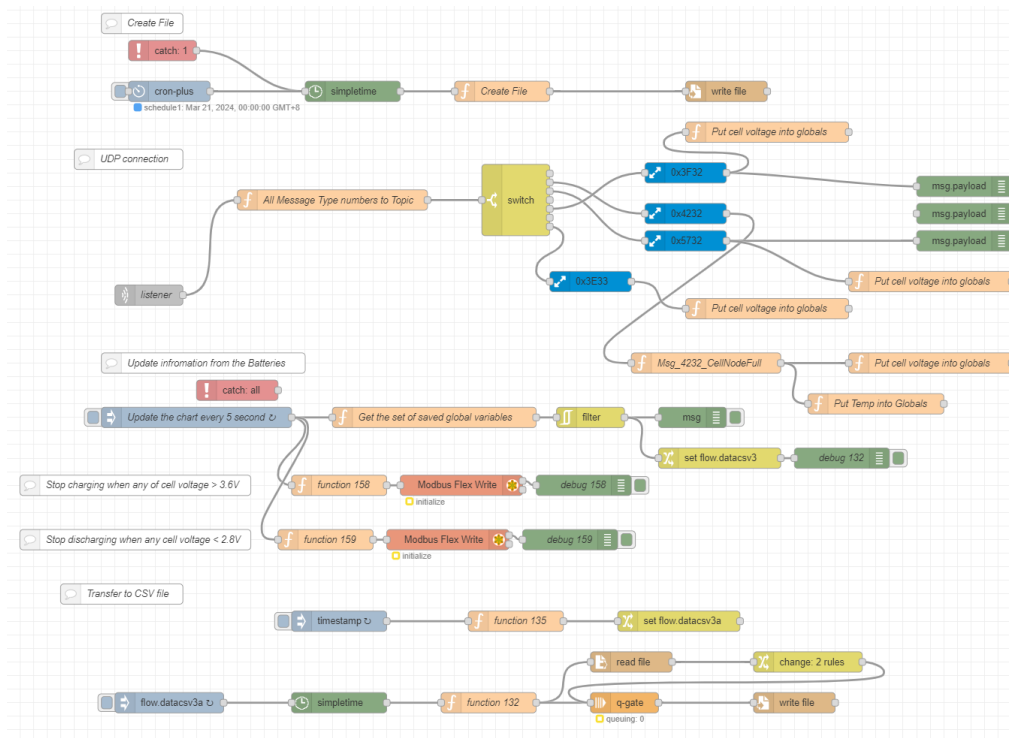


Figure 3.12: Retrieve Information of Battery from Watchmon4 Batrium

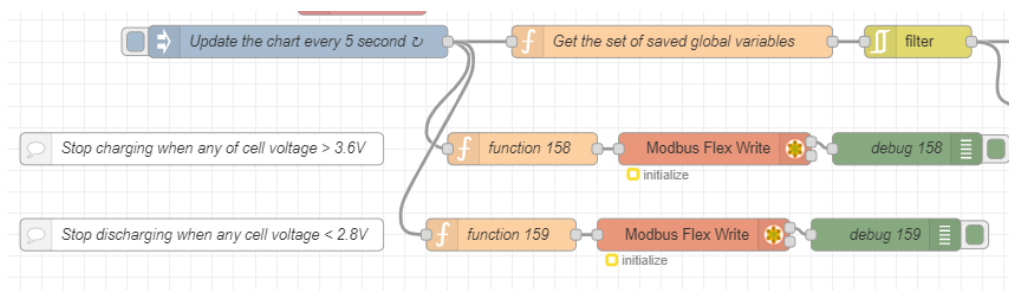


Figure 3.13: Protection for stop Charging and discharging when the voltage above the level or lower the level respectively.

### 3.7 State of Health (SOH) Estimation

In SOH estimations calculations is refer from the research paper of Bian et al., 2019 and Li et al., 2016. The rate of change of capacity (Q) with respect to voltage (V) ( $dQ/dV$ ) is calculated from the parameters is recorded during charging. At first the  $dQ/dV$  vs Cell voltage is plotted where shown in Figure 3.14: Graph of  $dQ/dV$  vs Cell Voltage. This graph can show us the three peak voltages can be used in further calculations which will be used in the formula

shown in equation of  $Q = Q_{max} \left[ \sum_{i=1}^n \frac{A_i}{\pi} \arctan \left( \frac{V - V_{0i}}{\frac{\omega_i}{2}} \right) + C \right]$

(3.1). The cell voltages data that collected when charging the batteries will not directly to be used but will give a moving average of each five voltages data to make the graph smoother and reduce the stage-like shape graph.

$$\text{In} \quad Q = Q_{max} \left[ \sum_{i=1}^n \frac{A_i}{\pi} \arctan \left( \frac{V-V_{0i}}{\frac{\omega_i}{2}} \right) + C \right]$$

(3.1) formula, calculated capacity or maximum capacity can be determined. The range of  $\omega_i, A_i, C$  and  $Q_{max}$  stated in equation  $Q =$

$$Q_{max} \left[ \sum_{i=1}^n \frac{A_i}{\pi} \arctan \left( \frac{V-V_{0i}}{\frac{\omega_i}{2}} \right) + C \right] \quad (3.1) \text{ is used}$$

but for  $Q_{max}$  is slightly change from 1.05 to 1.15 because during the charging process is ended earlier. In the voltage vs capacity graph, the regression model is used with the formula and range stated in  $Q =$

$$Q_{max} \left[ \sum_{i=1}^n \frac{A_i}{\pi} \arctan \left( \frac{V-V_{0i}}{\frac{\omega_i}{2}} \right) + C \right] \quad (3.1) \text{ for}$$

minimising SSR (Sum of Squares). The objective is to select the line that fits the data most closely and minimises the sum of squared residuals (SSR) and describes the relationship between voltage (the independent variable) and capacity (the dependent variable). The best fitting line is solve using the Excel solver function to minimize the SSR and the fitted graph is shown in Figure 3.15. Therefore, the  $Q_{max}$  can be determined to find the SOH.

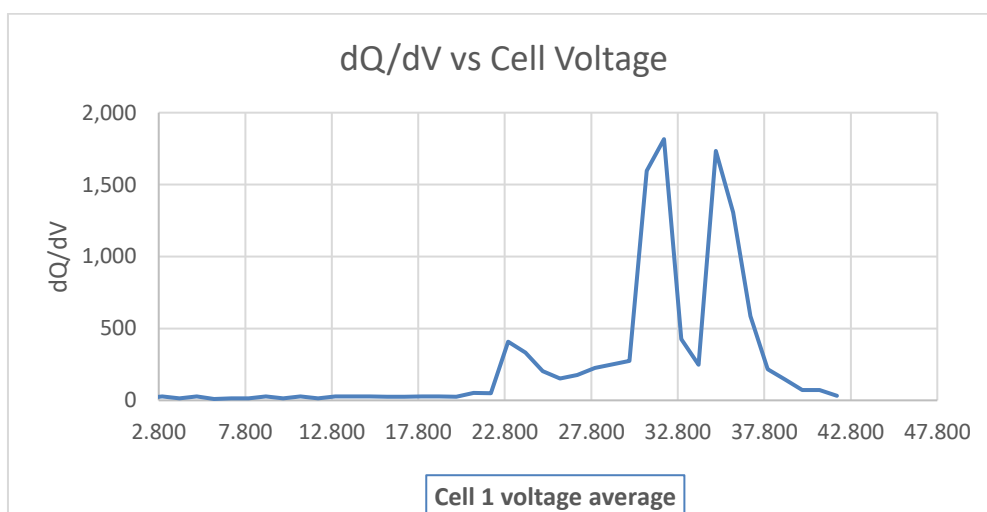


Figure 3.14: Graph of dQ/dV vs Cell Voltage

$$Q = Q_{max} \left[ \sum_{i=1}^n \frac{A_i}{\pi} \arctan \left( \frac{V - V_{0i}}{\frac{\omega_i}{2}} \right) + C \right] \quad (3.1)$$

where

$\omega_i \in [0,0.1]V, A_i \in [0,1.0], C \in [0.5,0.52]$  and  $Q_{max} \in [1,1.15] \times Q_{end}$

$Q = \text{Capacity (Ah)}$

$Q_{max} = \text{Maximum Capacity (Ah)}$

$A_i = \text{area below } i\text{th peak}$

$n = \text{number of peaks}$

$V_{0i} = \text{peaks Voltage}$

$\omega_i = \text{peak width}$

$C = \text{Constant produced by integral}$

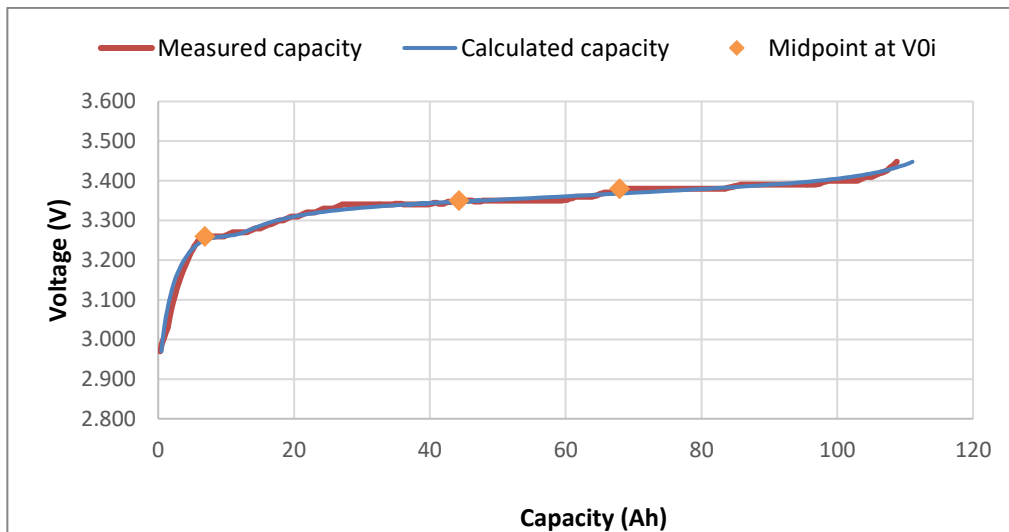


Figure 3.15: Graph of Voltage vs Capacity (Measured and Calculated)

### 3.8 Summary

In this methodology, includes a setup of monitoring system of a series of lithium-ion batteries, the Batrium Battery Management System (BMS), and using an inverter. This arrangement allows for real-time monitoring of the batteries' functioning and health, with the inverter functioning as an charging and discharging the batteries. All the parameters such as voltage, current, temperature, and state of charge are monitor by BMS. The BMS also will ensure cell balancing and protection against overcharging or over-discharging.

The design of the battery monitoring system setup makes use of node-red software to enable data interchange between the BMS and the inverter,

recording data to an Excel file for further investigation. The WatchMon CORE, Cell Monitors, ShuntMon2, and Expansion Board are some of the components that make up the Battery Monitoring System (BMS). Each one has a specific purpose in monitoring and managing the battery system.

Node-red facilitates inverter management and monitoring by offering features such as reading inverter, transferring data to CSV files for logging, and controlling the inverter's charging and discharging. The inverter is connected using Modbus communication, and data is sent and received by TCP/IP while for WatchMon CORE is communicated using UDP Listener. The Sunny Island Inverter, which has capabilities like Ethernet, WLAN, and integrated user interfaces for simple commissioning and configuration, is also used in this project to charge and discharge the batteries. Node-RED Dashboard is another tool used by the system to create dynamic data dashboards that track battery characteristics.



## CHAPTER 4

### RESULTS AND DISCUSSION

#### 4.1 Introduction

In this chapter, we will explore the results and discourse pertaining to the degradation rate of Li-ion batteries under various charging and discharging current profiles, this section will offer an in-depth examination of the research outcomes and the gathered data.

#### 4.2 Characteristics during Charging and Discharging

In this section will shows the graph characteristics during charging and discharging between the voltage, current and the capacity of the batteries where it can use for further determination in State of Health (SOH). There also a subsection where included temperature characteristics during charging and discharging using three different current profile.

##### 4.2.1 Part A: Capacity vs Shunt Current during Charging

All the graphs of measured capacity vs shunt current are shown under part A. In Figure 4.3, Figure 4.2 and Figure 4.3, show using almost constant current charging for 1kW, 1.5kW and 2kW power respectively, the measured capacity,  $Q$  (Ah) increases proportionally. It means it is charging the batteries. First of all, it makes it possible to gather crucial information on the behaviour of Li-ion batteries under various charging current profiles. Understanding the batteries' degradation over time and in different operating situations depends on this data which may assess the batteries' degradation rate under various profiles by measuring their capacity ( $Q$ ) following each charging cycle.

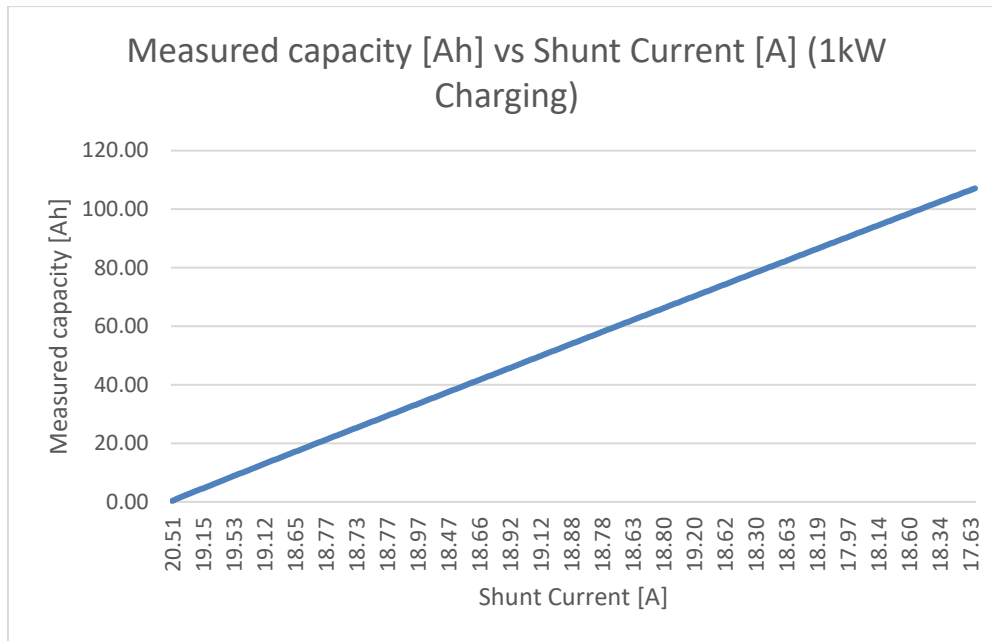


Figure 4.1: Graph of Shunt Measured Capacity against Shunt Current (1kW Charging)

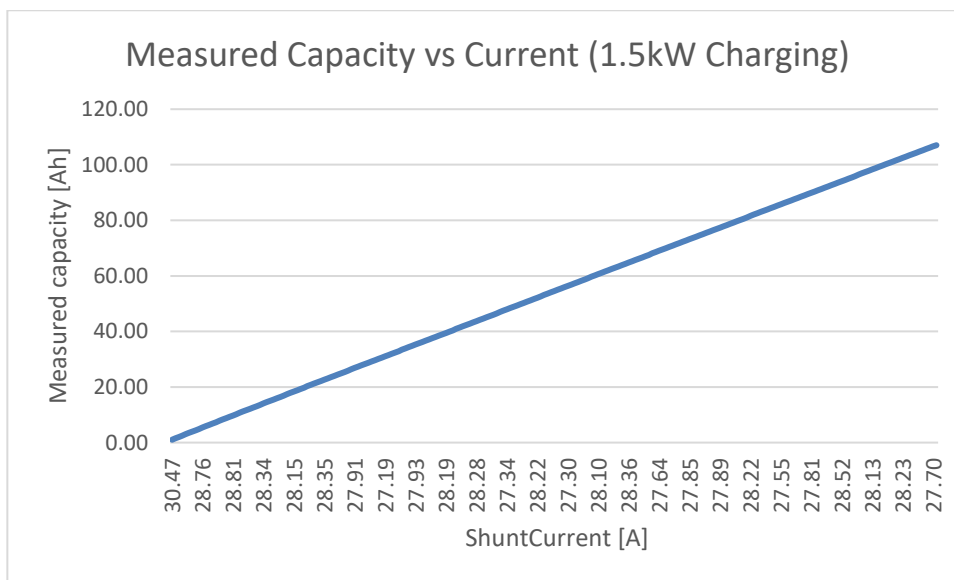


Figure 4.2: Graph of Shunt Measured Capacity against Shunt Current (1.5kW Charging)

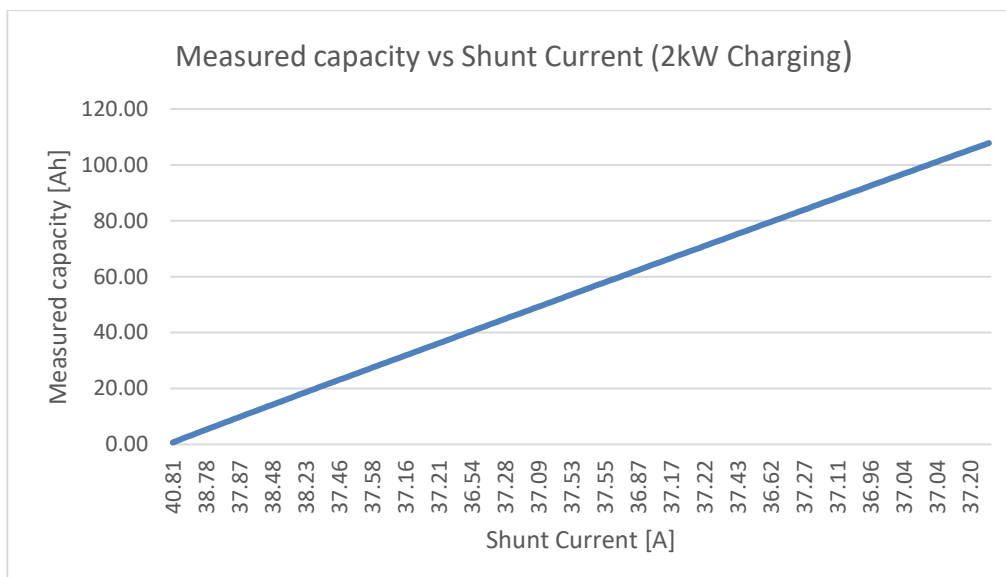


Figure 4.3: Graph of Shunt Measured Capacity against Shunt Current (2kW Charging)

#### 4.2.2 Part B: Shunt Voltage vs Capacity under Charging

In Figure 4.6, Figure 4.5 and Figure 4.6 which is part B display graphs of total voltage against measured capacity until different charging profile. All three graphs with different charging profiles shows the similar curve. For the initial stage, the three graphs can be seen that the total voltage increases linearly as the capacity of battery increases. This is because when the battery absorbs charge and the voltage incrementally rises, this first linear increase represents the early stage of charging. there is typically a plateau period during which further charging has little impact on the overall voltage. The reason for this plateau is that the battery saturates to the point where further charge does not appreciably raise the voltage. As the battery gets closer to full charge towards the conclusion of the charging process, the overall voltage begins to rise linearly once more. The battery is almost fully charged based on this last linear increase, and more charging will cause the voltage to spike.

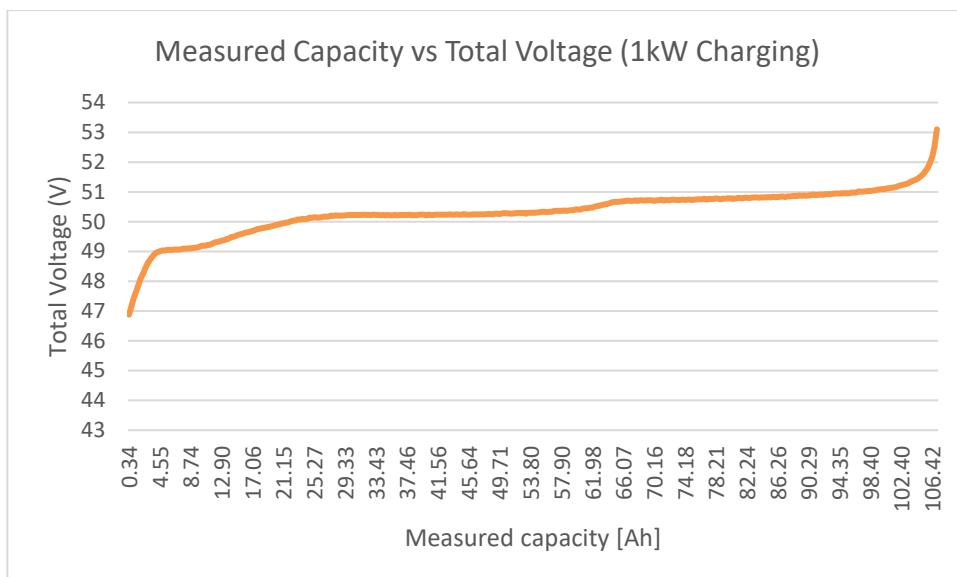


Figure 4.4: Graph of Total Voltage against Measured Capacity (1kW Charging)

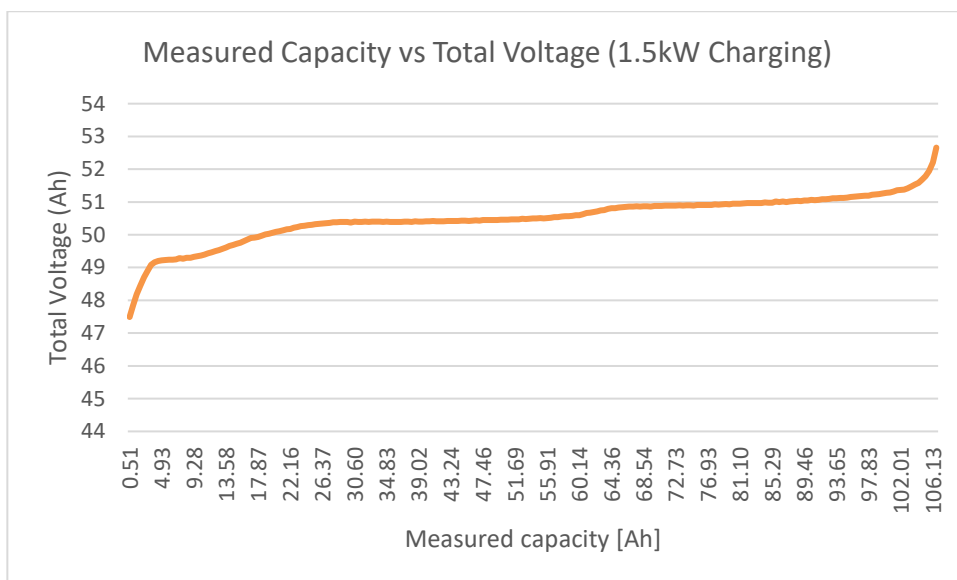


Figure 4.5: Graph of Total Voltage against Measured Capacity (1.5kW Charging)

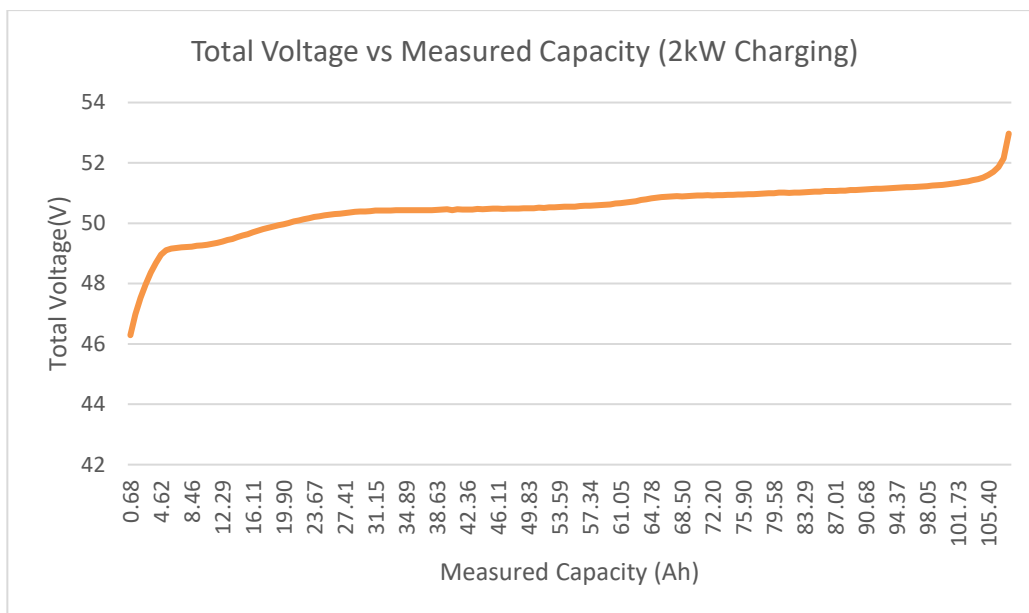


Figure 4.6: Graph of Total Voltage against Measured Capacity (2kW Charging)

### 4.2.3 Part C: Capacity vs Shunt Current under Discharging

In Part C shows the measured capacity against shunt current graphs for discharging profile. In Figure 4.7, Figure 4.8 and Figure 4.9, shows the three graphs of measured capacity against shunt current where the current almost constant under power of 1kW, 1.5kW and 2kW respectively. The three graphs shows that measured capacity, Q (Ah) decreases proportionally when discharging under constant current. It means it is discharging the batteries. Discharging the batteries where they gradually lose their charge after being used often to power gadgets like EV cars and smartphones. By discharging the batteries, we can future research in assessing the battery degradation characteristics. It is crucial for maximising battery management methods and offers significant insights into how batteries operate in different circumstances.

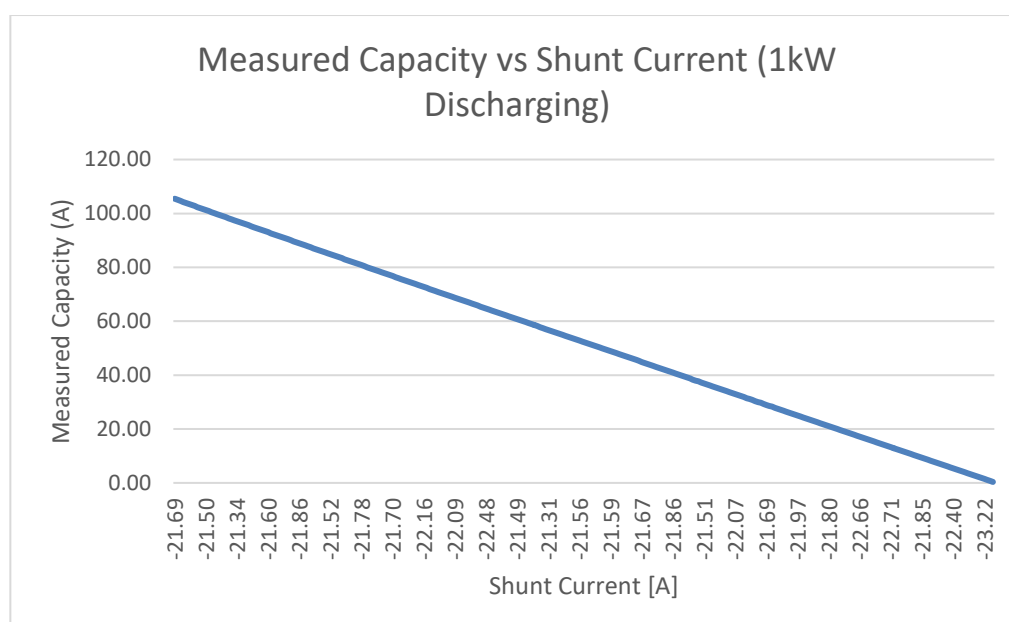


Figure 4.7: Graph of Shunt Measured Capacity against Shunt Current (1kW Discharging)

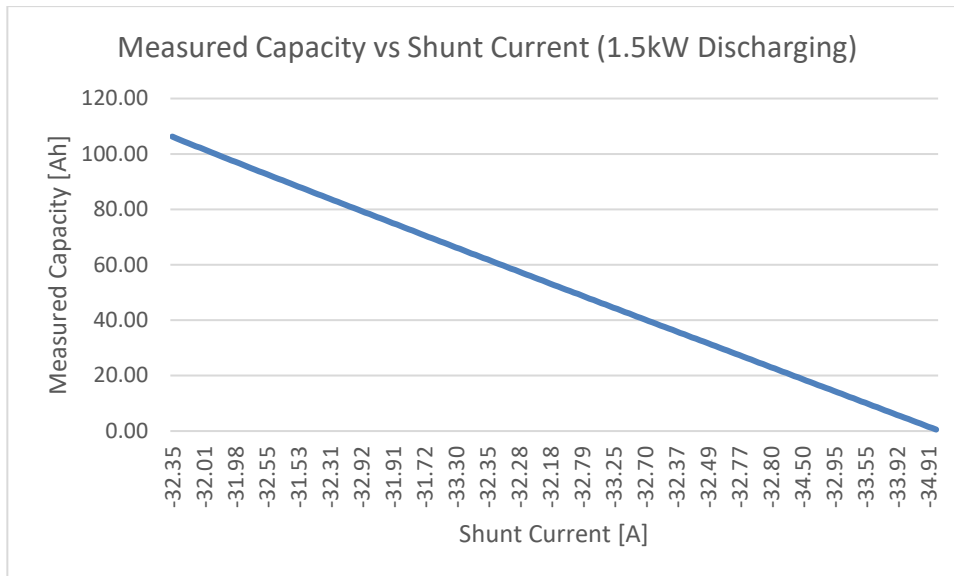


Figure 4.8: Graph of Shunt Measured Capacity against Shunt Current (1.5kW Discharging)

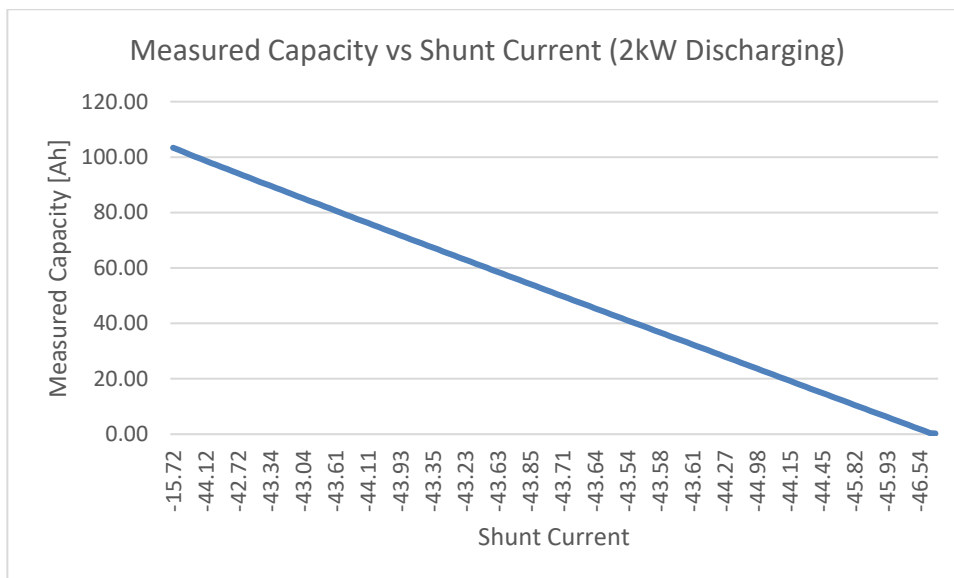


Figure 4.9: Graph of Shunt Measured Capacity against Shunt Current (2kW Discharging)

### 4.3 Part D: Voltage vs Capacity under Discharging

In Part D for Figure 4.10, Figure 4.11 and Figure 4.12 of discharging display graphs of total voltage against measured capacity until different discharging profile which is 1kW, 1.5kW and 2kW respectively. At the beginning phase of discharging, the total voltage drops rapidly. This rapid first fall shows the battery's rapid discharge. After the initial decrease, there comes a plateau period during which the overall voltage stays mostly consistent for the duration of the discharging operation. This plateau shows that the battery produces a steady voltage for most of the discharge cycle. As the battery gets closer to full discharge at the end, the total voltage decreases again. This can show that the battery is almost fully discharge or in drainage.

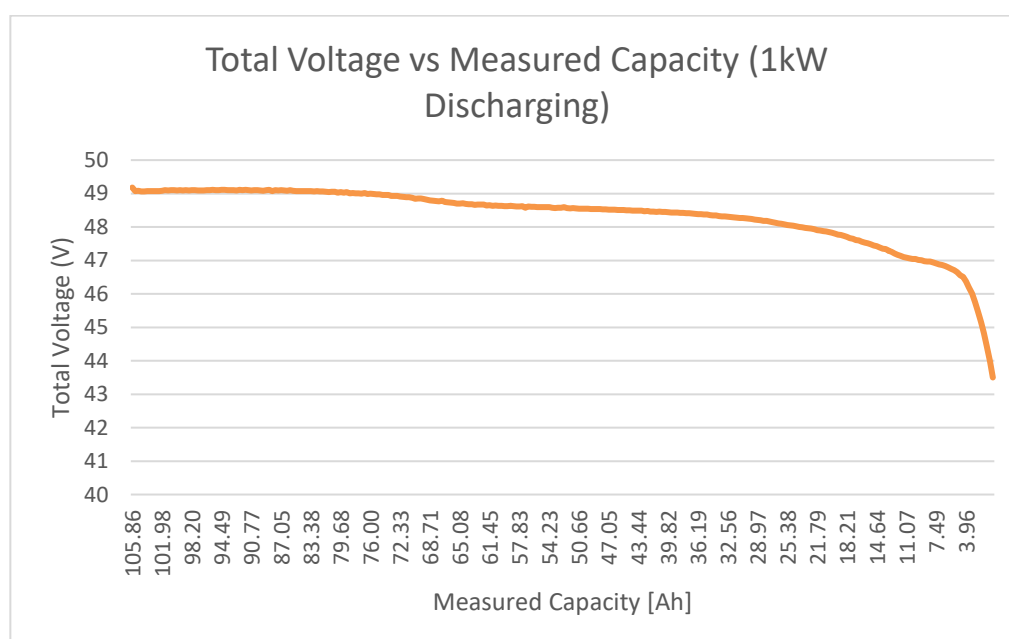


Figure 4.10: Graph of Total Voltage against Measured Capacity (1kW Discharging)



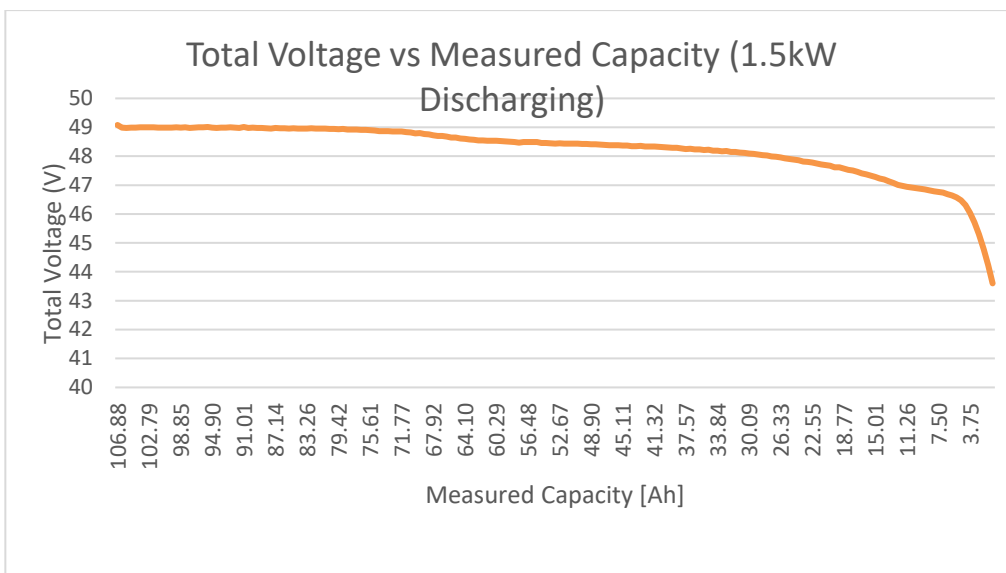


Figure 4.11: Graph of Total Voltage against Measured Capacity (1.5kW Discharging)

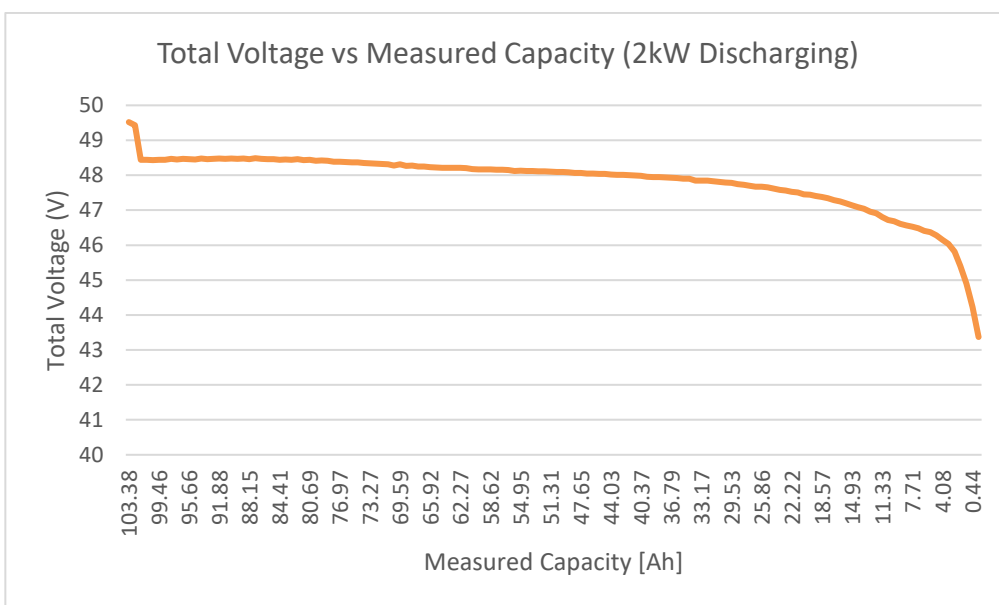


Figure 4.12: Graph of Total Voltage against Measured Capacity (2kW Discharging)

### 4.3.1 Charging and Discharging for Temperature Characteristics

The two sections where a) with Figure 4.13, Figure 4.14 and Figure 4.15 show temperature changes under different charging profiles while section b) with Figure 4.16, Figure 4.17 and Figure 4.18 shows temperature recorded under different discharging profiles. 1kW charging has the lowest peak temperature compared to other two charging profiles. The highest temperature among these charging profiles is 2kW where when charging it goes to the highest peak 39 °C while for discharging it goes to 41 °C. For 1kW charging and discharging, its highest temperature gain during end of the charging only at 28°C and 30°C for discharging and continue with 1.5kW, which highest temperature at 31°C and discharging is 34°C. Cell 6 has the highest temperature among the other cells.

According to Ma et al., 2018, high temperatures speed up the process of thermal ageing and might potentially reduce Lithium-ion batteries (LIB) lifespan. Another significant issue at high temperatures is heat production within the batteries. This shows that higher current (power) will increase the temperature during charging and discharging which can damage the battery. Therefore, to prevent the high temperature charging 1kW is the most suitable because it has the lowest peak temperature which compares to 1.5kW and 2kW profiles. It gives the most damage to the batteries because very high current charging and discharging profiles give a high rise of temperature.

**a) Temperature with current during charging of 1kW, 1.5kW and 2kW**

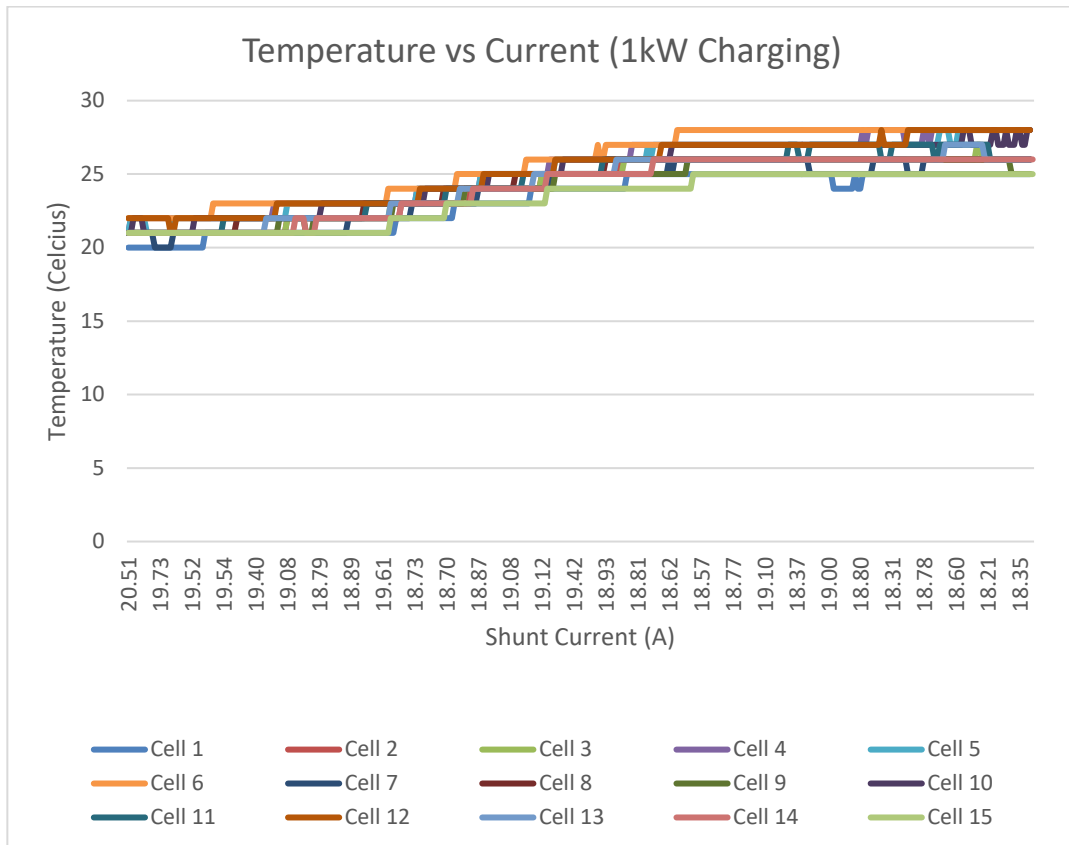


Figure 4.13: Graph of Temperature for 1kW Charging.

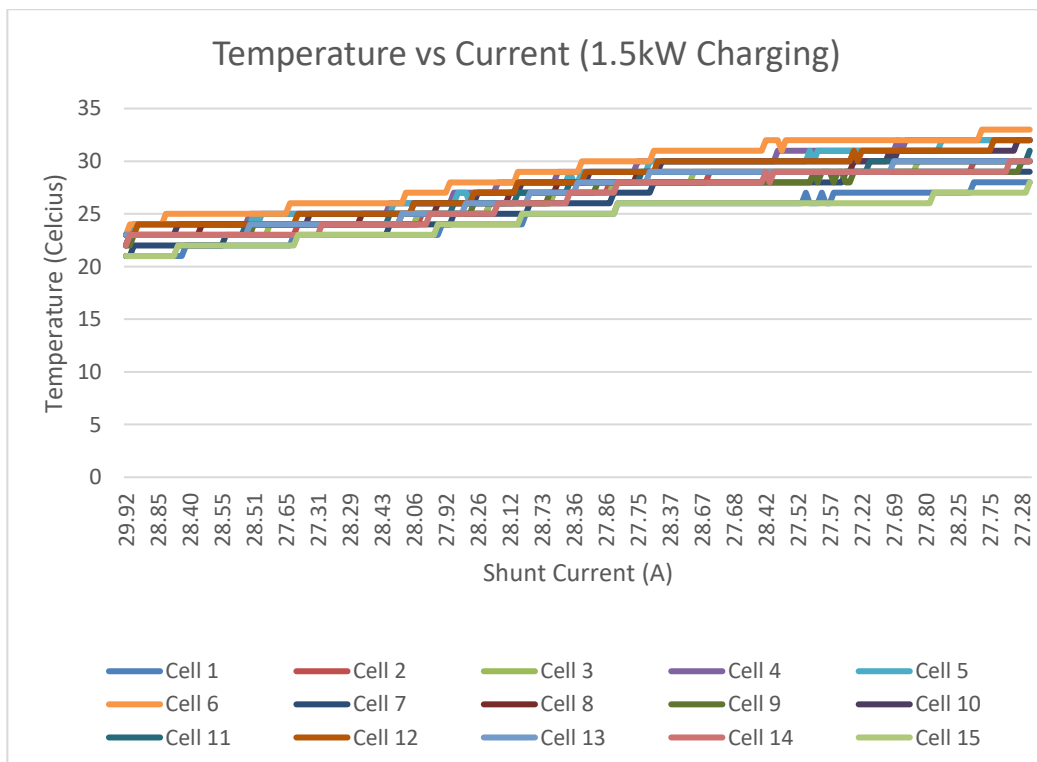


Figure 4.14: Graph of Temperature for 1.5kW Charging.





#### 4.4 Summary

Various graphs and statistics on battery performance are included in this chapter. In this chapter, the measured capacity (Ah) grows proportionately with practically constant current charging, as shown in graphs in the first section of the article, which gives insights from charging situations. In order to emphasise the significance of these chemical processes in effective and secure charging procedures, voltage plateaus during charging are explained as being symptomatic of various chemical reactions within the battery. To track the status of charging, the link between voltage and capacity is also covered. The chapter explores discharge scenarios, showing that in constant current discharge, measured capacity (Ah) and current have an inversely proportional relationship. The figures demonstrate how voltage plateaus are equally important in understanding battery behaviour during discharge as they are during charging. For the purpose of evaluating battery performance and estimating runtime, the relationship between battery capacity and shunt voltage during discharging is shown. Moreover, the temperature graphs during charging and discharging also shown, this gives a valuable insight how the temperature increases during charging and discharging.

## CHAPTER 5

### ESTIMATED RESULTS OF SOH USING ICA METHOD

#### 5.1 Incremental capacity analysis (ICA-based) SOC estimation of batteries (SOH Estimation)

In the Section 5.1.1 , it gives every charging profile of dQ/dV Graph to determine the peak voltage while in section 5.1.2 shows the Voltage vs Measured and Calculated Capacity Graph to determine the maximum capacity and State of Health (SOH).

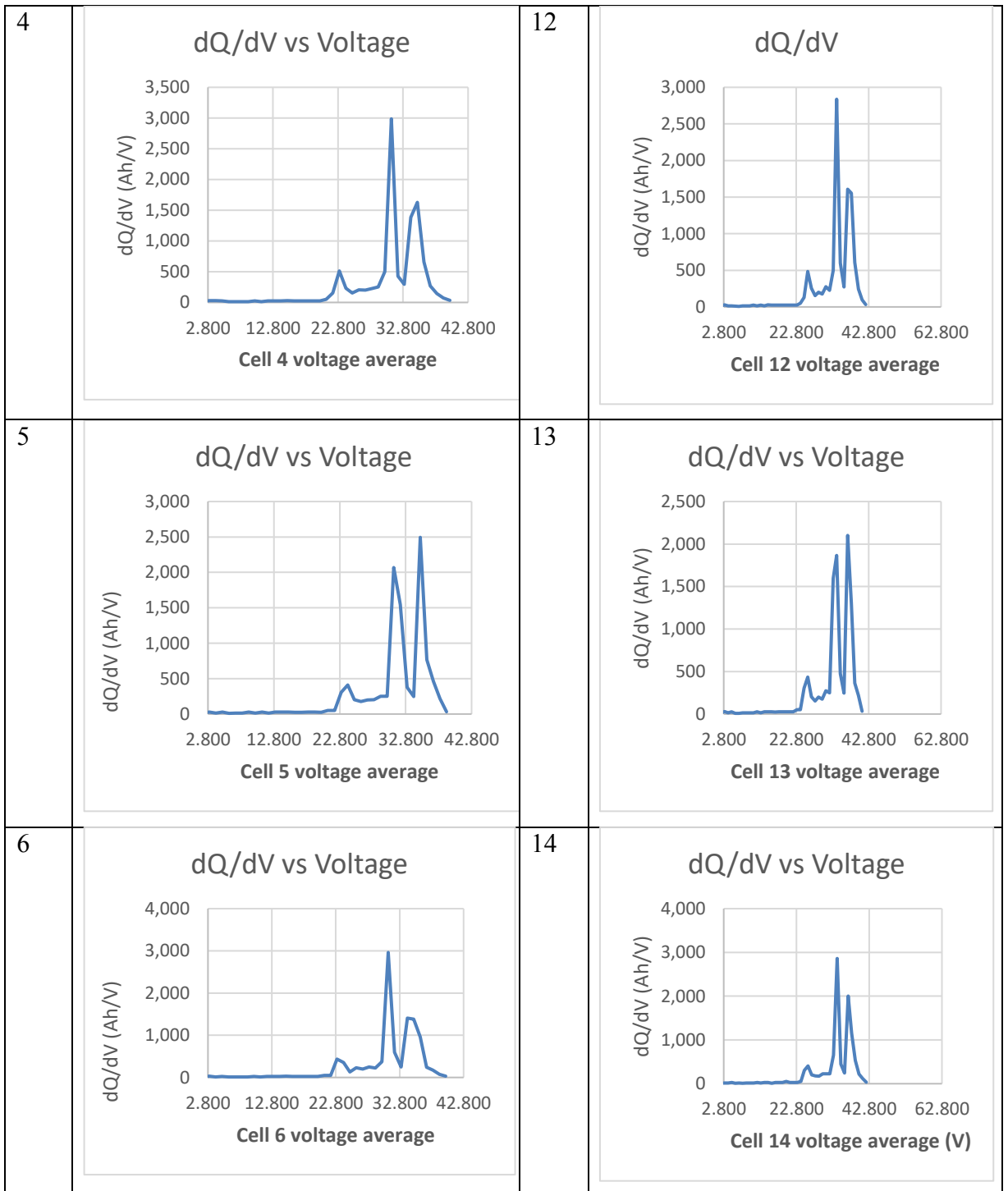
##### 5.1.1 dQ/dV Graph (Three Peaks Voltage)

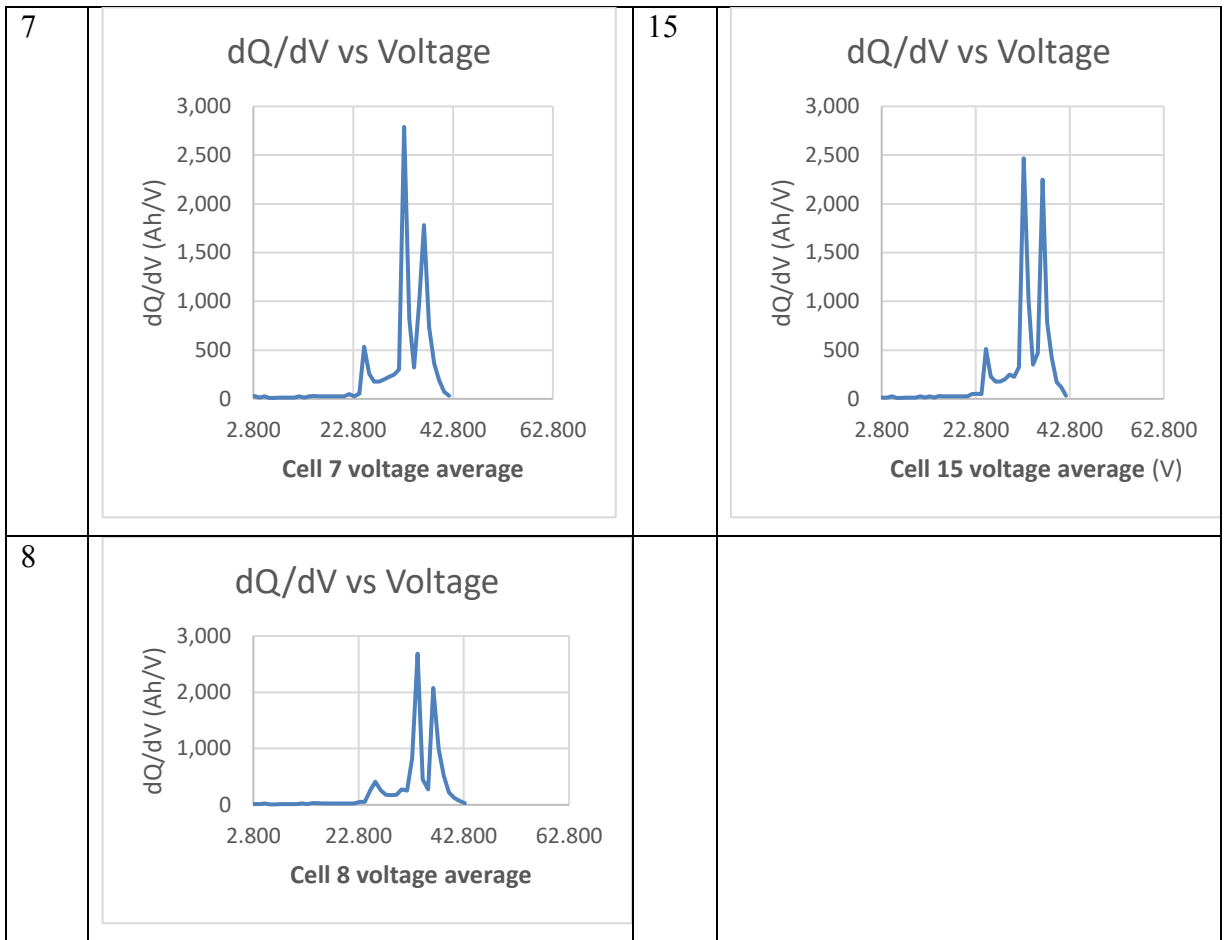
In this section of the Table 5.1, all the dQ/dV graphs under different cells is plot under the charging profiles of 0.8kW and other tables will be in Appendix C. For this graph where the change of capacity divides the change of cell voltage in every point is plotted in graph as mentioned in State of Health (SOH) Estimation in section 3.7. Each IC curve is dependent on voltage interval (dV). According to Huang, 2019, the capacity of Incremental Capacity Analysis (ICA) to convert cell voltage plateaus into easily recognizable dQ/dV peaks on Incremental Capacity (IC) curves is a significant benefit. The peaks indicate the cell's phase transition features during the intercalation and de-intercalation of lithium ions in the active materials. This change offers a more straightforward and enlightening method for examining the behavior of the battery and comprehending its causes of degradation. From the three peak values can determine the peak voltage. With these each peak voltage can further determine the analytical graph for Voltage vs Calculated graphs for each cell to determine the maximum capacity and State of Health.

Table 5.1: Table with Graph of dQ/dV vs voltage points (0.8kW Charging)

Cell	Graph of dQ/dV vs Cell Voltage	Cell	Graph of dQ/dV vs Cell Voltage
1	<p><b>dQ/dV vs Cell Voltage</b></p> <p>Axis Title</p> <p>Cell 1 voltage average</p>	9	<p><b>dQ/dV vs Voltage</b></p> <p>dQ/dV (Ah/V)</p> <p>Cell 9 voltage average</p>
2	<p><b>dQ/dV vs Voltage</b></p> <p>dQ/dV (Ah/V)</p> <p>Cell 2 voltage average</p>	10	<p><b>dQ/dV vs Voltage</b></p> <p>dQ/dV (Ah/V)</p> <p>Cell 10 voltage average</p>
3	<p><b>dQ/dV vs Voltage</b></p> <p>dQ/dV (Ah/V)</p> <p>Cell 3 voltage average</p>	11	<p><b>dQ/dV vs Voltage</b></p> <p>dQ/dV (Ah/V)</p> <p>Cell 11 voltage average</p>







### 5.1.2 Voltage vs Capacity Curve of Measured and Analytical

The Table 5.2 is showing 15 cells of Voltage against Measured and Calculated Capacity under 0.8kW current profiles. The rest of the curve of other charging profiles of 1kW, 1.5kW and 2kW under Appendix D. In this section, the

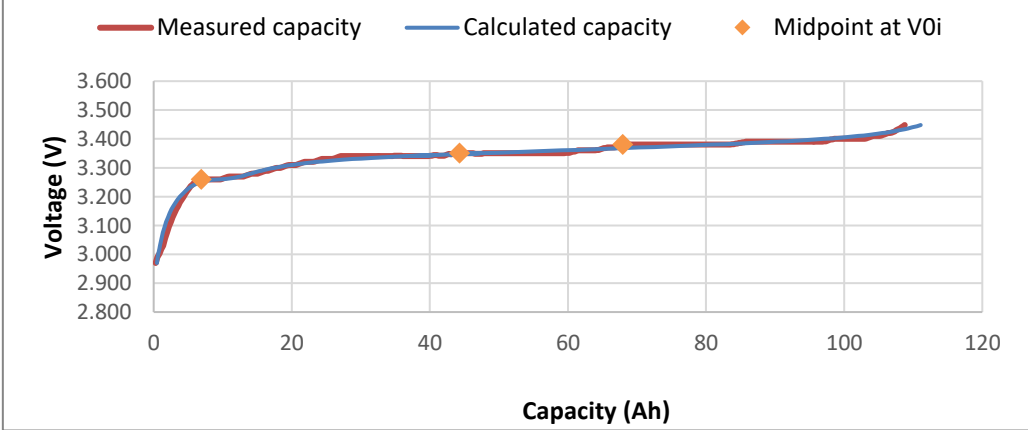
calculated curve is from equation of  $Q = Q_{max} \left[ \sum_{i=1}^n \frac{A_i}{\pi} \arctan \left( \frac{V-V_{0i}}{\frac{\omega_i}{2}} \right) + C \right]$

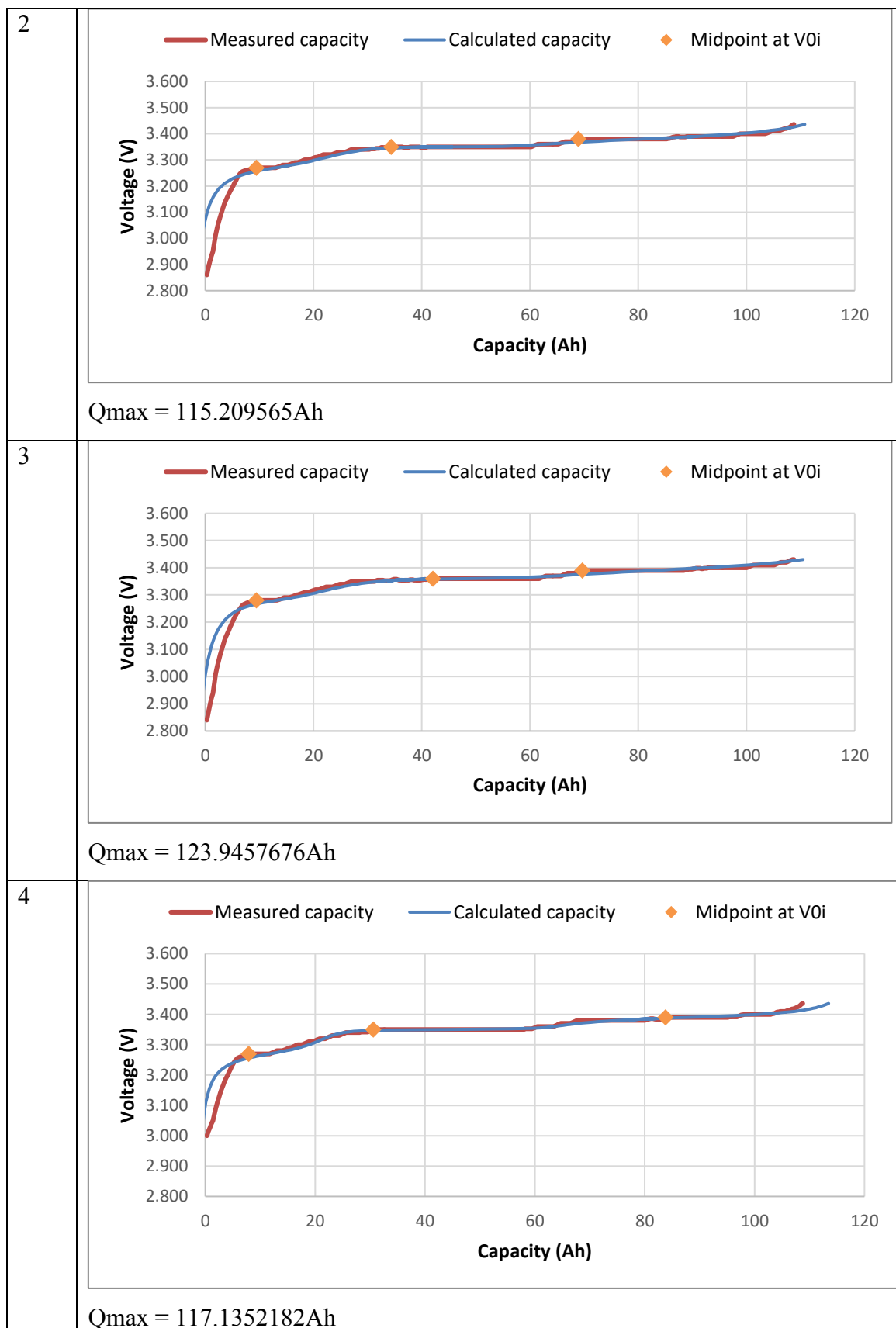
(3.1) which mention in Chapter 3. In this formula parameters of  $V_{0i}$  is the three peak voltage which is determine from  $dQ/dV$  graphs. Using the solver function of excel, with the range stated in equation  $Q =$

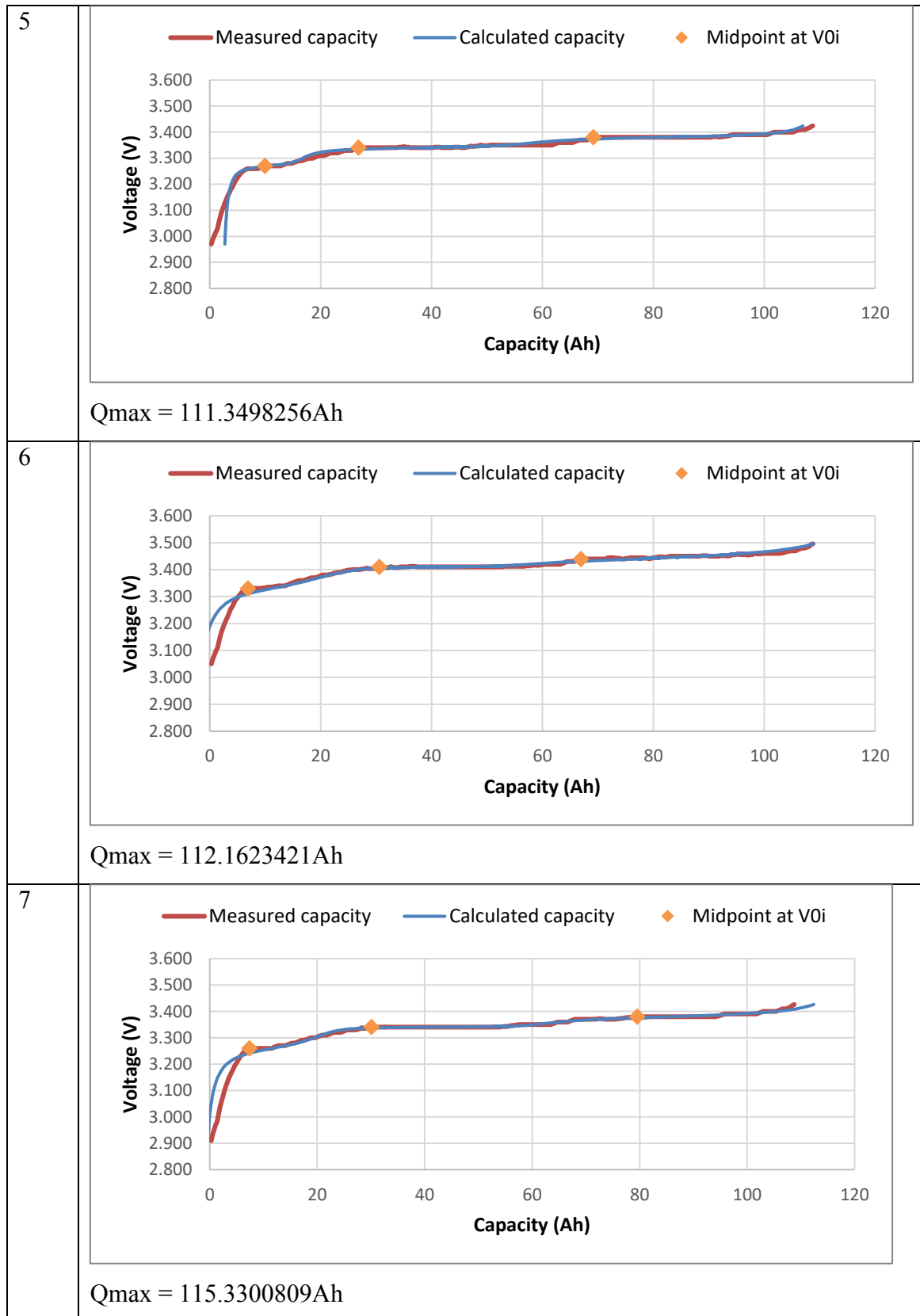
$$Q_{max} \left[ \sum_{i=1}^n \frac{A_i}{\pi} \arctan \left( \frac{V-V_{0i}}{\frac{\omega_i}{2}} \right) + C \right] \quad (3.1) \text{ to make}$$

the calculated capacity curve smaller difference to measured capacity curve where it can find the maximum capacity of each charging profiles. From each table's charging profiles, the average maximum capacity ( $Q_{max}$ ), is determined. Using this average maximum capacity values of each charging profiles, to determine state of health (SOH) of 1kW,1.5kW and 2kW charging profiles.

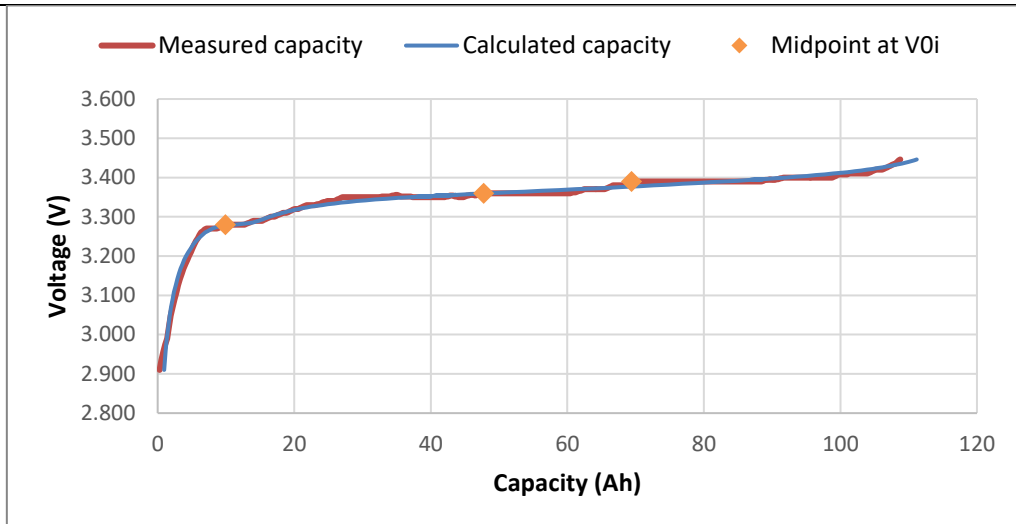
Table 5.2: Table of Voltage vs Capacity Curve with Calculated Maximum Capacity (0.8kW Charging)

Cell	Graph of Voltage vs Measured and Calculated Capacity with the Maximum Capacity ( $Q_{max}$ ) Value
1	 <p data-bbox="341 1800 663 1832">Qmax = 108.7685472Ah</p>



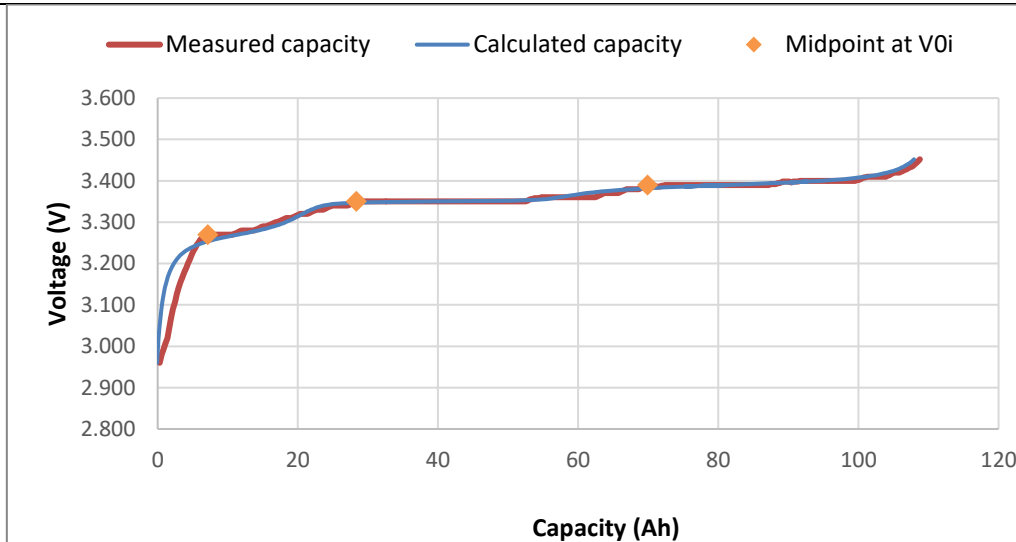


8



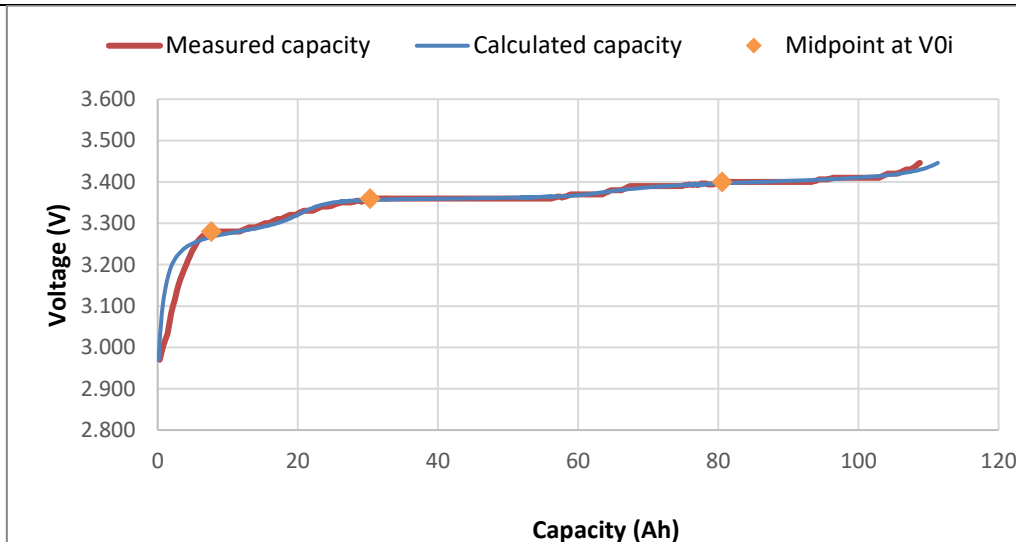
$Q_{max} = 118.6739577Ah$

9

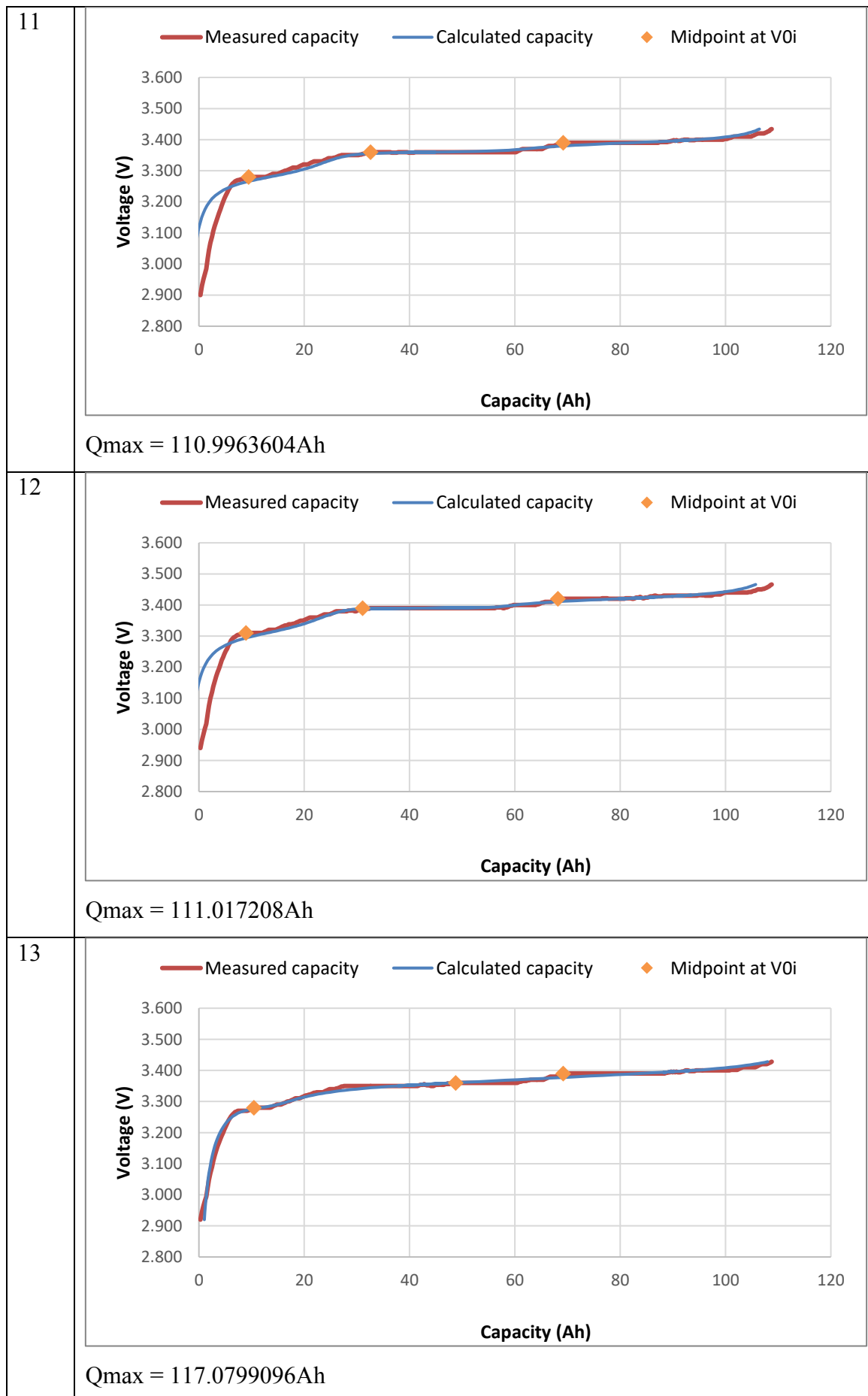


$Q_{max} = 110.9388486Ah$

10



$Q_{max} = 113.9417315Ah$



<p>14</p>	<p>Qmax = 114.9743092Ah</p>
<p>15</p>	<p>Qmax = 111.4192487Ah</p>
<p>Average Maximum Capacity = 114.6644686Ah</p>	



## CHAPTER 6

### STATE OF HEATH (SOH), DEGRDADATION RATE AND OPTIMAL CURRENT PROFILES ANALYSIS

#### 6.1 Comparison of Analytical and Measured Results

In this section, analytical and measured capacity will be compared, and the State of Heath (SOH) Curve will show to understand the SOH of Li-ion Battery with calculation proof its heath of Battery under different current profile. The calculation and discussion of SOH, degradation rate and optimal current profiles will be explained.

Table 6.1: Comparison of Analytical vs Measured Results

	<b>Capacity (Ah) Measured</b>	<b>Capacity (Ah) Average Calculated</b>	<b>Percentage Difference (%)</b>
<b>0.8kW(14A - 15A)</b>	<b>108.7685472</b>	<b>114.6644686</b>	<b>5.141890508</b>
<b>2kW (37A-40A)</b>	<b>107.8193467</b>	<b>112.6808053</b>	<b>4.314362701</b>
<b>1kW (18A -19A)</b>	<b>105.2651135</b>	<b>106.2513644</b>	<b>0.928224253</b>
<b>1kW (18A -19A)</b>	<b>107.0954165</b>	<b>109.291622</b>	<b>2.009491133</b>
<b>1.5kW (27A - 28A)</b>	<b>107.0334946</b>	<b>107.2938129</b>	<b>0.242621876</b>
<b>1.5kW (27A - 28A)</b>	<b>107.2656092</b>	<b>107.9778</b>	<b>0.659571445</b>
<b>1kW (18A -19A)</b>	<b>107.3191875</b>	<b>107.4223902</b>	<b>0.096071874</b>
<b>1kW (18A -19A)</b>	<b>106.5618179</b>	<b>107.3409915</b>	<b>0.72588639</b>

From Table 6.1, we can see the measured and average computed capacities for various charging profiles are shown in the comparison table, along with the percentage differences between them. These variations provide insight on the calculating method's accuracy and its consequences for estimating the SOH. The range of percentage discrepancies between the computed and measured capacity is 5.142% to 0.096%. All things considered, there is a modest overestimation of the estimated capacities in comparison to the actual capacities; the biggest discrepancy is shown for the 0.8kW charging profile (5.142%). They may be some factors why at first charging of 0.8kW has the highest percentage difference because maybe the original rated capacity is built higher

a little compared to the stated rated capacity. There are also some possible factors include measurement flaws, intrinsic faults in the calculating process, and differences in battery behaviour throughout testing. Additionally, there's a chance that some factors impacting capacity were not fully taken into consideration in the calculation process, which resulted in differences.

## 6.2 SOH, Degradation rate and Optimal Current Profiles Evaluation

### 6.2.1 Analysis of State of Health

In Figure 6.1 present the graphs of maximum capacity under different charging profiles. The formula for state of health (SOH) is  $SOH (\%) = \frac{Q_{max}}{Rated\ Capacity} \times 100(\%)$ . The SOH is same as the maximum capacity due to the Rated capacity is 100Ah. It can be seen the trend of the Figure 6.2 which is SOH against current profiles and Figure 6.3 where both Maximum capacity and SOH is plotted in the same graphs, shows when charging and discharging under different current profiles the SOH is decreasing. The higher the current profiles the more the SOH decreases. In the graphs can gives us a trendline equation which is  $y = 0.343x^2 - 3.947x + 118.49$ . The equation could assist on identify patterns or trends in data that aren't visible when looking at the raw values. The plotted graph with trendline visually represents the trend, making it easier to analyse and explain the data.

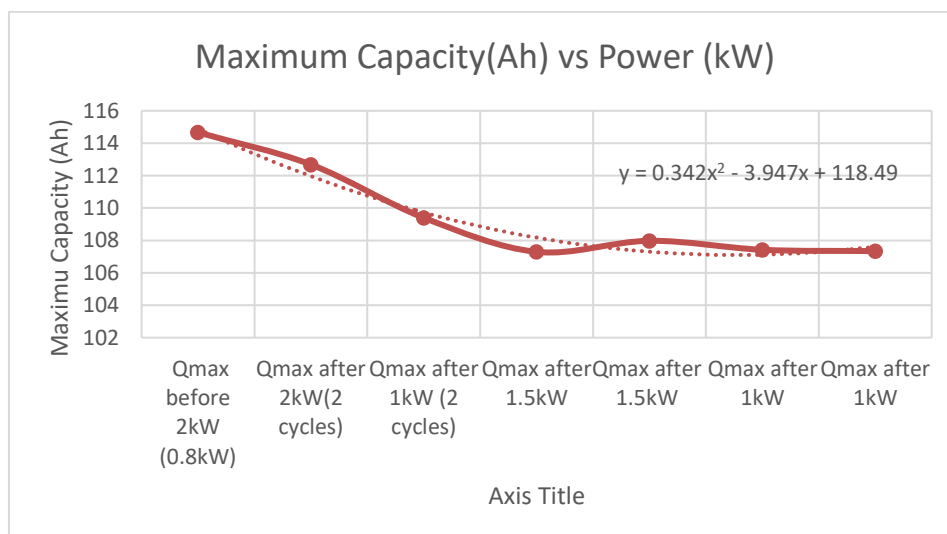


Figure 6.1: Analytical Graphs for Maximum Capacity

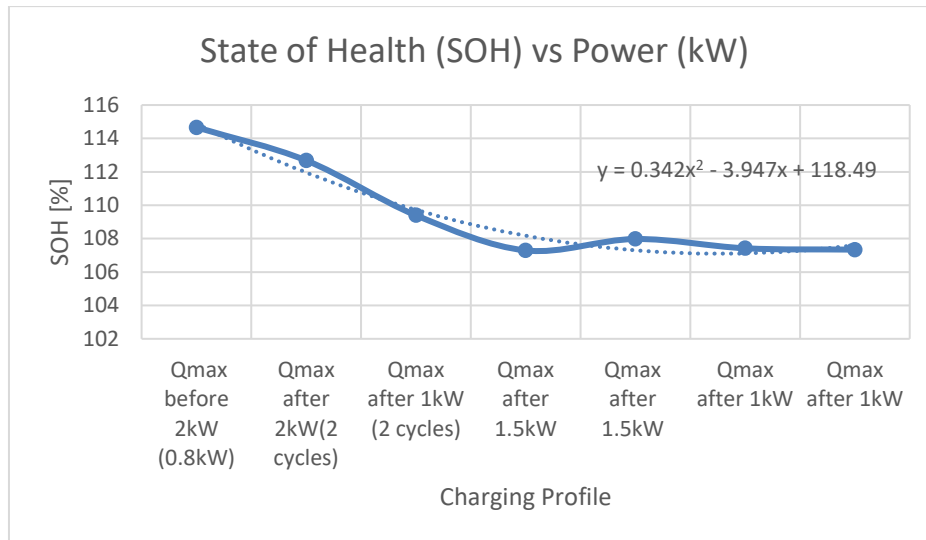


Figure 6.2: Analytical Graphs for State of Health (SOH)

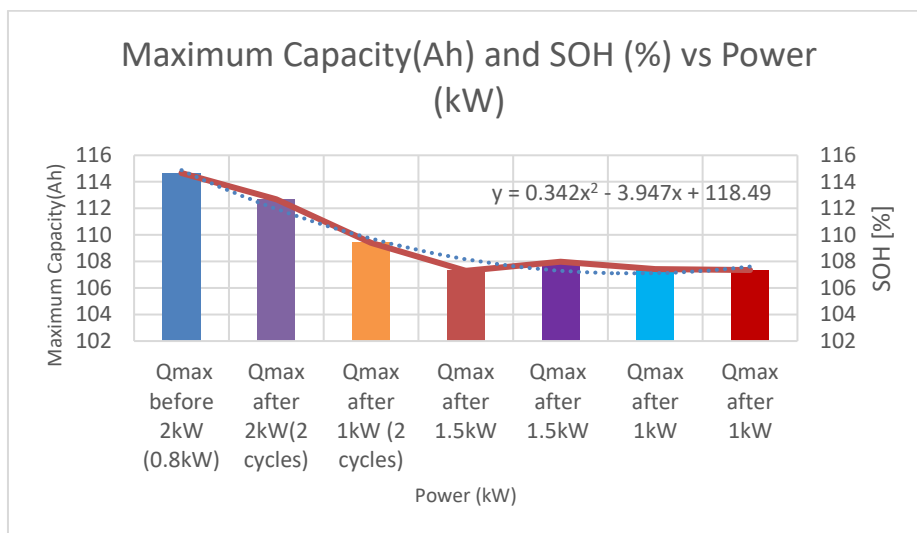


Figure 6.3: Analytical Graphs with SOH and Maximum Capacity

### 6.2.2 Comparative Analysis of Battery Degradation and State of Health (SOH) under Different Charging Profiles

From graphs of Figure 6.1 gives the information of this calculation comparison. By using before and after cycling maximum capacity ( $Q_{max}$ ) by different current profile to determine their changes in State of Health (SOH) and degradation rate of the batteries. The comparison calculation is shown below:

#### 1. For 2kW (37A-40A) charging profile:

$$Q_{max} \text{ before cycling} = 114.6644686\text{Ah}$$

$$Q_{max} \text{ after cycling} = 112.6808053\text{Ah}$$

$$SOH = \frac{112.6808053}{114.6644686} \times 100\% \approx 98.26\%$$

$$\text{Degradation Rate} = \frac{114.6644686 - 112.6808053}{114.6644686} \times 100\% \approx 1.73\%$$

#### 2. For 1.5kW (27A-28A) charging profile:

$$Q_{max} \text{ before cycling} = 107.2938129$$

$$Q_{max} \text{ after cycling} = 107.9778$$

$$SOH = \frac{107.9778}{107.2938129} \times 100\% \approx 100.64\%$$

$$\text{Degradation Rate} = \frac{107.2938129 - 107.9778}{107.2938129} \times 100\% \approx -0.64\%$$

#### 3. For 1kW (18A-19A) charging profile (excluding one data point):

$$Q_{max} \text{ before cycling} = 107.3409915$$

$$Q_{max} \text{ after cycling} = 107.4223902$$

$$SOH = \frac{107.4223902}{107.3409915} \times 100\% \approx 100.08\%$$

$$\text{Degradation Rate} = \frac{107.3409915 - 107.4223902}{107.3409915} \times 100\% \approx -0.08\%$$

In the comparison of different charging and discharging current profiles is shown in the comparison calculation above. For 1kW there is one point excluded due to the sudden drop and unstable calculations. To make more consistent another two points for 1kW is calculated. In the explanation of State of Health (SOH), for 2kW (37A-40A) charging profiles, it approximately shows is 98.26% of state of health which experienced some degradation but still in good condition. While in 1kW (18-19A) and 1.5kW (27A-28A) give a 100.64% and

100.08% of SOH. This implies that there hasn't been much degradation or perhaps a tiny improvement in the battery over time.

In the degradation rate, in 2kW (37A-40A) charging and discharging profiles, the degradation rate is around 1.73%, indicating a moderate rate of battery degradation. The negative degradation rates for 1kW and 1.5kW might suggest problems in the State of Health (SOH) estimate, which could be caused by variations in temperature, anomalies in the sensor, or mistakes in the analysis.

According to the study, the 1kW charging profile is the most optimal one as it has a greater State of Health (SOH) and a slower rate of degradation than the 2kW and 1.5kW profiles. During the SOH estimation, 2kW charging profile which have the higher of degradation rate compared to the other two. In comparison to the 2kW and 1.5kW charging profiles, the study indicates that the 1kW charging profile has a slightly greater SOH and a slower rate of degradation. Due to its low degradation and high SOH, the 1kW charging profile may be thought of as the best current profile for charging the batteries.

### **6.3 Summary**

Examining the degradation characteristics of Li-ion batteries under various charging and discharging settings is the main goal of this early results chapter. With the ICA Method in previous chapter, it gives a further analysis for this chapter. It shows how the SOH is estimated using Incremental capacity analysis (ICA-based) SOC estimation. The SOH is calculated then is compared with the measured SOH with a table where it can be seen that the percentage difference is quite low. The State of Health (SOH), degradation rate and identify the optimal under different charging and discharging current profiles for this project is discussed in this chapter.

## CHAPTER 7

### CONCLUSION AND RECCOMENDATIONS

#### 7.1 Conclusions

In conclusions, the objectives of are achieved which the objectives are to measure the State of Health (SOH) under various charging and discharging current profiles, determine the rate of degradation of Li-ion batteries, and identify the optimal profile with the slowest degradation rate of batteries. The research here show that the batteries' SOH values ranged from around 98.26% to 100.64%. The degradation is in the range of -0.63% to 1.73% which the rate shows the less degradation. The negative degradations may be due to reasons. One of reasons may be the SOH estimations may not be accurate or the longer cycles of this batteries of charging and discharging should be done to give more accurate degradation rate. Other factors could be anomalies in sensor. This emphasises how crucial it is to choose the right charging and discharging patterns in order to preserve battery health. According to the study, the best charging and discharging currents for reducing degradation rates and maintaining SOH is 1kW which is 18A to 19A constant current profiles. This shows that the current profiles can guaranteed optimal battery performance over time while also minimising degradation. The temperature graphs also show that 37A to 40A (2kW) charging profiles has the highest temperature compared to 18A to 19 A(1kW) charging and discharging profiles and 27A to 28A (1.5kW) charging and discharging profiles. The higher the temperature will damage the batteries. 1kW has the lowest temperature, this gives the best current for the charging and discharging profiles.

Therefore, this research can further our knowledge of the mechanisms underlying degradation of batteries and offers insightful information for developing Li-ion battery solutions that are more robust and efficient in our real life. The findings highlight to choose the right charging and discharging profiles in order to maximise battery longevity and performance.

## 7.2 Recommended of Future Work

In the recommendation of future work, the charging and discharging process should be more consistent with time. This is because to show more accurate results compare to not consistent during the time between different current profiles. Long-term cycle life testing in various charging and discharging scenarios might offer a more complete understanding of the physics driving degradation of batteries. This process should be going longer to have a more obvious State of Health (SOH) and degradation curve.

Another future study is the voltage should be more decimal points which is hard to be solve. This is because the Batrium battery monitoring system (BMS) is one two decimal points voltage which is hard to be calculated in our SOH estimation. Others BMS should be consider to or try to do more research to change the voltage's decimal to have 3 or 4 decimals to gives a more accurate results during the calculations.

Lastly, machine learning algorithms also can be implemented in this study. This can optimise charging and discharging procedures based on our historical data. This may result in longer-lasting batteries and better battery performance.

## REFERENCES

- accautomation.ca. (n.d.). *Node-RED Modbus RTU / TCP Communication | ACC Automation*. [online] Available at: <https://accautomation.ca/node-red-modbus-rtu-tcp-communication/#:~:text=Modbus%20is%20a%20master%2Dslave> [Accessed 12 Sep. 2023].
- Appelman, M., Venugopal, P., & Rietveld, G. (2022). Impact of Discharge Current Profiles on Li-ion Battery Pack Degradation. *2022 IEEE 20th International Power Electronics and Motion Control Conference, PEMC 2022*, 474–480. <https://doi.org/10.1109/PEMC51159.2022.9962917>
- Batrium Knowledge / Wiki. (n.d.). *Batrium Products*. [online] Available at: <https://wiki.batrium.com/product> [Accessed 12 Sep. 2023].
- Battery Degradation: Maximizing Battery Life & Performance, n.d. [www.exro.com](https://www.exro.com/industry-insights/battery-degradation-explained). Available at: <https://www.exro.com/industry-insights/battery-degradation-explained> [Accessed 19 July 2023].
- Bian, X., Liu, L., & Yan, J. (2019). A model for state-of-health estimation of lithium ion batteries based on charging profiles. *Energy*, *177*, 57–65. <https://doi.org/10.1016/j.energy.2019.04.070>
- Birkl, C.R., Roberts, M.R., McTurk, E., Bruce, P.G. & Howey, D.A., 2017. Degradation diagnostics for lithium ion cells. *Journal of Power Sources*, [e-journal] 341, pp.373–386. Available at: <https://doi.org/10.1016/j.jpowsour.2016.12.011>
- Chen, G., Liu, Z., & Su, H. (2020). An optimal fast-charging strategy for lithium-ion batteries via an electrochemical–thermal model with intercalation-induced stresses and film growth. *Energies*, *13*(9). <https://doi.org/10.3390/en13092388>
- Curtis, T., 2023. Do Electric Car Batteries Degrade Over Time? *Car Sloth*. Available at: <https://www.carsloth.com/advice/do-electric-car-batteries-degrade> [Accessed 28 June 2023].
- de Mendonça, P. R. C., Monteiro, M. M., Scavarda, L. F., & Rocha, J. (2020). Challenges and Barriers of Performance Measurement Systems: Lessons from Different Initiatives Within One Single Organization. In A. Leiras, C. A. González-Calderón, I. de Brito Junior, S. Villa, & H. T. Y. Yoshizaki (Eds.), *Operations Management for Social Good* (pp. 659–668). Springer International Publishing.
- docs.opennms.com. (n.d.). *UDP Listener*. [online] Available at: <https://docs.opennms.com/horizon/32/reference/telemetryd/listeners/udp.html#:~:text=Use%20the%20UDP%20listener%20to> [Accessed 12 Sep. 2023].



Edge, J. S., O’Kane, S., Prosser, R., Kirkaldy, N. D., Patel, A. N., Hales, A., Ghosh, A., Ai, W., Chen, J., Yang, J., Li, S., Pang, M. C., Bravo Diaz, L., Tomaszewska, A., Marzook, M. W., Radhakrishnan, K. N., Wang, H., Patel, Y., Wu, B., & Offer, G. J. (2021). Lithium ion battery degradation: what you need to know. In *Physical Chemistry Chemical Physics* (Vol. 23, Issue 14, pp. 8200–8221). Royal Society of Chemistry. Available at: <https://doi.org/10.1039/d1cp00359c>

Gao, Z., Xie, H., Yang, X., Niu, W., Li, S., & Chen, S. (2022). The Dilemma of C-Rate and Cycle Life for Lithium-Ion Batteries under Low Temperature Fast Charging. *Batteries*, 8(11). <https://doi.org/10.3390/batteries8110234>

Han, X., Lu, L., Zheng, Y., Feng, X., Li, Z., Li, J. & Ouyang, M., 2019. A review on the key issues of the lithium ion battery degradation among the whole life cycle. In *eTransportation* (Vol. 1). Available at: <https://doi.org/10.1016/j.etrans.2019.100005>

Huang, M. (2019). Incremental capacity analysis-based impact study of diverse usage patterns on lithium-ion battery aging in electrified vehicles. *Batteries*, 5(3). <https://doi.org/10.3390/batteries5030059>

International Energy Agency, 2021. Global EV Outlook 2021 Accelerating ambitions despite the pandemic. Available at: <https://www.iea.org/reports/global-ev-outlook-2021/policies-to-promote-electric-vehicle-deployment> [Accessed 29 July 2023].

Introduction to Lithium-ion Batteries - Yuasa UK, n.d. Yuasa. Available at: <https://www.yuasa.co.uk/info/industrial-applications/introduction-to-lithium-ion-batteries/> [Accessed 10 July 2023].

Li, J., Adewuyi, K., Lotfi, N., Landers, R. G., & Park, J. (2018). A single particle model with chemical/mechanical degradation physics for lithium ion battery State of Health (SOH) estimation. *Applied Energy*, 212, 1178–1190. <https://doi.org/https://doi.org/10.1016/j.apenergy.2018.01.011>

Li, X., Jiang, J., Wang, L. Y., Chen, D., Zhang, Y., & Zhang, C. (2016). A capacity model based on charging process for state of health estimation of lithium ion batteries. *Applied Energy*, 177, 537–543. <https://doi.org/https://doi.org/10.1016/j.apenergy.2016.05.109>

Lv, H., Huang, X., & Liu, Y. (2020). Analysis on pulse charging–discharging strategies for improving capacity retention rates of lithium-ion batteries. *Ionics*, 26(4), 1749–1770. <https://doi.org/10.1007/s11581-019-03404-8>

Ma, S., Jiang, M., Tao, P., Song, C., Wu, J., Wang, J., Deng, T., & Shang, W. (2018). Temperature effect and thermal impact in lithium-ion batteries: A review. *Progress in Natural Science: Materials International*, 28(6), 653–666. <https://doi.org/https://doi.org/10.1016/j.pnsc.2018.11.002>

nodered.org. (n.d.). *About* : *Node-RED*. [online] Available at: <https://nodered.org/about/>.

O’Kane, S. E. J., Ai, W., Madabattula, G., Alonso-Alvarez, D., Timms, R., Sulzer, V., Edge, J. S., Wu, B., Offer, G. J., & Marinescu, M. (2022). Lithium-ion battery degradation: how to model it. *Physical Chemistry Chemical Physics*, 24(13), 7909–7922. <https://doi.org/10.1039/d2cp00417h>

Pistorio, F., Clerici, D., Mocera, F., & Somà, A. (2022). Review on the Experimental Characterization of Fracture in Active Material for Lithium-Ion Batteries. In *Energies* (Vol. 15, Issue 23). MDPI. <https://doi.org/10.3390/en15239168>

Ren, F., Wu, Y., Zuo, W., Zhao, W., Pan, S., Lin, H., Yu, H., Lin, J., Lin, M., Yao, X., Brezesinski, T., Gong, Z., & Yang, Y. (2024). Visualizing the SEI formation between lithium metal and solid-state electrolyte. *Energy Environ. Sci.*, 17(8), 2743–2752. <https://doi.org/10.1039/D3EE03536K>

Shacklett, M. (2021). *TCP/IP: What is TCP/IP and How Does it Work?* [online] SearchNetworking. Available at: <https://www.techtarget.com/searchnetworking/definition/TCP-IP>.

Simolka, M., Heger, J. F., Kaess, H., Biswas, I., & Friedrich, K. A. (2020). Influence of cycling profile, depth of discharge and temperature on commercial LFP/C cell ageing: post-mortem material analysis of structure, morphology and chemical composition. *Journal of Applied Electrochemistry*, 50(11), 1101–1117. <https://doi.org/10.1007/s10800-020-01465-6>

SMA. (n.d.). SMA Sunny Island 4.4M/6.0H/8.0H Datasheet. [Product datasheet]. Europe Solar Store. [https://www.europe-solarstore.com/download/sma/SMA\\_Sunny\\_Island\\_4.4M\\_6.0H\\_8.0H\\_DATA\\_SHEET.pdf](https://www.europe-solarstore.com/download/sma/SMA_Sunny_Island_4.4M_6.0H_8.0H_DATA_SHEET.pdf)

Sui, X., Świerczyński, M., Teodorescu, R., & Stroe, D. I. (2021). The degradation behavior of lifepo4/c batteries during long-term calendar aging. *Energies*, 14(6). <https://doi.org/10.3390/en14061732>

Tomaszewska, A., Chu, Z., Feng, X., O’Kane, S., Liu, X., Chen, J., Ji, C., Endler, E., Li, R., Liu, L., Li, Y., Zheng, S., Vetterlein, S., Gao, M., Du, J., Parkes, M., Ouyang, M., Marinescu, M., Offer, G., & Wu, B. (2019). Lithium-ion battery fast charging: A review. *ETransportation*, 1, 100011. <https://doi.org/https://doi.org/10.1016/j.etrans.2019.100011>

Vivek, n.d. Battery Degradation – VAST Enterprise Solutions. Available at: <https://vastenterprisesolutions.com/2021/07/12/battery-degradation/> [Accessed 29 July 2023].

Xiong, S., 2019. A study of the factors that affect lithium ion battery degradation. Mospace.umssystem.edu. Available at: <https://hdl.handle.net/10355/73777> [Accessed 5 July 2023].

Xu, R., Yang, Y., Yin, F., Liu, P., Cloetens, P., Liu, Y., Lin, F., & Zhao, K. (2019). Heterogeneous damage in Li-ion batteries: Experimental analysis and theoretical modeling. *Journal of the Mechanics and Physics of Solids*, 129, 160–183. <https://doi.org/https://doi.org/10.1016/j.jmps.2019.05.003>

Yang, Z., Huang, H. & Lin, F., 2022. Sustainable Electric Vehicle Batteries for a Sustainable World: Perspectives on Battery Cathodes, Environment, Supply Chain, Manufacturing, Life Cycle, and Policy. *Advanced Energy Materials*, 12(26), 2200383. Available at: <https://doi.org/10.1002/aenm.202200383>

## APPENDICES

## Appendix A: BMS UDP



Watchmon SW 1.0.30 UDP Outbound protocol

Shunt SoC	41	uint8	-5% to +105%	0.5% / bit and 5% offset
Shunt Voltage	42	Uint16		Multiple (100) according to setup
Shunt Current	44	Float	mA	(+ charge , - discharge)
Shunt Status	48	Uint8	Timeout = 0, Discharging = 1, Idle = 2, Charging = 4	
Shunt RX ticks	49	Uint8		

## Telemetry - Combined Status Rapid Info - payload formatting

Identifier: 0x3E32 - Recommended to monitor

Frequency: 294 milliseconds

Data Length: 50 bytes

Version 2

Field	Offset	Data Type	Format / Range	Resolution / Notes
Min Cell Voltage	8	Uint16	0 to 6,500 mV	1mV / bit and nil offset
Max Cell Voltage	10	Uint16	0 to 6,500 mV	1mV / bit and nil offset
Min Cell Volt Reference	12	Uint8	0 to 250	Node Identifier
Max Cell Volt Reference	13	Uint8	0 to 250	Node Identifier
Min Cell Temperature	14	uint8	-40°C to 125°C	1°C/bit and 40°C offset
Min Cell Temperature	15	uint8	-40°C to 125°C	1°C/bit and 40°C offset
Min Cell Temp Reference	16	Uint8	0 to 250	Node Identifier
Max Cell Temp Reference	17	Uint8	0 to 250	Node Identifier
Min Cell Bypass Current	18	Uint16	0 to 2,500 mA	1mA / bit and nil offset
Max Cell Bypass Current	20	Uint16	0 to 2,500 mA	1mA / bit and nil offset
Min Cell Bypass Ref ID	22	Uint8	0 to 250	Node Identifier
Max Cell Bypass Ref ID	23	Uint8	0 to 250	Node Identifier
Min Bypass Temperature	24	uint8	-40°C to 125°C	1°C/bit and 40°C offset
Min Bypass Temperature	25	uint8	-40°C to 125°C	1°C/bit and 40°C offset
Min Bypass Temp Ref ID	26	Uint8	0 to 250	Node Identifier
Max Bypass Temp Ref ID	27	Uint8	0 to 250	Node Identifier
Average Cell Voltage	28	Uint16	0 to 6,500 mV	1mV / bit and nil offset
Average Cell Temperature	30	uint8	-40°C to 125°C	1°C/bit and 40°C offset
Num# of Cells Above Initial Bypass	31	Uint8	0 to 250	
Num# of Cells Above Final Bypass	32	Uint8	0 to 250	
Num# of Cells in Bypass	33	Uint8	0 to 250	
Num# of Cells Overdue	34	Uint8	0 to 250	
Num# of Cells Active	35	Uint8	0 to 250	
Num# of Cells in System	36	Uint8	0 to 250	
CMU port TX NodeID	37	Uint8		
CMU port RX NodeID	38	Uint8		
CMU port RX USN	39	Uint8	0 to 254	Serial number packet counter
Shunt Voltage	40	Uint16		Multiple (100) according to setup
Shunt Amp	42	Float	mA	(+ charge , - discharge)
Shunt Power	46	Float	VA	(+ charge , - discharge)

## Appendix B: Modbus Address of Sunny Island Inverter

### 7 Assignment Tables

#### 7.1 Information on Assignment Tables

The following subsections are sorted by unit ID. Each contains a table of the Modbus registers which can be accessed using this unit ID. The tables present the following information:

Information	Explanation
ADR	Decimal Modbus register
Description/number codes	Short description of the Modbus register and the number codes used
CNT	Number of assigned Modbus registers
Type	Data type: <ul style="list-style-type: none"> <li>• U = Unsigned Value</li> <li>• S = Signed Value</li> <li>• 16, 32 or 64 = size of the register in bits</li> </ul>
Format	Data format of the saved value: <ul style="list-style-type: none"> <li>• FIXn means that in the register value the decimal point is shifted by n digits.</li> <li>• TAGLIST means that only the given values appear.</li> </ul>
Access	Access type: <ul style="list-style-type: none"> <li>• RO = Read Only</li> <li>• RW = Read Write</li> <li>• WO = Write Only</li> </ul>

#### 7.2 Measured Values and Parameters Selected

The following table contains a selection of the measured values and parameters provided by the Sunny Island via the SMA Modbus profile. These measured values and parameters are relevant for reading Modbus registers, for parameterization and for power specification.

ADR	Description/number codes	CNT	Type	Format	Access
30053	Device type: 9331: Sunny Island 3.0M-12 9332: Sunny Island 4.4M-12 9333: Sunny Island 6.0H-12 9334: Sunny Island 8.0H-12 9474: Sunny Island 4.4M-13 9475: Sunny Island 6.0H-13 9476: Sunny Island 8.0H-13 9486: Sunny Island 5.0H-13	2	U32	TAGLIST	RO
30201	Status: 35: Error (Alm) 303: Off 307: Ok 455: Warning (Wrm)	2	U32	TAGLIST	RO

ADR	Description/number codes	CNT	Type	Format	Access
30845	Current battery state of charge Value range: 0% to 100%	2	U32	FIX0	RO
30775	Power in W	2	S32	FIX0	RO
30843	Battery current in A	2	S32	FIX3	RO
30849	Battery temperature in °C	2	U32	FIX0	RO
30851	Battery voltage in V	2	U32	FIX0	RO
30917	Generator status: 303: Off 1392: Error (Flt) 1787: Initialization (Init) 1788: Ready (Rdy) 1789: Warm-up (Warming) 1790: Synchronize (Syn) 1791: Activated (ConnAct) 1792: Re-synchronize (ReSyn) 1793: Generator separation (GnDscon) 1794: shut-off delay (StopDl) 1795: blocked (Lok) 1796: Locked after error (FltLok) 16777213: Information not available (NaNStt)	2	U32	TAGLIST	RO
31009	Lower discharge limit for self-consumption range in %	2	U32	FIX0	RO
33003	Operating status: 235: Parallel grid operation (GriOp) 1463: Backup (Bck) 2677: Operation at generator, at external input (SttGnOp) 3664: Emergency charge mode (EmgCha) 16777213: Information not available (NaNStt)	2	U32	TAGLIST	RO
40149	Active power setpoint in W	2	S32	FIX0	WO
40151	Active and reactive power control via communication: 802: active (Act) 803: inactive (Ina)	2	U32	TAGLIST	WO
40210 <sup>10)</sup>	Operating mode Active power setpoint: 303: Off 1077: Manual setting in W (WCnst) 1078: Manual setpoint in % of the nominal device power (WCnstNom) 1079: External setpoint (WCtlCom)	2	U32	TAGLIST	WO

<sup>10)</sup> This parameter can only be read or written if a logon has taken place using the SMA Grid Guard code.

## Appendix C: dQ/dV Graphs for 1kW,1.5kW and 2kW

Table 0.1: Table with Graph of dQ/dV vs voltage points (2kW Charging)

Cell	Graph of dQ/dV vs Cell Voltage	Cell	Graph of dQ/dV vs Cell Voltage
1	<p style="text-align: center;"><b>dQ/dV vs Voltage</b></p> <p style="text-align: center;"><b>Cell 1 voltage average (V)</b></p>	9	<p style="text-align: center;"><b>dQ/dV vs Voltage</b></p> <p style="text-align: center;"><b>Cell 9 voltage average</b></p>
2	<p style="text-align: center;"><b>dQ/dV vs Voltage</b></p> <p style="text-align: center;"><b>Cell 2 voltage average</b></p>	10	<p style="text-align: center;"><b>dQ/dV vs Voltage</b></p> <p style="text-align: center;"><b>Cell 10 voltage average</b></p>
3	<p style="text-align: center;"><b>dQ/dV vs Voltage</b></p> <p style="text-align: center;"><b>Cell 3 voltage average</b></p>	11	<p style="text-align: center;"><b>dQ/dV vs Voltage</b></p> <p style="text-align: center;"><b>Cell 11 voltage average</b></p>

<p>4</p>	<p style="text-align: center;"><b>dQ/dV vs Voltage</b></p> <p style="text-align: center;"><b>Cell 4 voltage average</b></p>	<p>12</p>	<p style="text-align: center;"><b>dQ/dV vs Voltage</b></p> <p style="text-align: center;"><b>Cell 12 voltage average</b></p>
<p>5</p>	<p style="text-align: center;"><b>dQ/dV vs Voltage</b></p> <p style="text-align: center;"><b>Cell 5 voltage average</b></p>	<p>13</p>	<p style="text-align: center;"><b>dQ/dV vs Voltage</b></p> <p style="text-align: center;"><b>Cell 13 voltage average</b></p>
<p>6</p>	<p style="text-align: center;"><b>dQ/dV vs Voltage</b></p> <p style="text-align: center;"><b>Cell 6 voltage average</b></p>	<p>14</p>	<p style="text-align: center;"><b>dQ/dV vs Voltage</b></p> <p style="text-align: center;"><b>Cell 14 voltage average</b></p>



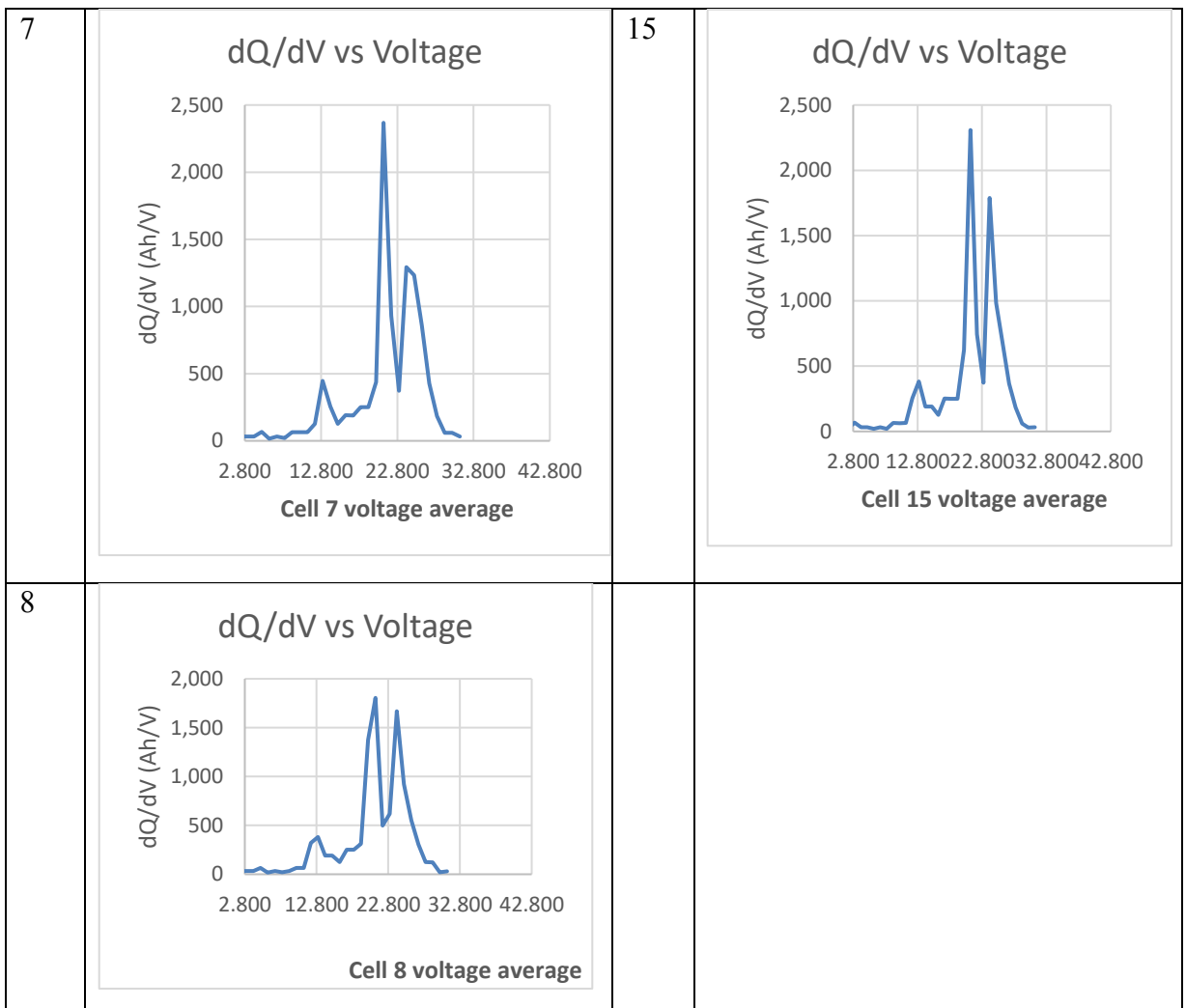


Table 0.2: Table with Graph of dQ/dV vs voltage points (1kW Charging after 2 cycles)

Cell	Graph of dQ/dV vs Cell Voltage	Cell	Graph of dQ/dV vs Cell Voltage
1	<p style="text-align: center;"><b>dQ/dV vs Voltage</b></p> <p style="text-align: center;"><b>Cell 1 voltage average</b></p>	9	<p style="text-align: center;"><b>dQ/dV vs Voltage</b></p> <p style="text-align: center;"><b>Cell 9 voltage average</b></p>
2	<p style="text-align: center;"><b>dQ/dV vs Voltage</b></p> <p style="text-align: center;"><b>Cell 2 voltage average</b></p>	10	<p style="text-align: center;"><b>dQ/dV vs Voltage</b></p> <p style="text-align: center;"><b>Cell 10 voltage average</b></p>
3	<p style="text-align: center;"><b>dQ/dV vs Voltage</b></p> <p style="text-align: center;"><b>Cell 3 voltage average</b></p>	11	<p style="text-align: center;"><b>dQ/dV vs Voltage</b></p> <p style="text-align: center;"><b>Cell 11 voltage average</b></p>

<p>4</p>	<p style="text-align: center;"><b>dQ/dV vs Voltage</b></p> <p style="text-align: center;"><b>Cell 4 voltage average</b></p>	<p>12</p>	<p style="text-align: center;"><b>dQ/dV vs Voltage</b></p> <p style="text-align: center;"><b>Cell 12 voltage average</b></p>
<p>5</p>	<p style="text-align: center;"><b>dQ/dV vs Voltage</b></p> <p style="text-align: center;"><b>Cell 5 voltage average</b></p>	<p>13</p>	<p style="text-align: center;"><b>dQ/dV vs Voltage</b></p> <p style="text-align: center;"><b>Cell 13 voltage average</b></p>
<p>6</p>	<p style="text-align: center;"><b>dQ/dV vs Voltage</b></p> <p style="text-align: center;"><b>Cell 6 voltage average</b></p>	<p>14</p>	<p style="text-align: center;"><b>dQ/dV vs Voltage</b></p> <p style="text-align: center;"><b>Cell 14 voltage average</b></p>

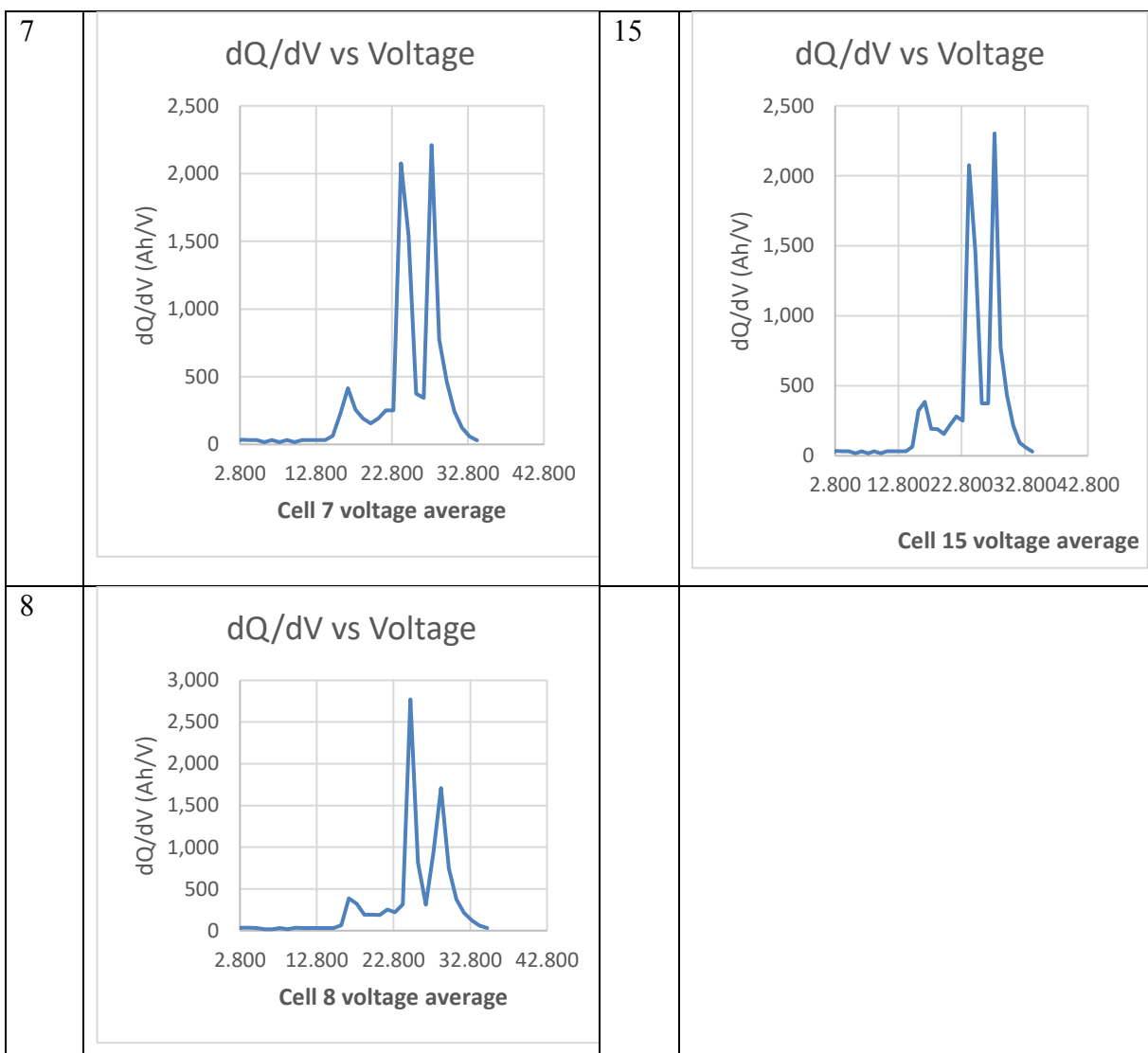
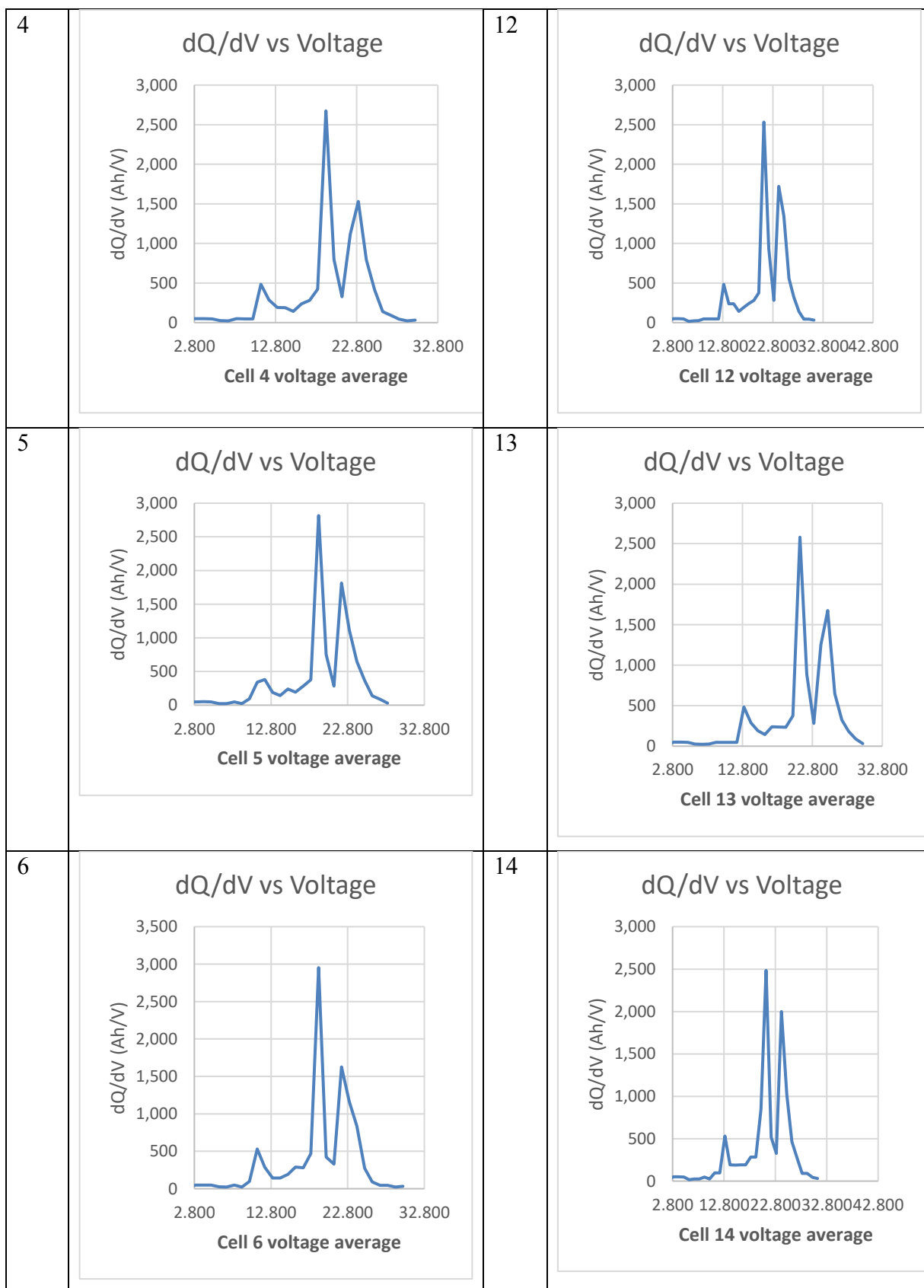


Table 0.3: Table with Graph dQ/dV vs voltage points (1<sup>st</sup> 1.5kW Charging)

Cell	Graph of dQ/dV vs Cell Voltage	Cell	Graph of dQ/dV vs Cell Voltage
1	<p style="text-align: center;"><b>dQ/dV vs Voltage</b></p> <p style="text-align: center;"><b>Cell 1 voltage average</b></p>	9	<p style="text-align: center;"><b>dQ/dV vs Voltage</b></p> <p style="text-align: center;"><b>Cell 9 voltage average</b></p>
2	<p style="text-align: center;"><b>dQ/dV vs Voltage</b></p> <p style="text-align: center;"><b>Cell 2 voltage average</b></p>	10	<p style="text-align: center;"><b>dQ/dV vs Voltage</b></p> <p style="text-align: center;"><b>Cell 10 voltage average</b></p>
3	<p style="text-align: center;"><b>dQ/dV vs Voltage</b></p> <p style="text-align: center;"><b>Cell 3 voltage average</b></p>	11	<p style="text-align: center;"><b>dQ/dV vs Voltage</b></p> <p style="text-align: center;"><b>Cell 11 voltage average</b></p>



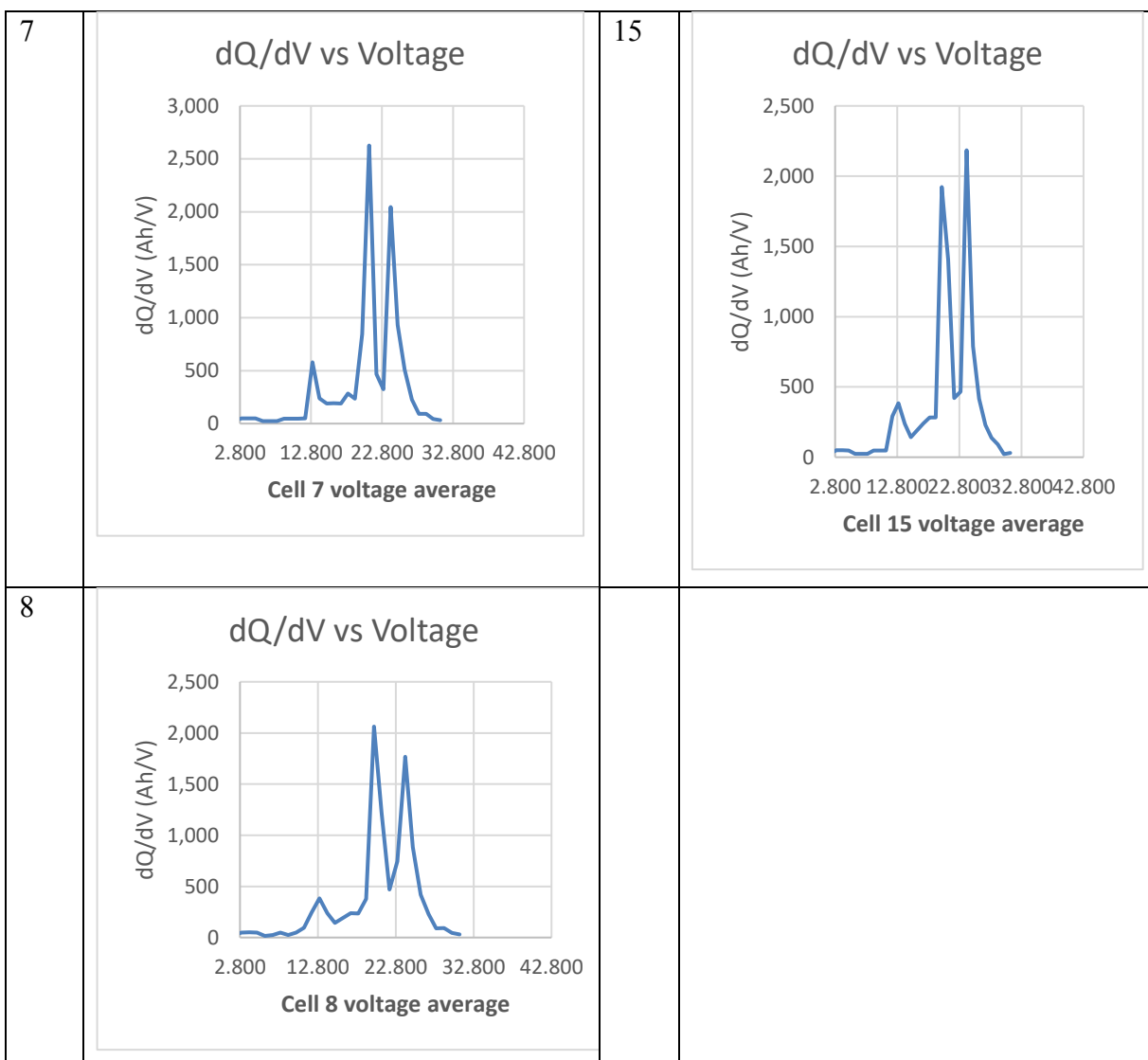
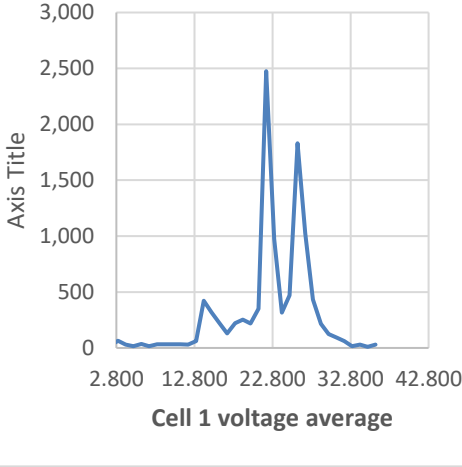
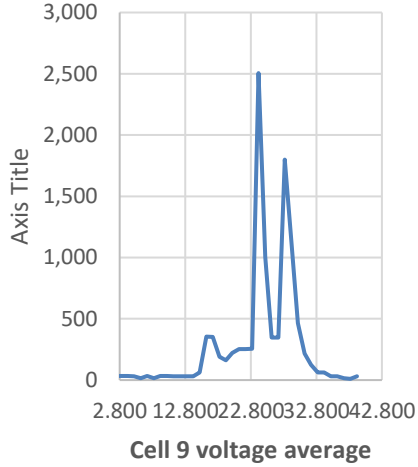
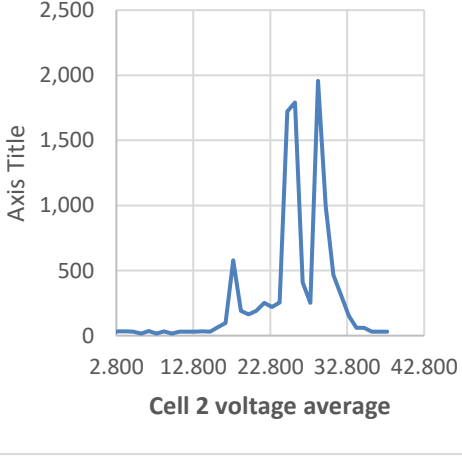
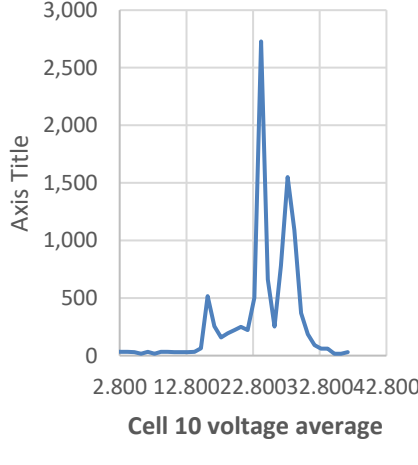


Table 0.4: Table with Graph dQ/dV vs voltage points (2<sup>nd</sup> 1.5kW Charging)

Cell	Graph of dQ/dV vs Cell Voltage	Cell	Graph of dQ/dV vs Cell Voltage
1	<p style="text-align: center;"><b>dQ/dV vs Voltage</b></p>  <p style="text-align: center;"><b>Cell 1 voltage average</b></p>	9	<p style="text-align: center;"><b>dQ/dV vs Voltage</b></p>  <p style="text-align: center;"><b>Cell 9 voltage average</b></p>
2	<p style="text-align: center;"><b>dQ/dV vs Voltage</b></p>  <p style="text-align: center;"><b>Cell 2 voltage average</b></p>	10	<p style="text-align: center;"><b>dQ/dV vs Voltage</b></p>  <p style="text-align: center;"><b>Cell 10 voltage average</b></p>



<p>3</p>	<p style="text-align: center;"><b>dQ/dV vs Voltage</b></p> <p style="text-align: center;"><b>Cell 3 voltage average</b></p>	<p>11</p>	<p style="text-align: center;"><b>dQ/dV vs Voltage</b></p> <p style="text-align: center;"><b>Cell 11 voltage average</b></p>
<p>4</p>	<p style="text-align: center;"><b>dQ/dV vs Voltage</b></p> <p style="text-align: center;"><b>Cell 4 voltage average</b></p>	<p>12</p>	<p style="text-align: center;"><b>dQ/dV vs Voltage</b></p> <p style="text-align: center;"><b>Cell 12 voltage average</b></p>
<p>5</p>	<p style="text-align: center;"><b>dQ/dV vs Voltage</b></p> <p style="text-align: center;"><b>Cell 5 voltage average</b></p>	<p>13</p>	<p style="text-align: center;"><b>dQ/dV vs Voltage</b></p> <p style="text-align: center;"><b>Cell 13 voltage average</b></p>

<p>6</p>	<p style="text-align: center;"><b>dQ/dV vs Voltage</b></p> <p style="text-align: center;"><b>Cell 6 voltage average</b></p>	<p>14</p>	<p style="text-align: center;"><b>dQ/dV vs Voltage</b></p> <p style="text-align: center;"><b>Cell 14 voltage average</b></p>
<p>7</p>	<p style="text-align: center;"><b>dQ/dV vs Voltage</b></p> <p style="text-align: center;"><b>Cell 7 voltage average</b></p>	<p>15</p>	<p style="text-align: center;"><b>dQ/dV vs Voltage</b></p> <p style="text-align: center;"><b>Cell 15 voltage average</b></p>
<p>8</p>	<p style="text-align: center;"><b>dQ/dV vs Voltage</b></p> <p style="text-align: center;"><b>Cell 8 voltage average</b></p>	Empty cell	

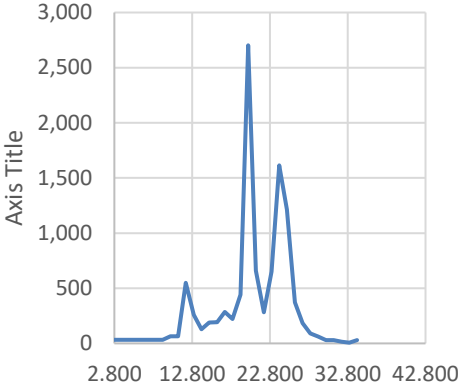
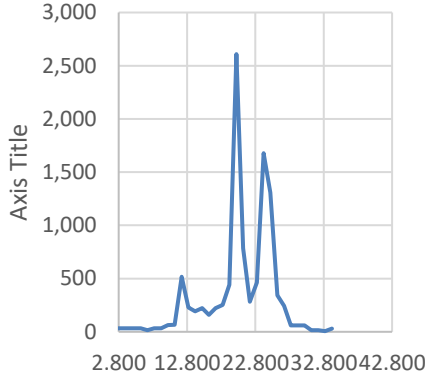
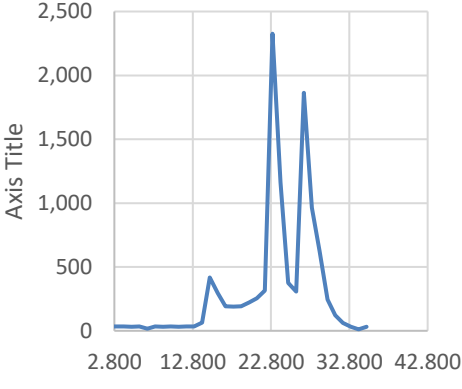
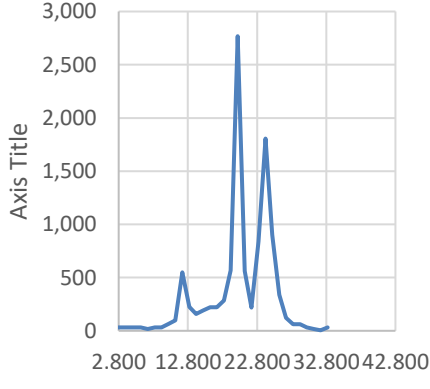
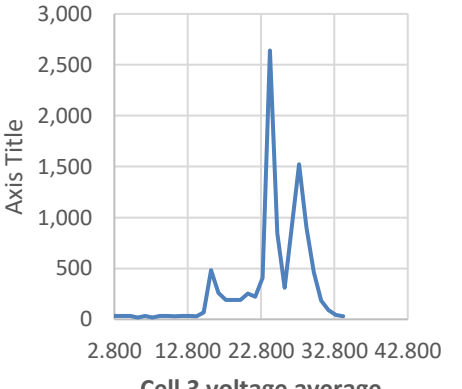
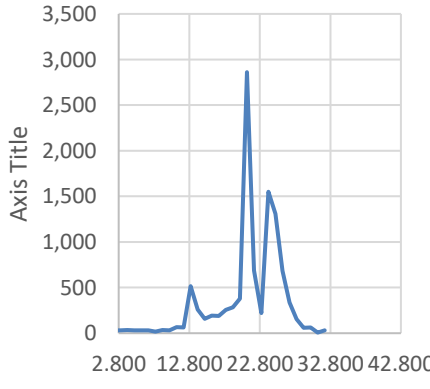
Table 0.5: Table with Graph dQ/dV vs voltage points (1<sup>st</sup> 1kW Charging)

Cell	Graph of dQ/dV vs Cell Voltage	Cell	Graph of dQ/dV vs Cell Voltage
1	<p style="text-align: center;"><b>dQ/dV vs Voltage</b></p> <p style="text-align: center;"><b>Cell 1 voltage average</b></p>	9	<p style="text-align: center;"><b>dQ/dV vs Voltage</b></p> <p style="text-align: center;"><b>Cell 9 voltage average</b></p>
2	<p style="text-align: center;"><b>dQ/dV vs Voltage</b></p> <p style="text-align: center;"><b>Cell 2 voltage average</b></p>	10	<p style="text-align: center;"><b>dQ/dV vs Voltage</b></p> <p style="text-align: center;"><b>Cell 10 voltage average</b></p>

<p>3</p>	<p style="text-align: center;"><b>dQ/dV vs Voltage</b></p> <p style="text-align: center;"><b>Cell 3 voltage average</b></p>	<p>11</p>	<p style="text-align: center;"><b>dQ/dV vs Voltage</b></p> <p style="text-align: center;"><b>Cell 11 voltage average</b></p>
<p>4</p>	<p style="text-align: center;"><b>dQ/dV vs Voltage</b></p> <p style="text-align: center;"><b>Cell 4 voltage average</b></p>	<p>12</p>	<p style="text-align: center;"><b>dQ/dV vs Voltage</b></p> <p style="text-align: center;"><b>Cell 12 voltage average</b></p>
<p>5</p>	<p style="text-align: center;"><b>dQ/dV vs Voltage</b></p> <p style="text-align: center;"><b>Cell 5 voltage average</b></p>	<p>13</p>	<p style="text-align: center;"><b>dQ/dV vs Voltage</b></p> <p style="text-align: center;"><b>Cell 13 voltage average</b></p>

<p>6</p>	<p style="text-align: center;"><b>dQ/dV vs Voltage</b></p> <p style="text-align: center;"><b>Cell 6 voltage average</b></p>	<p>14</p>	<p style="text-align: center;"><b>dQ/dV vs Voltage</b></p> <p style="text-align: center;"><b>Cell 14 voltage average</b></p>
<p>7</p>	<p style="text-align: center;"><b>dQ/dV vs Voltage</b></p> <p style="text-align: center;"><b>Cell 7 voltage average</b></p>	<p>15</p>	<p style="text-align: center;"><b>dQ/dV vs Voltage</b></p> <p style="text-align: center;"><b>Cell 15 voltage average</b></p>
<p>8</p>	<p style="text-align: center;"><b>dQ/dV vs Voltage</b></p> <p style="text-align: center;"><b>Cell 8 voltage average</b></p>		

Table 0.6: Table with Graph dQ/dV vs voltage points (2<sup>nd</sup> 1kW Charging)

Cell	Graph of dQ/dV vs Cell Voltage	Cell	Graph of dQ/dV vs Cell Voltage
1	<p style="text-align: center;"><b>dQ/dV vs Voltage</b></p>  <p style="text-align: center;"><b>Cell 1 voltage average</b></p>	9	<p style="text-align: center;"><b>dQ/dV vs Voltage</b></p>  <p style="text-align: center;"><b>Cell 9 voltage average</b></p>
2	<p style="text-align: center;"><b>dQ/dV vs Voltage</b></p>  <p style="text-align: center;"><b>Cell 2 voltage average</b></p>	10	<p style="text-align: center;"><b>dQ/dV vs Voltage</b></p>  <p style="text-align: center;"><b>Cell 10 voltage average</b></p>
3	<p style="text-align: center;"><b>dQ/dV vs Voltage</b></p>  <p style="text-align: center;"><b>Cell 3 voltage average</b></p>	11	<p style="text-align: center;"><b>dQ/dV vs Voltage</b></p>  <p style="text-align: center;"><b>Cell 11 voltage average</b></p>

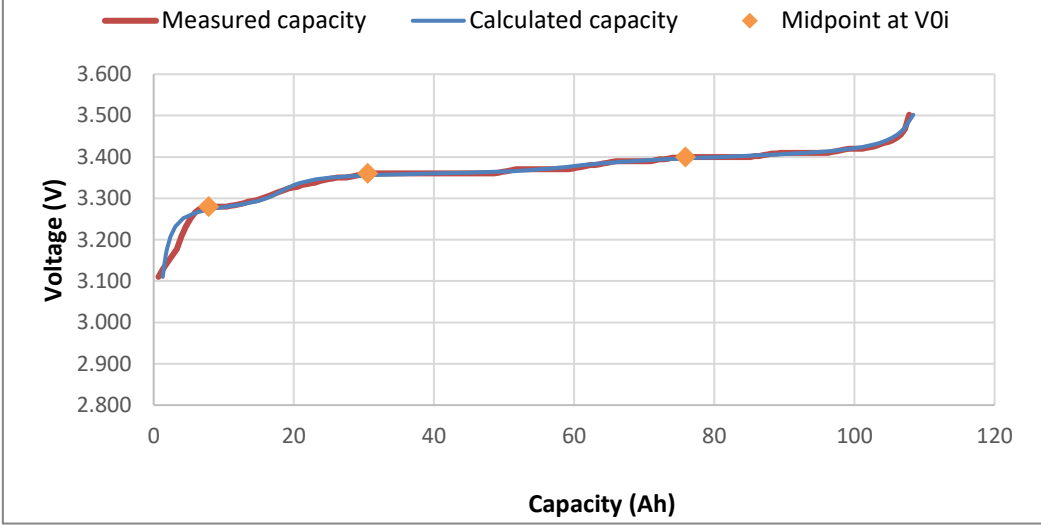
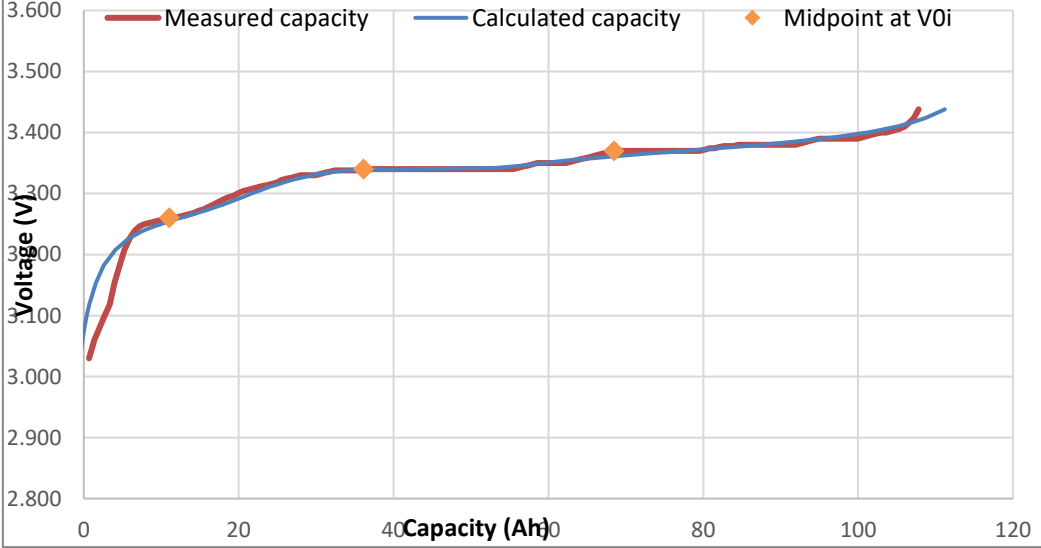
<p>4</p>	<p style="text-align: center;"><b>dQ/dV vs Voltage</b></p> <p style="text-align: center;"><b>Cell 4 voltage average</b></p>	<p>12</p>	<p style="text-align: center;"><b>dQ/dV vs Voltage</b></p> <p style="text-align: center;"><b>Cell 12 voltage average</b></p>
<p>5</p>	<p style="text-align: center;"><b>dQ/dV vs Voltage</b></p> <p style="text-align: center;"><b>Cell 5 voltage average</b></p>	<p>13</p>	<p style="text-align: center;"><b>dQ/dV vs Voltage</b></p> <p style="text-align: center;"><b>Cell 13 voltage average</b></p>
<p>6</p>	<p style="text-align: center;"><b>dQ/dV vs Voltage</b></p> <p style="text-align: center;"><b>Cell 6 voltage average</b></p>	<p>14</p>	<p style="text-align: center;"><b>dQ/dV vs Voltage</b></p> <p style="text-align: center;"><b>Cell 14 voltage average</b></p>

<p>7</p>	<p style="text-align: center;"><b>dQ/dV vs Voltage</b></p> <p style="text-align: center;"><b>Cell 7 voltage average</b></p>	<p>15</p>	<p style="text-align: center;"><b>dQ/dV vs Voltage</b></p> <p style="text-align: center;"><b>Cell 15 voltage average</b></p>
<p>8</p>	<p style="text-align: center;"><b>dQ/dV vs Voltage</b></p> <p style="text-align: center;"><b>Cell 8 voltage average</b></p>		

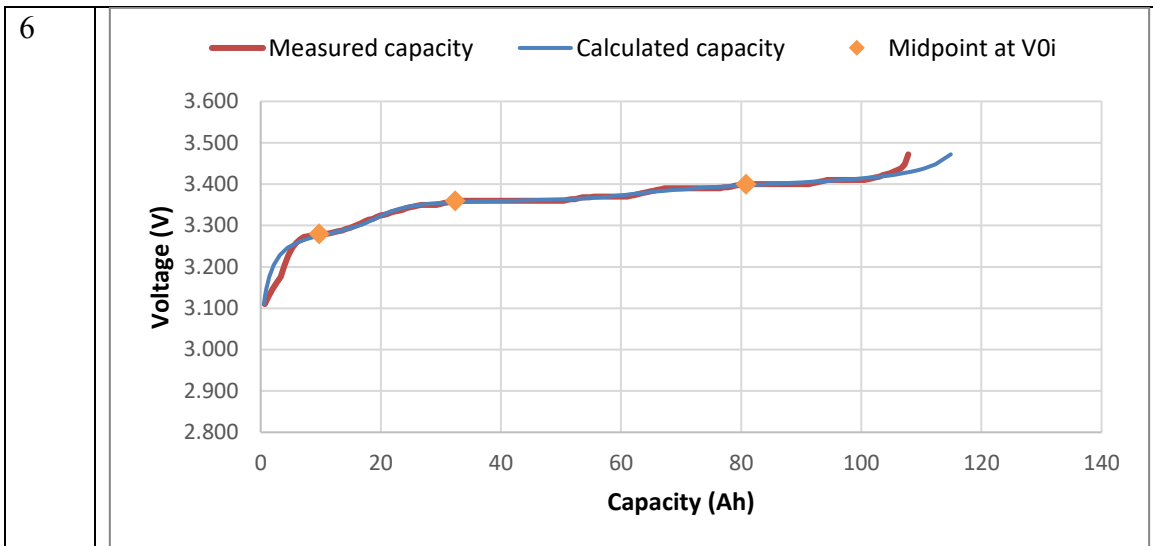


Appendix D: Voltage vs Measured and Calculated capacity of individual Cell

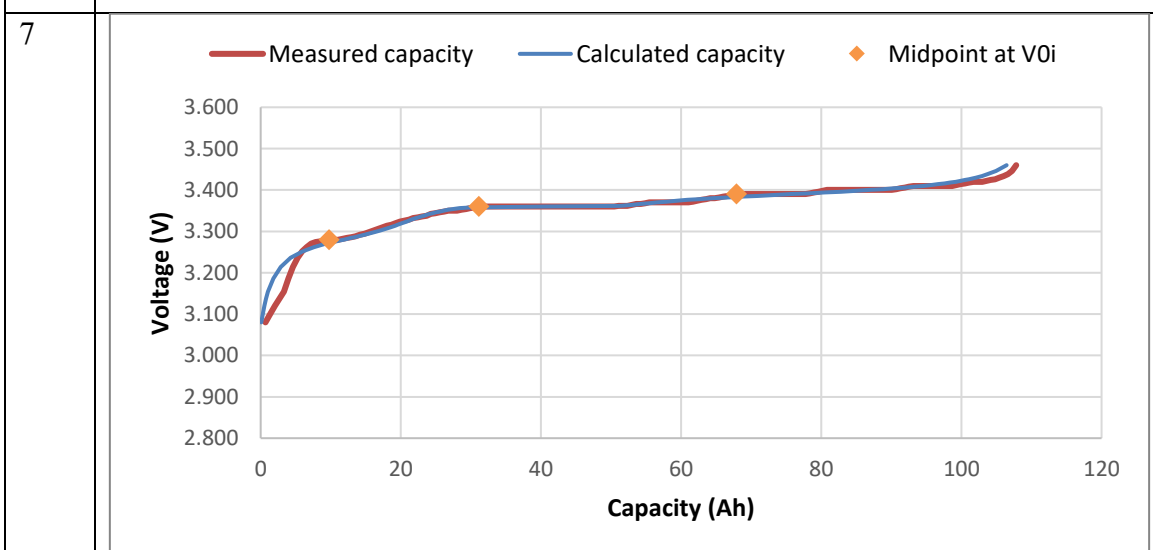
Table 0.7: Table of Voltage vs Capacity Curve with Calculated Maximum Capacity (2kW Charging after 2 cycles)

Cell	Graph of Voltage vs Measured and Calculated Capacity with the Maximum Capacity (Qmax) Value
1	 <p>Qmax = 108.2403297Ah</p>
2	 <p>Qmax = 114.639643Ah</p>

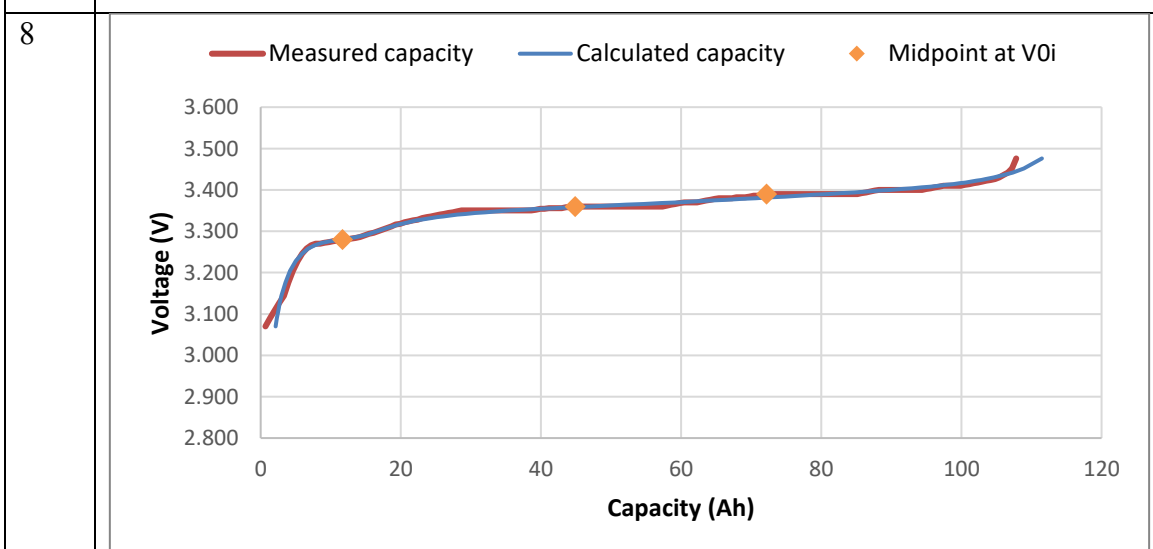
<p>3</p>	<p>Qmax = 119.4510906Ah</p>
<p>4</p>	<p>Qmax = 107.8195136Ah</p>
<p>5</p>	<p>Qmax = 110.7966191Ah</p>



Qmax = 117.3071285Ah



Qmax = 109.4878019Ah



	<p><math>Q_{max} = 115.0491542Ah</math></p>
<p>9</p>	<p>— Measured capacity    — Calculated capacity    ◆ Midpoint at <math>V_{0i}</math></p> <p>Y-axis: Voltage (V) from 2.800 to 3.600 X-axis: Capacity (Ah) from 0 to 120</p>
<p>10</p>	<p><math>Q_{max} = 113.837098Ah</math></p> <p>— Measured capacity    — Calculated capacity    ◆ Midpoint at <math>V_{0i}</math></p> <p>Y-axis: Voltage (V) from 2.800 to 3.600 X-axis: Capacity (Ah) from 0 to 120</p> <p><math>Q_{max} = 110.1002228Ah</math></p>

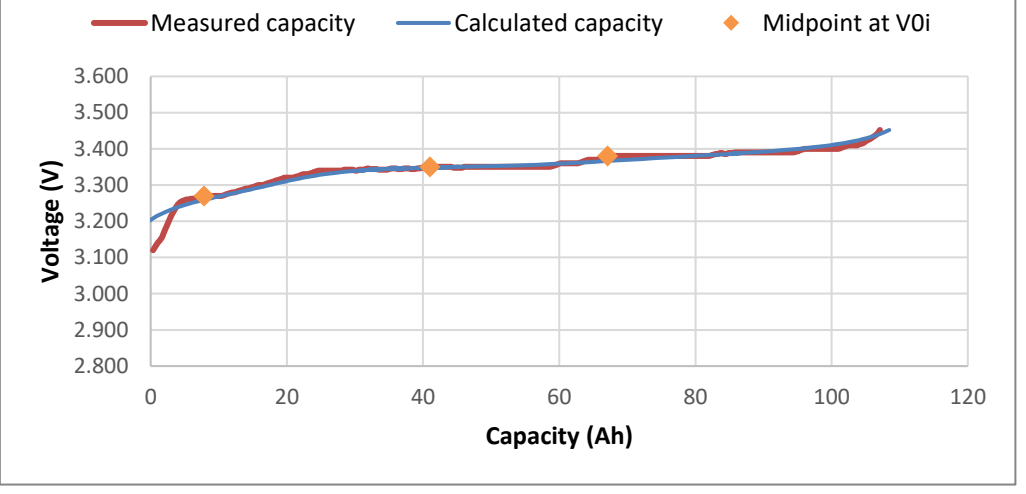
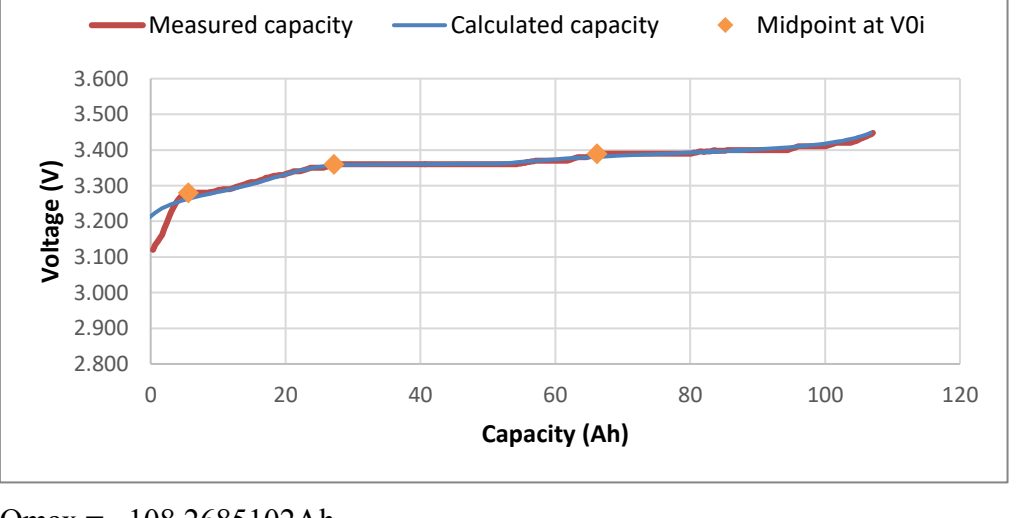
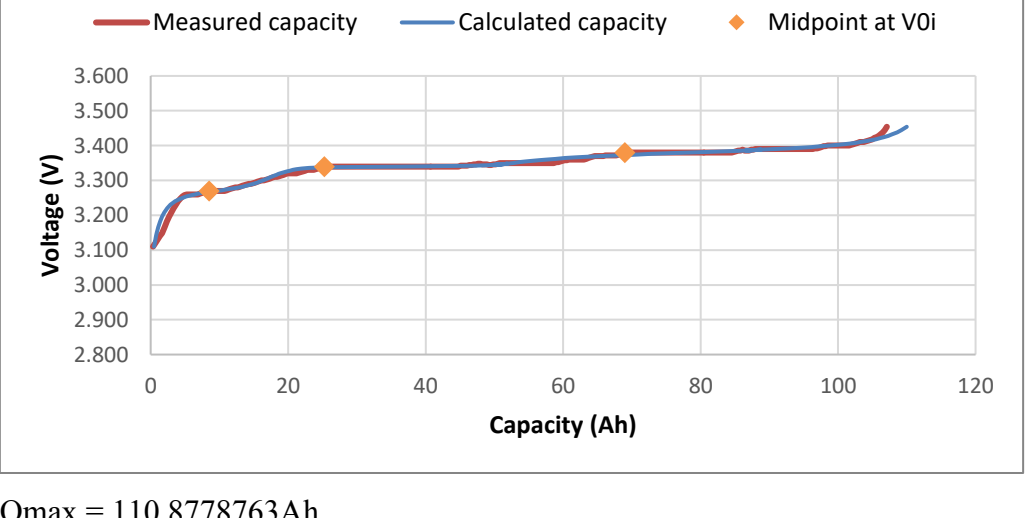
<p>11</p>	<p>Qmax = 110.3763721Ah</p>
<p>12</p>	<p>Qmax = 116.5964111Ah</p>
<p>13</p>	

	<p><math>Q_{max} = 115.1711045Ah</math></p>
<p>14</p>	<p><math>Q_{max} = 112.9738412Ah</math></p>
<p>15</p>	<p><math>Q_{max} = 108.3657497Ah</math></p>
<p>Average Maximum Capacity = 112.6808053Ah</p>	

Table 0.8: Table of Voltage vs Capacity Curve with Calculated Maximum Capacity (1kW Charging after 2 cycles)

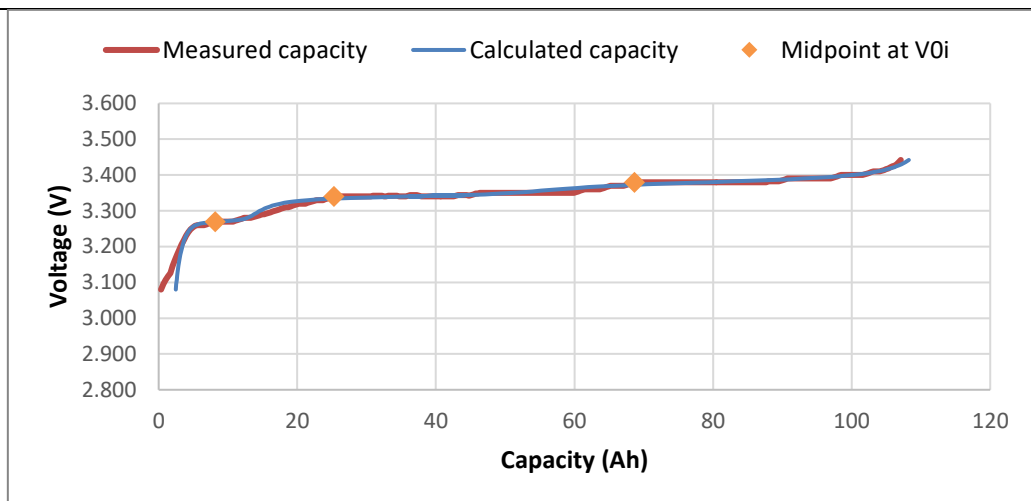
<p>Cell</p>	<p>Graph of Voltage vs Measured and Calculated Capacity with the Maximum Capacity (<math>Q_{max}</math>) Value</p>
-------------	--

<p>1</p>	<p>Qmax = 109.5498548Ah</p>
<p>2</p>	<p>Qmax = 111.6784106Ah</p>
<p>3</p>	<p>Qmax = 108.9827685Ah</p>

<p>4</p>	 <p>Qmax = 108.1606994Ah</p>
<p>5</p>	 <p>Qmax = 108.2685102Ah</p>
<p>6</p>	 <p>Qmax = 110.8778763Ah</p>

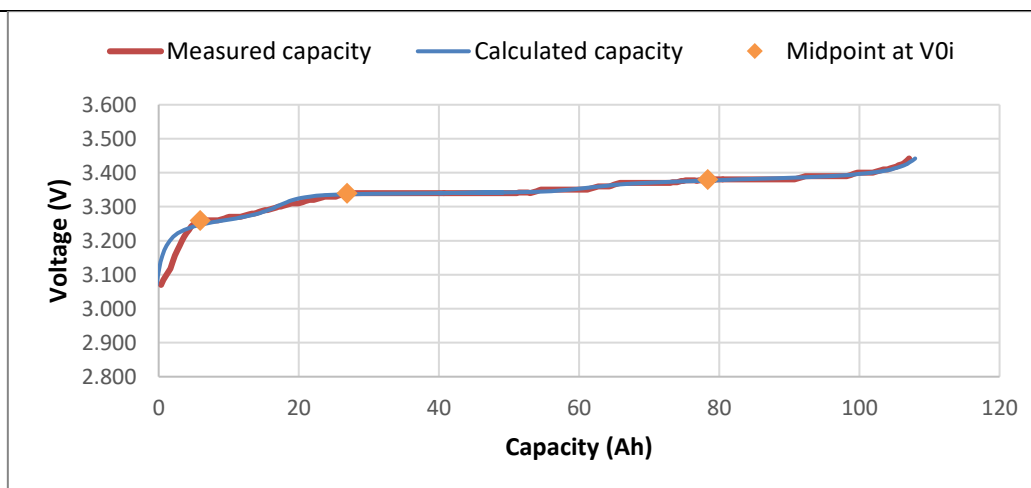


7



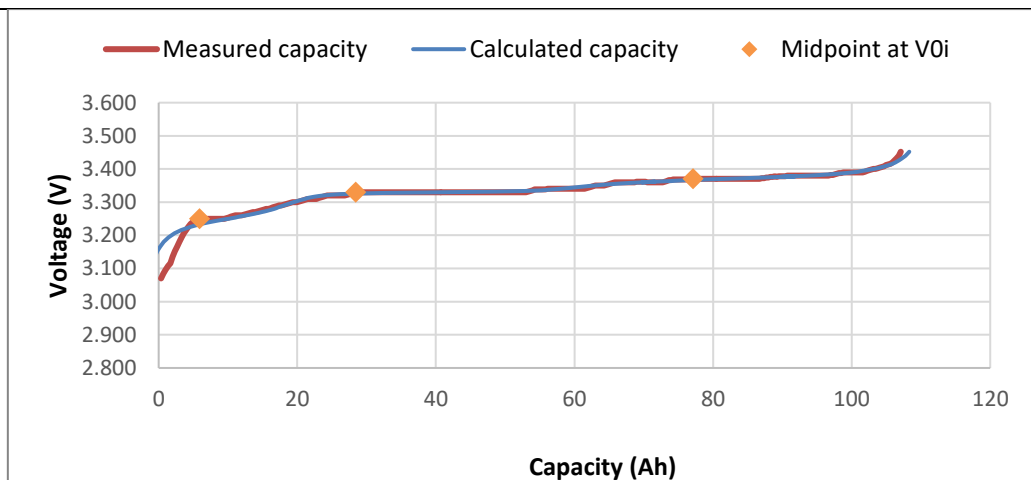
$Q_{max} = 110.784204\text{Ah}$

8

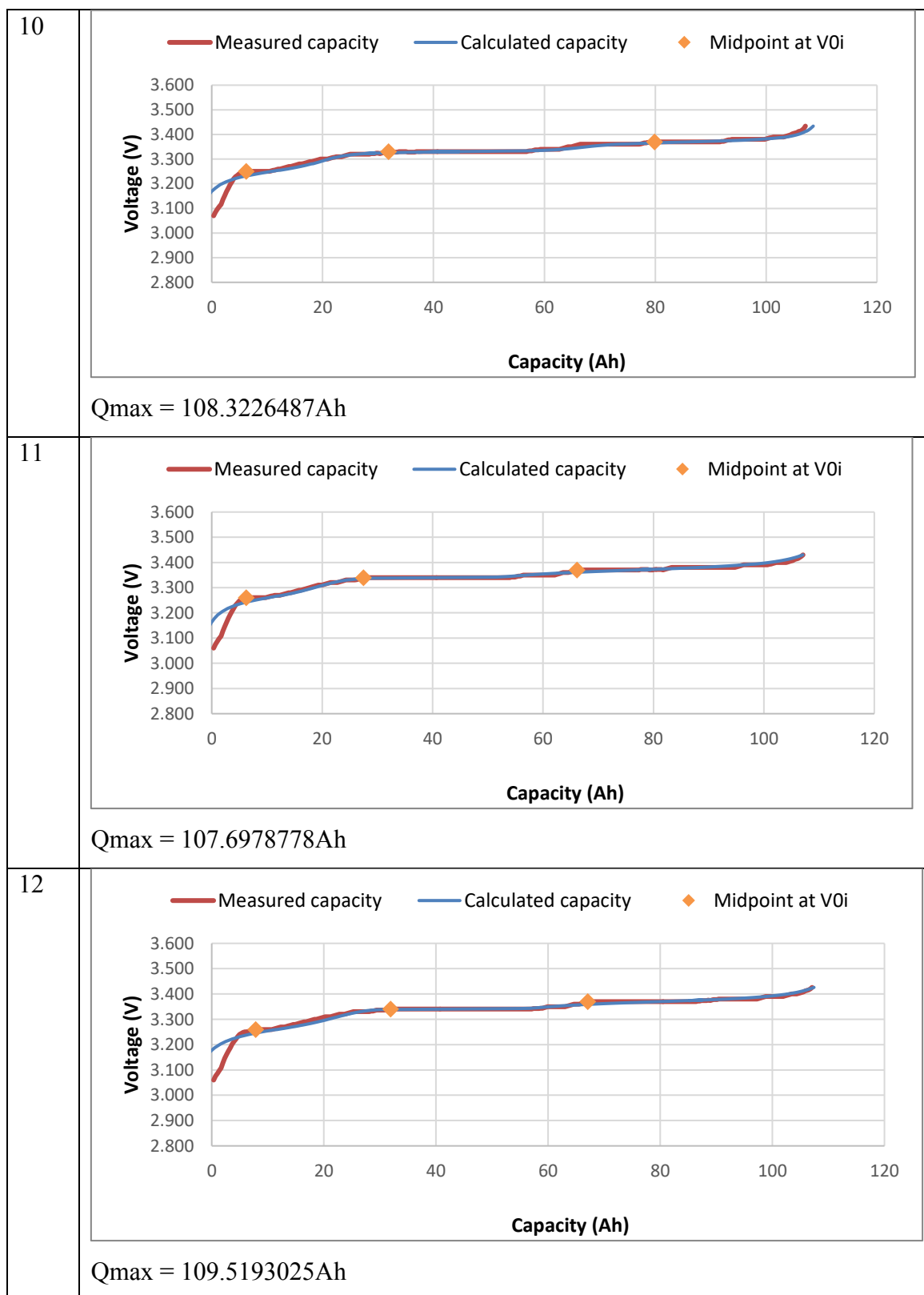


$Q_{max} = 107.3383198\text{Ah}$

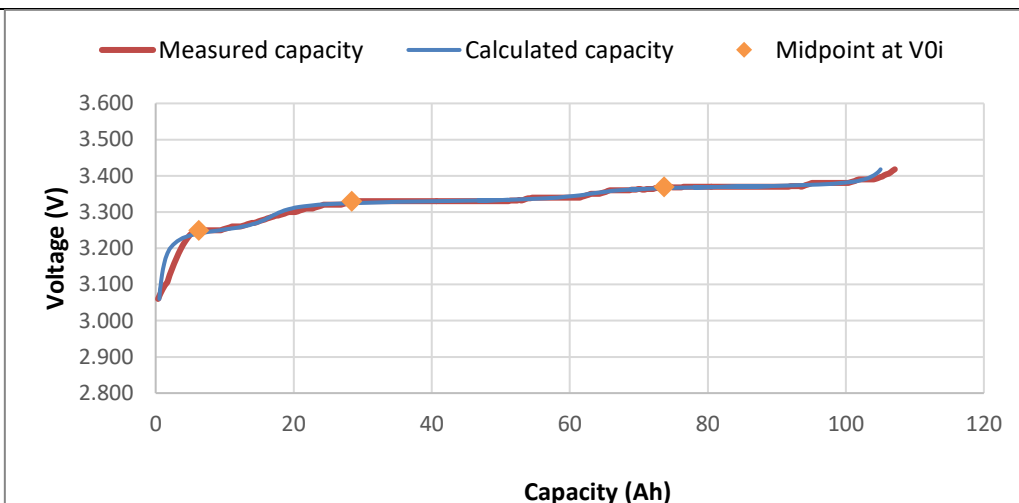
9



$Q_{max} = 108.9854225\text{Ah}$

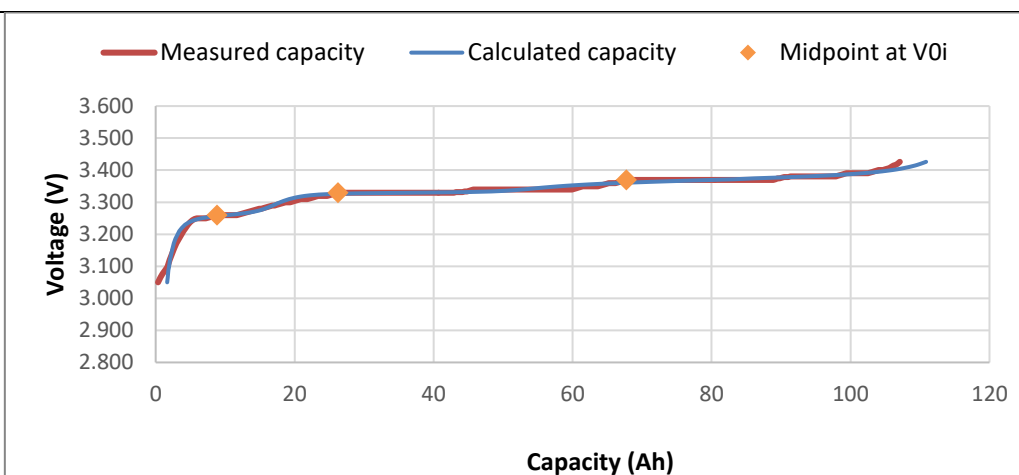


13



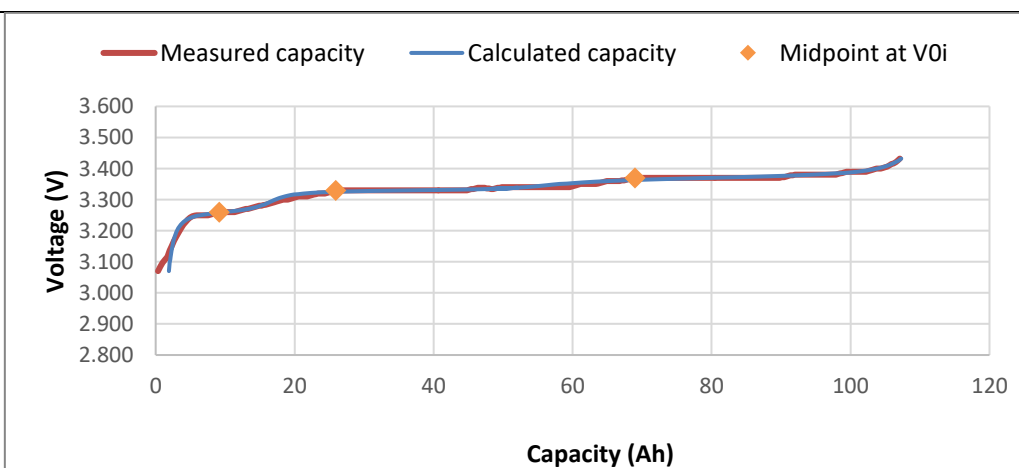
Qmax = 107.1538965Ah

14



Qmax = 113.6852131Ah

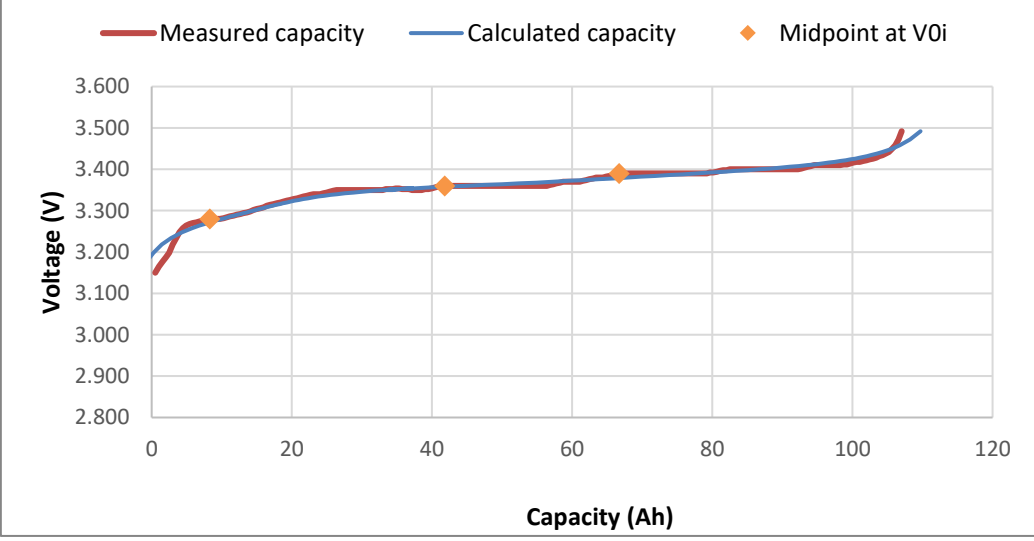
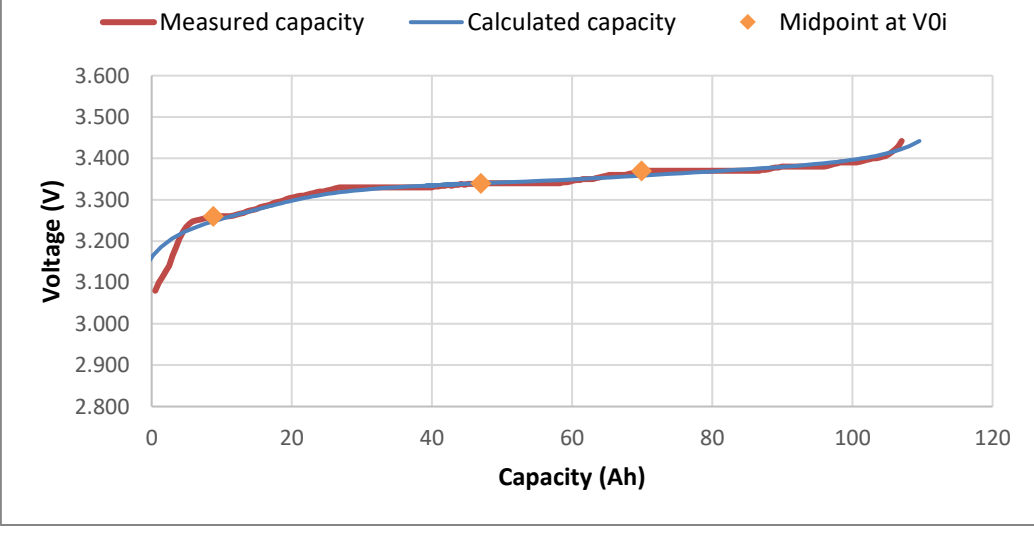
15



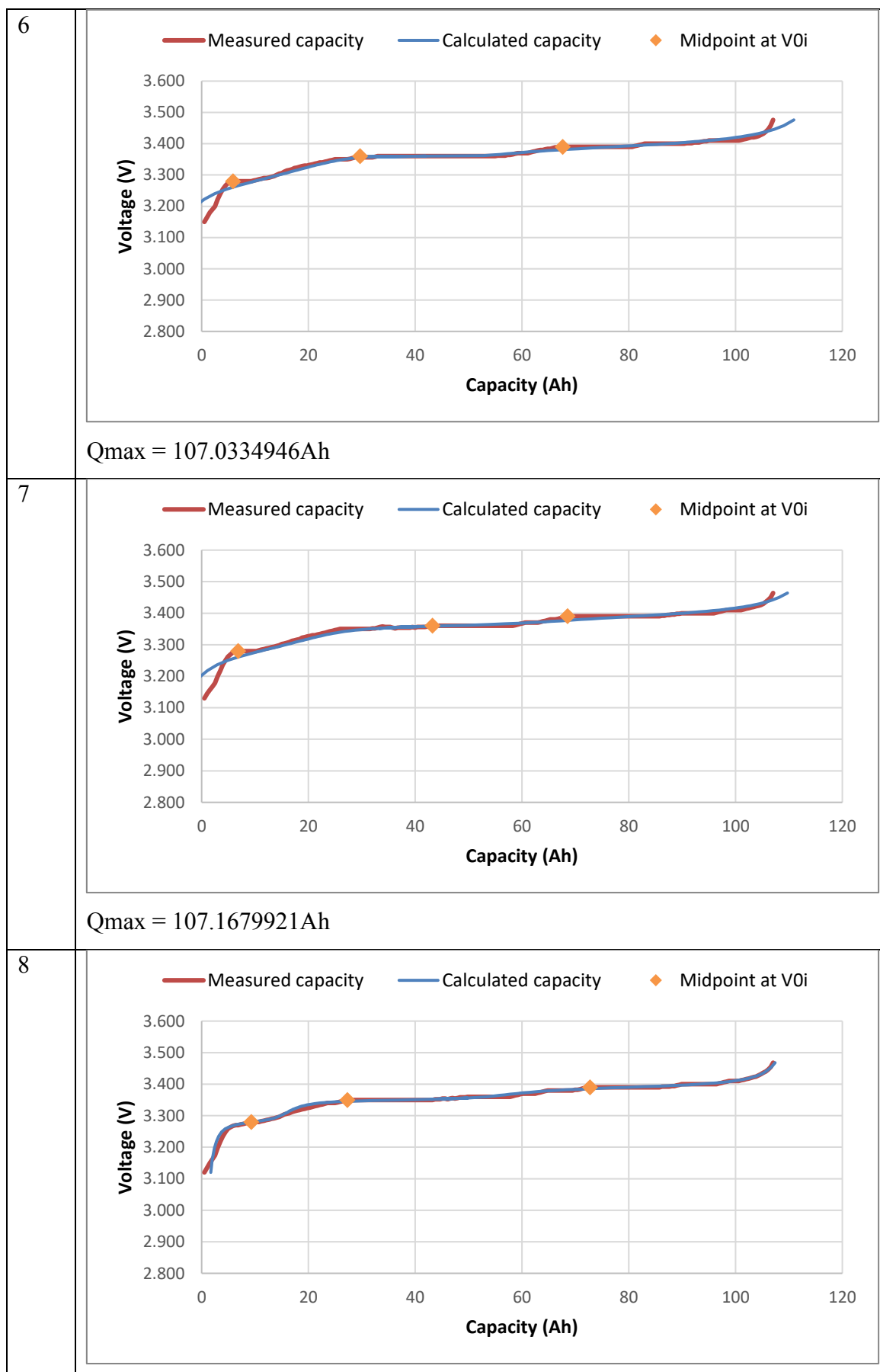
Qmax = 110.0605384Ah

Average Maximum Capacity = 109.3965659Ah

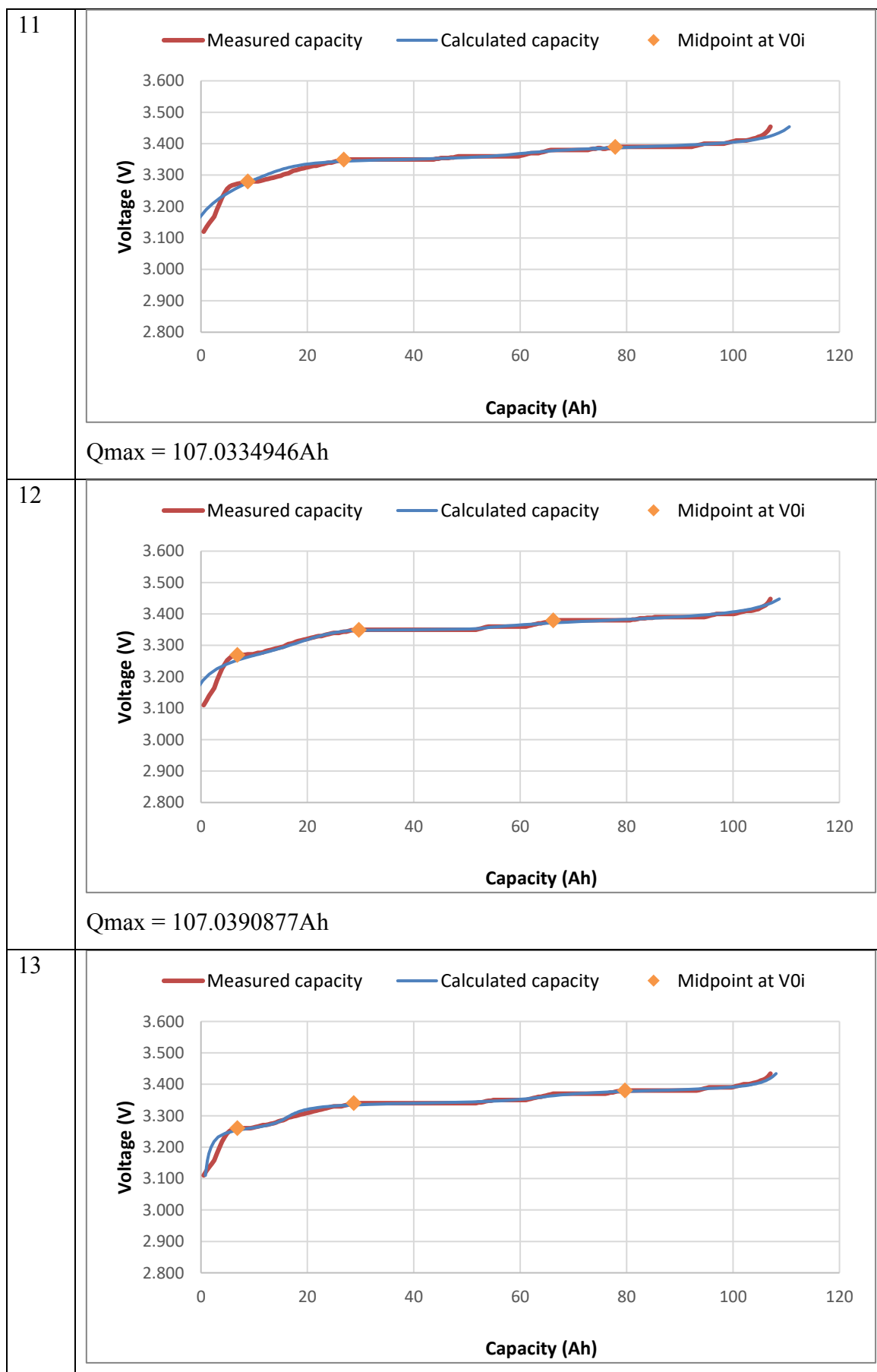
Table 0.9: Table of Voltage vs Capacity Curve with Calculated Maximum Capacity (1<sup>st</sup> 1.5kW Charging)

Cell	Graph of Voltage vs Measured and Calculated Capacity with the Maximum Capacity (Qmax) Value
1	 <p>Qmax = 107.0334946Ah</p>
2	 <p>Qmax = 108.9923822Ah</p>

<p>3</p>	<p>Qmax = 107.0334946Ah</p>
<p>4</p>	<p>Qmax = 107.0334946Ah</p>
<p>5</p>	<p>Qmax = 107.0334946Ah</p>



	<p><math>Q_{max} = 107.0334946Ah</math></p>
<p>9</p>	<p><math>Q_{max} = 107.0334946Ah</math></p>
<p>10</p>	<p><math>Q_{max} = 107.0334946Ah</math></p>





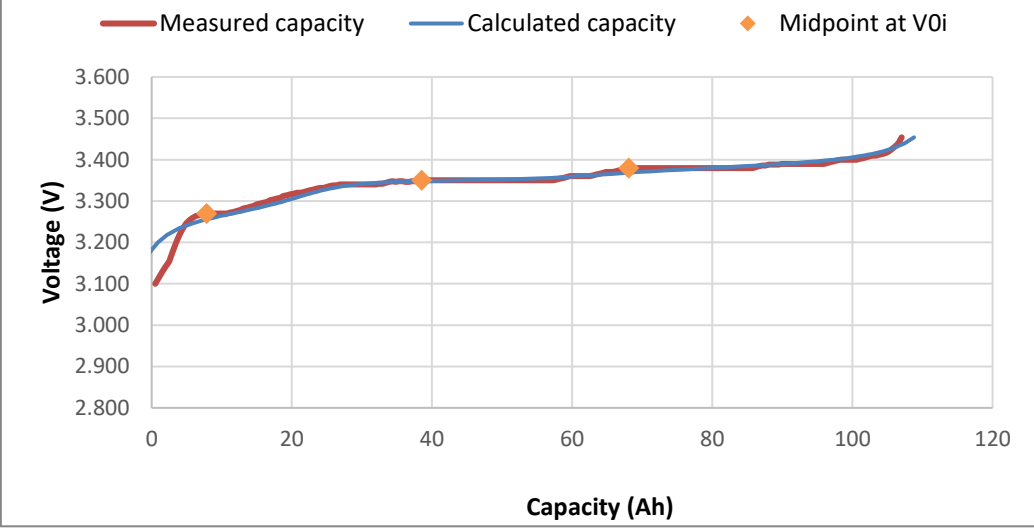
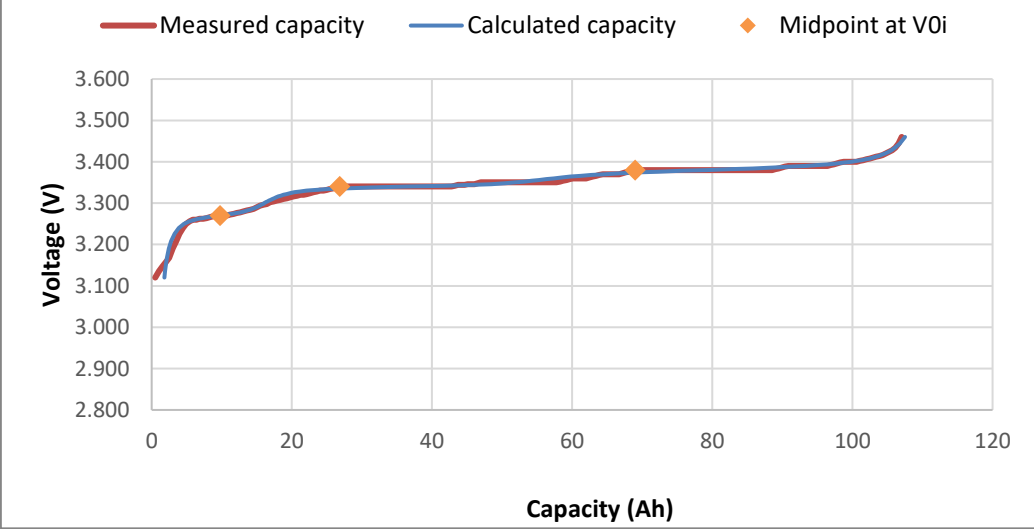
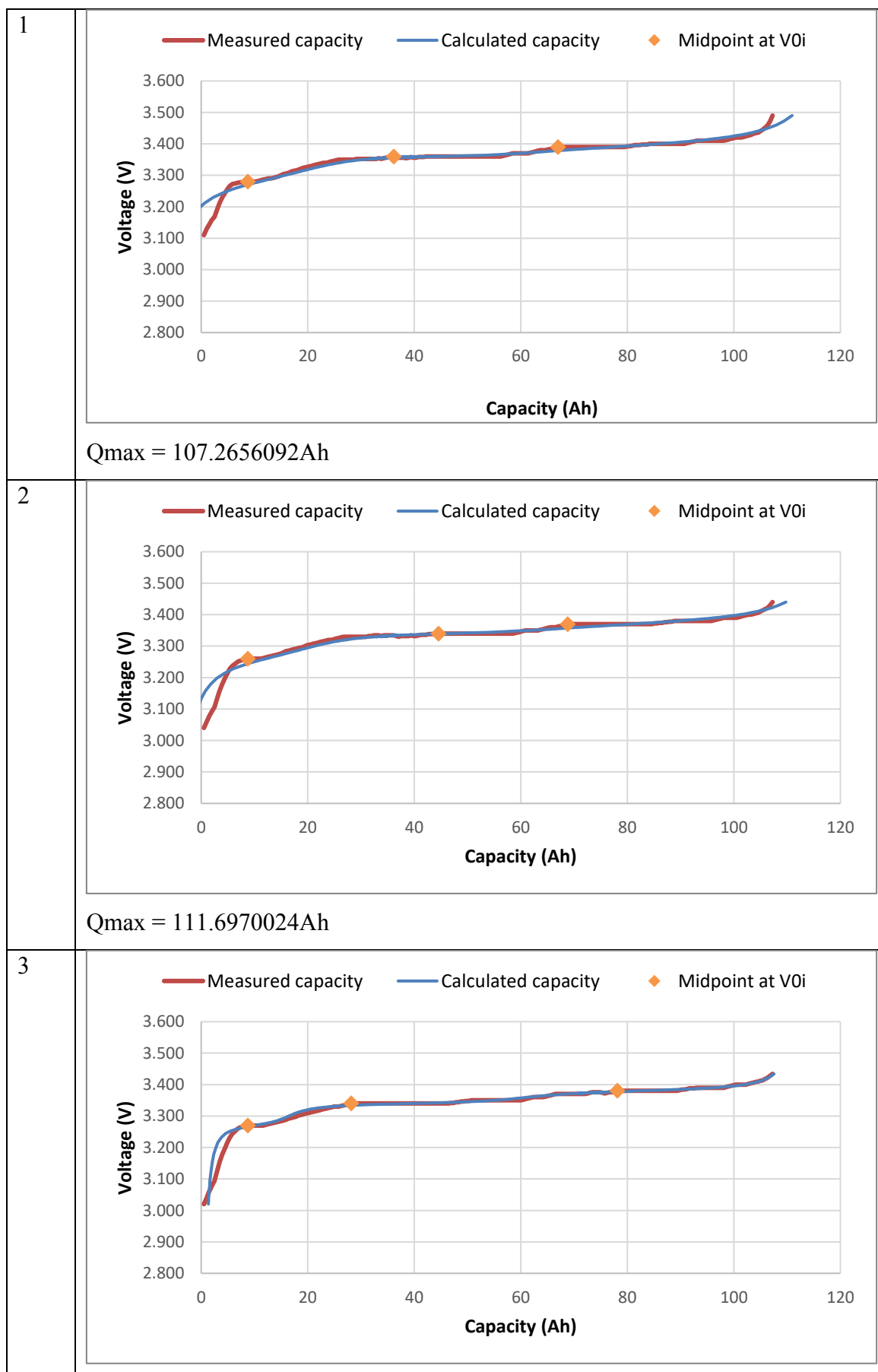
	<p><math>Q_{max} = 107.0334946Ah</math></p>
<p>14</p>	 <p><math>Q_{max} = 108.8392904Ah</math></p>
<p>15</p>	 <p><math>Q_{max} = 107.0334946Ah</math></p>
<p>Average Maximum Capacity = 107.2938129Ah</p>	

Table 0.10: Table of Voltage vs Capacity Curve with Calculated Maximum Capacity (2<sup>nd</sup> 1.5kW Charging)

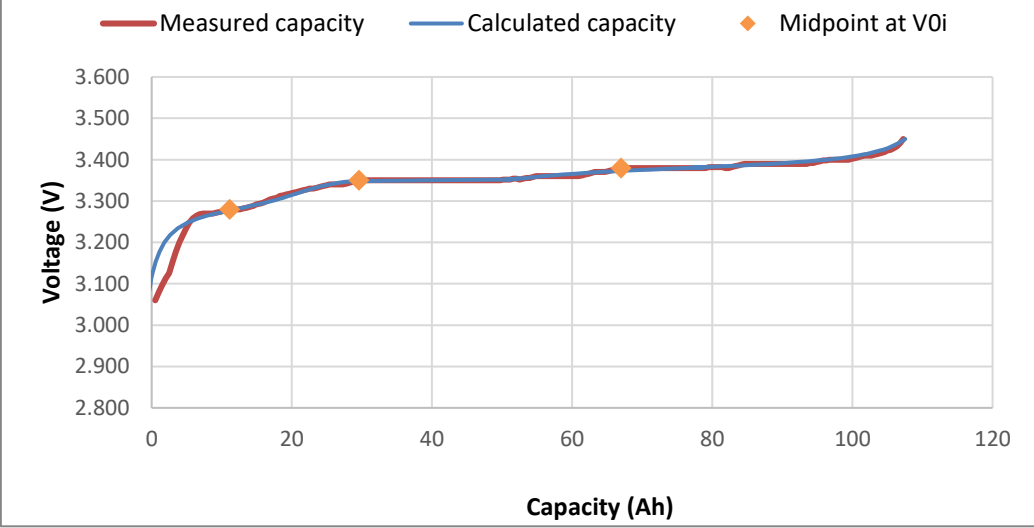
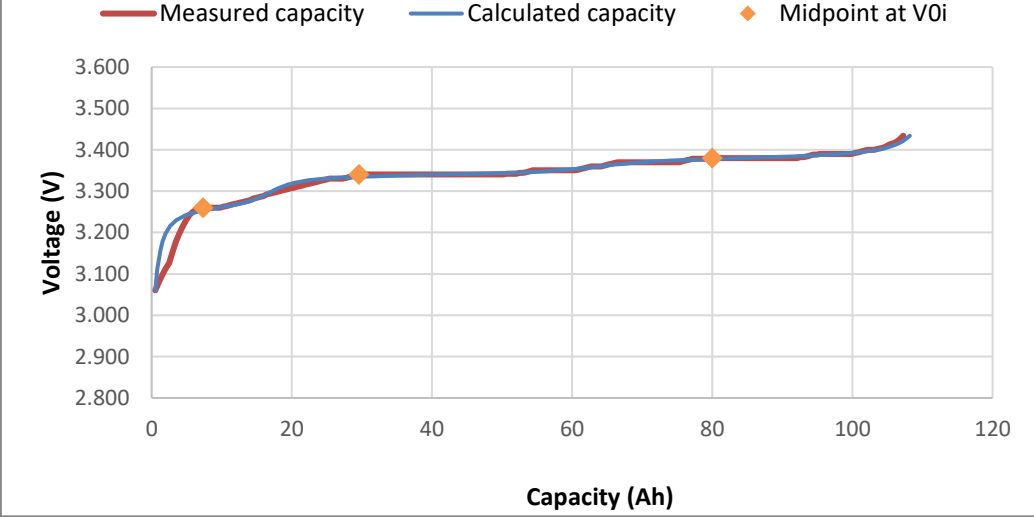
<p>Cell</p>	<p>Graph of Voltage vs Measured and Calculated Capacity with the Maximum Capacity (<math>Q_{max}</math>) Value</p>
-------------	--



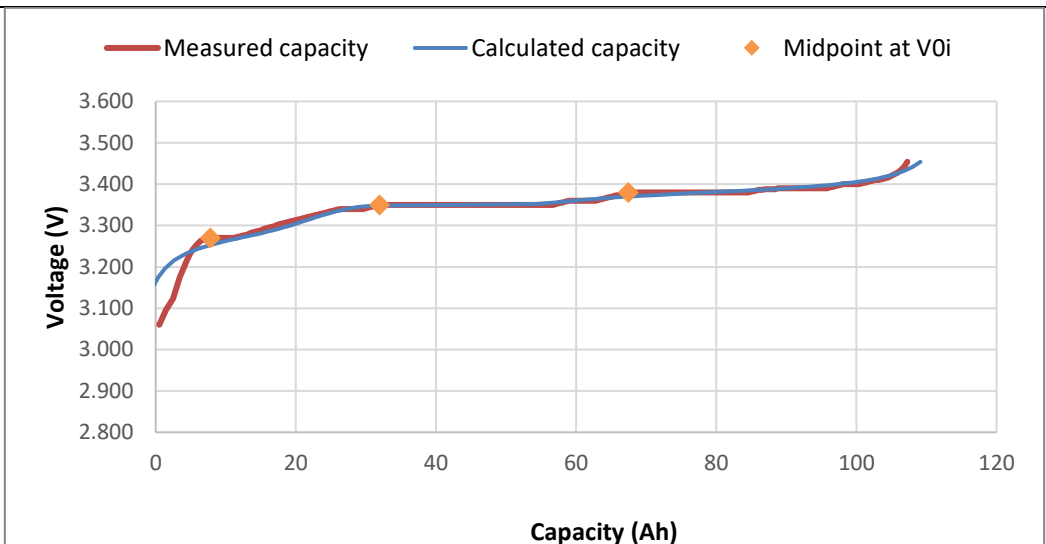
<p>4</p>	<p>Qmax = 108.9916198Ah</p> <p>— Measured capacity    — Calculated capacity    ◆ Midpoint at V0i</p> <p>3.600 3.500 3.400 3.300 3.200 3.100 3.000 2.900 2.800</p> <p>0 20 40 60 80 100 120</p> <p>Capacity (Ah)</p>
<p>5</p>	<p>Qmax = 107.2656092Ah</p> <p>— Measured capacity    — Calculated capacity    ◆ Midpoint at V0i</p> <p>3.600 3.500 3.400 3.300 3.200 3.100 3.000 2.900 2.800</p> <p>0 20 40 60 80 100 120</p> <p>Capacity (Ah)</p>
<p>6</p>	<p>Qmax = 107.2656092Ah</p> <p>— Measured capacity    — Calculated capacity    ◆ Midpoint at V0i</p> <p>3.600 3.500 3.400 3.300 3.200 3.100 3.000 2.900 2.800</p> <p>0 20 40 60 80 100 120</p> <p>Capacity (Ah)</p>

	<p><math>Q_{max} = 107.2656092Ah</math></p>
<p>7</p>	<p>— Measured capacity    — Calculated capacity    ◆ Midpoint at <math>V_{0i}</math></p> <p>3.600 3.500 3.400 3.300 3.200 3.100 3.000 2.900 2.800</p> <p>0    20    40    60    80    100    120</p> <p>Capacity (Ah)</p> <p>Voltage (V)</p>
<p>8</p>	<p>— Measured capacity    — Calculated capacity    ◆ Midpoint at <math>V_{0i}</math></p> <p>3.600 3.500 3.400 3.300 3.200 3.100 3.000 2.900 2.800</p> <p>0    20    40    60    80    100    120</p> <p>Capacity (Ah)</p> <p>Voltage (V)</p>
	<p><math>Q_{max} = 107.2656092Ah</math></p>

<p>9</p>	<p>— Measured capacity    — Calculated capacity    ◆ Midpoint at V0i</p> <p>Qmax = 107.2656092Ah</p>
<p>10</p>	<p>— Measured capacity    — Calculated capacity    ◆ Midpoint at V0i</p> <p>Qmax = 107.2656092Ah</p>
<p>11</p>	<p>— Measured capacity    — Calculated capacity    ◆ Midpoint at V0i</p>

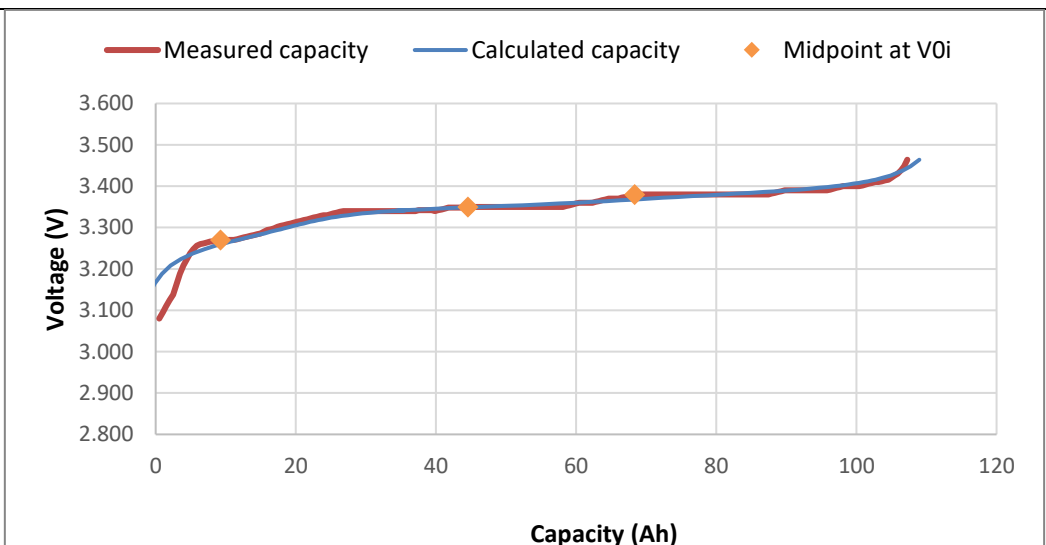
	<p><math>Q_{max} = 111.7910666\text{Ah}</math></p>
<p>12</p>	 <p><math>Q_{max} = 107.2656092\text{Ah}</math></p>
<p>13</p>	 <p><math>Q_{max} = 107.2656092\text{Ah}</math></p>

14



Qmax = 107.2656092Ah

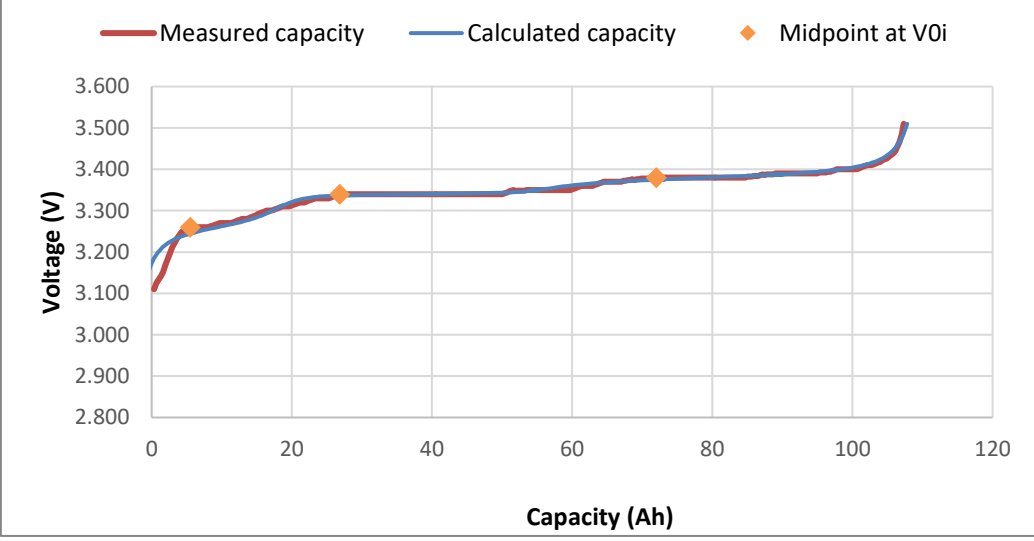
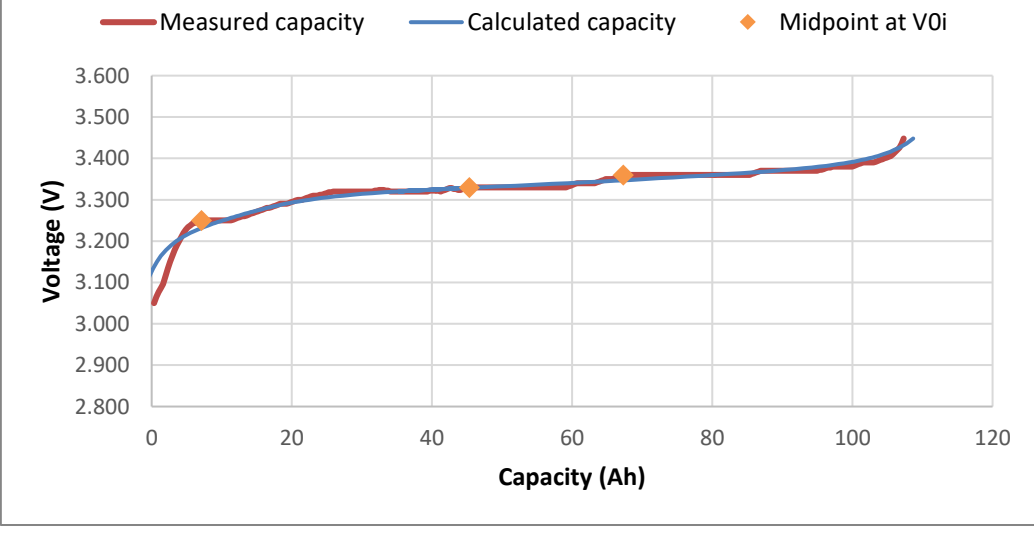
15



Qmax = 107.2656092Ah

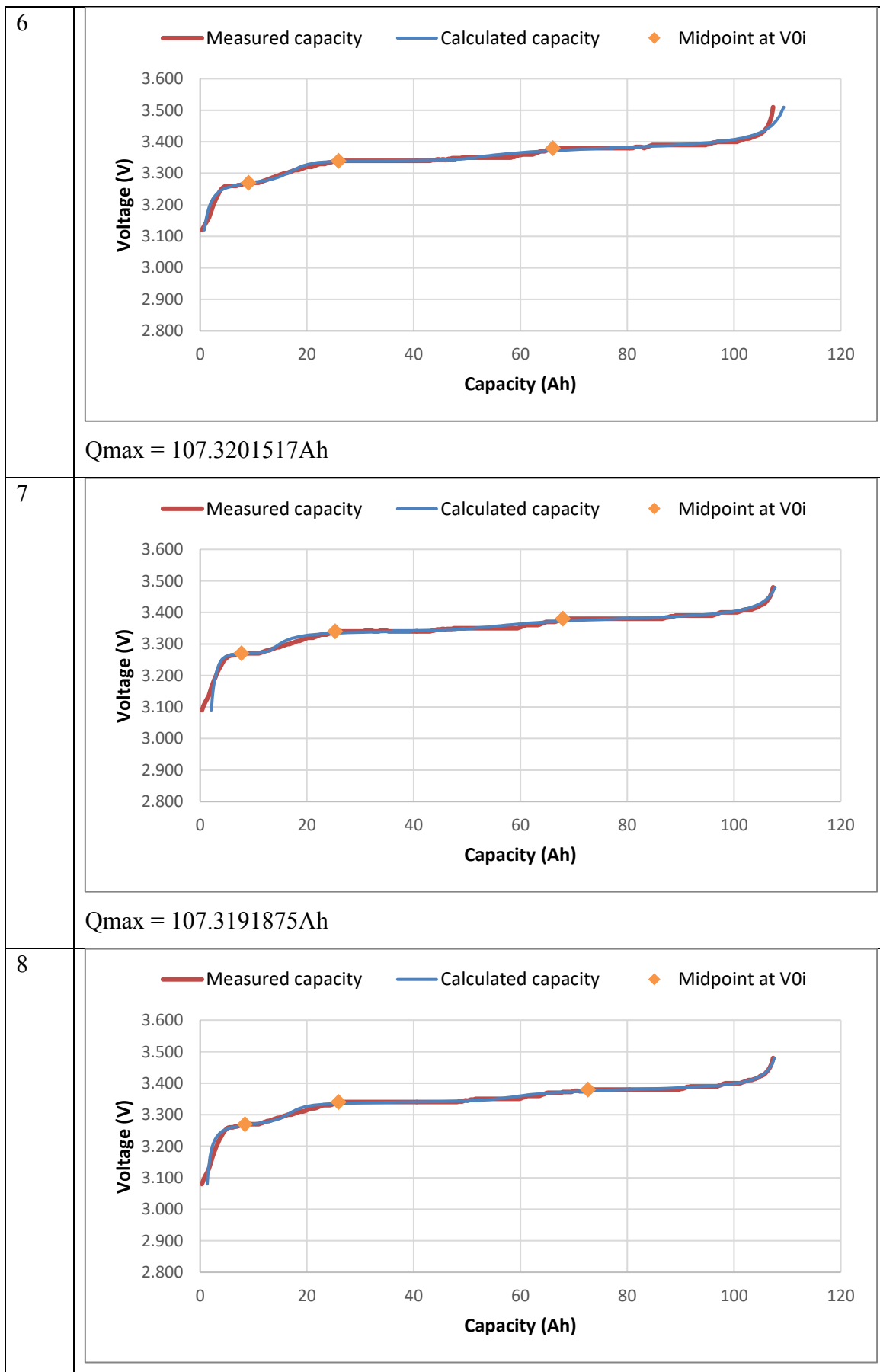
Average Maximum Capacity = 107.2938129Ah

Table 0.11: Table of Voltage vs Capacity Curve with Calculated Maximum Capacity (1<sup>st</sup> 1kW Charging)

Cell	Graph of Voltage vs Measured and Calculated Capacity with the Maximum Capacity (Qmax) Value
1	 <p>Qmax = 107.3191875Ah</p>
2	 <p>Qmax = 107.3191875Ah</p>



<p>3</p>	<p>Qmax = 108.8641681Ah</p>
<p>4</p>	<p>Qmax = 107.3191875Ah</p>
<p>5</p>	<p>Qmax = 107.3191875Ah</p>

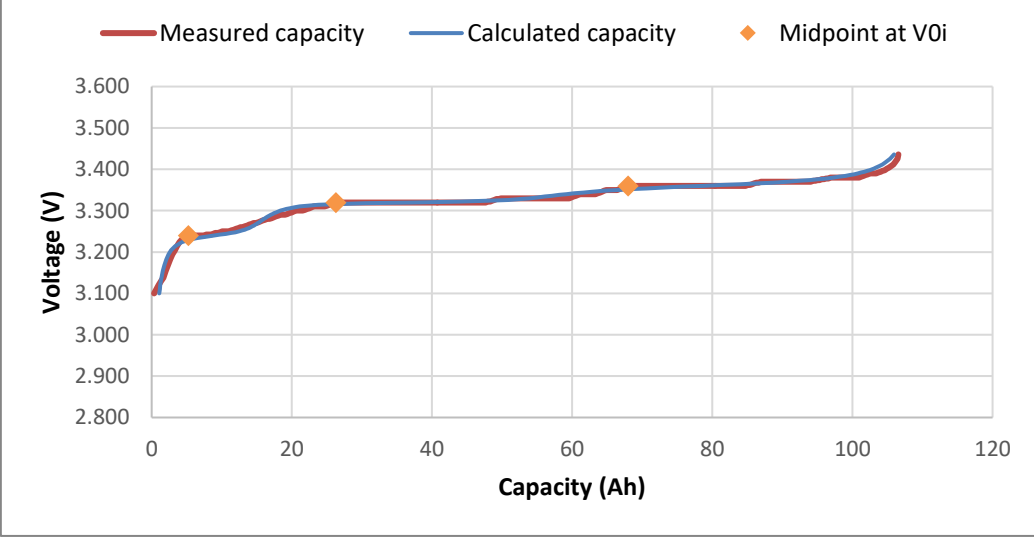
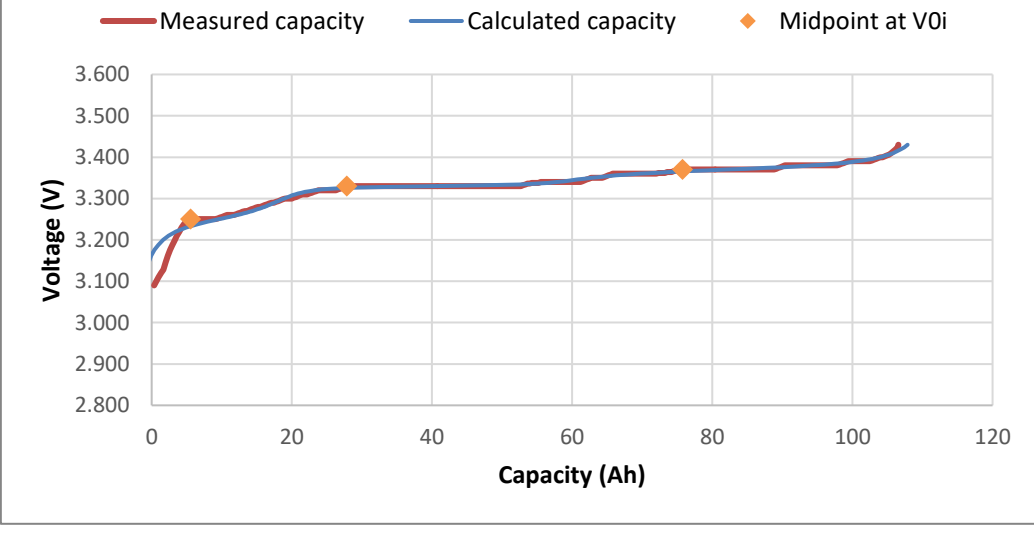


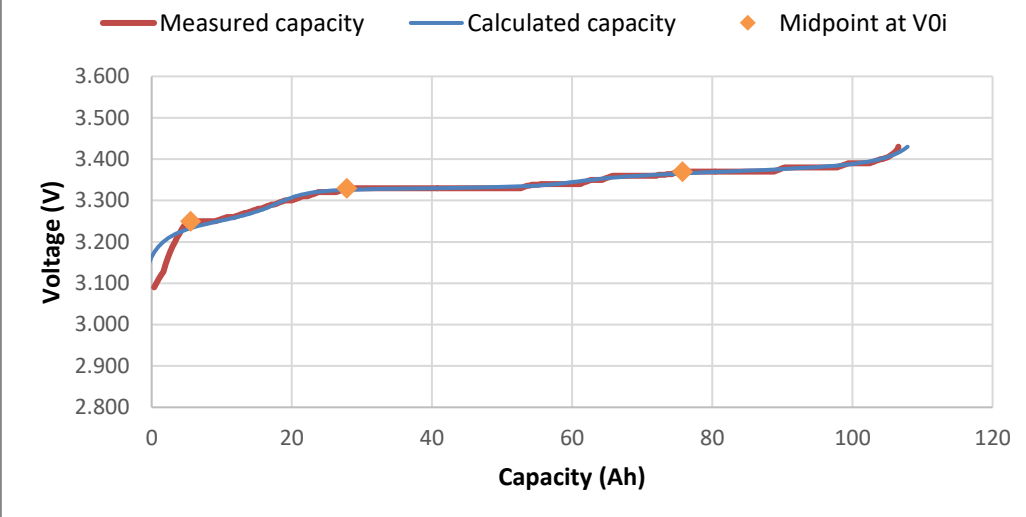
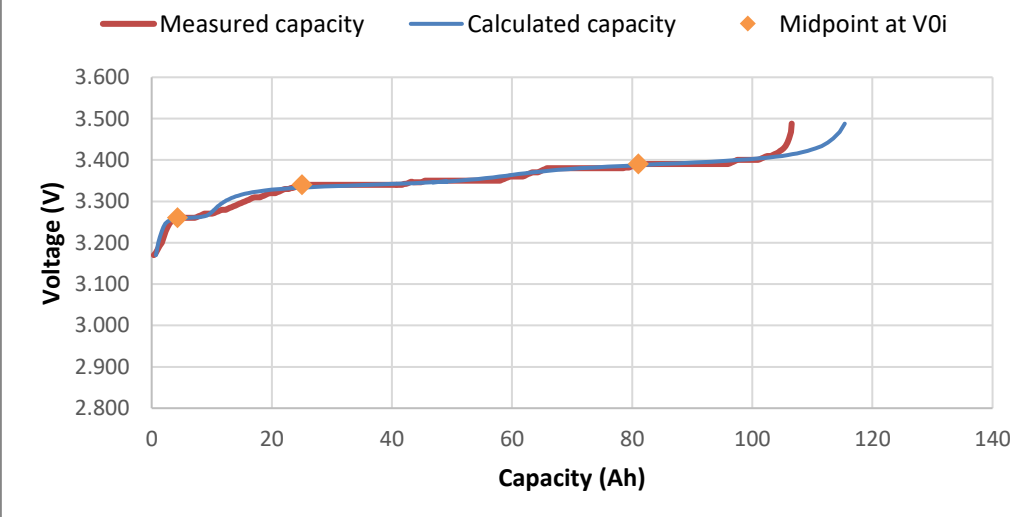
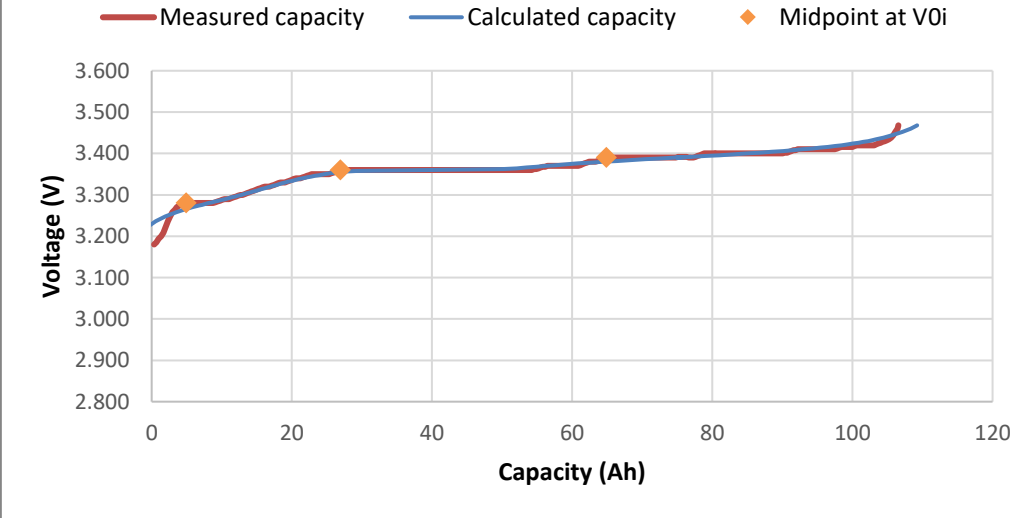
	<p><math>Q_{max} = 107.3191875Ah</math></p>
<p>9</p>	<p><math>Q_{max} = 107.3191875Ah</math></p>
<p>10</p>	<p><math>Q_{max} = 107.3191875Ah</math></p>

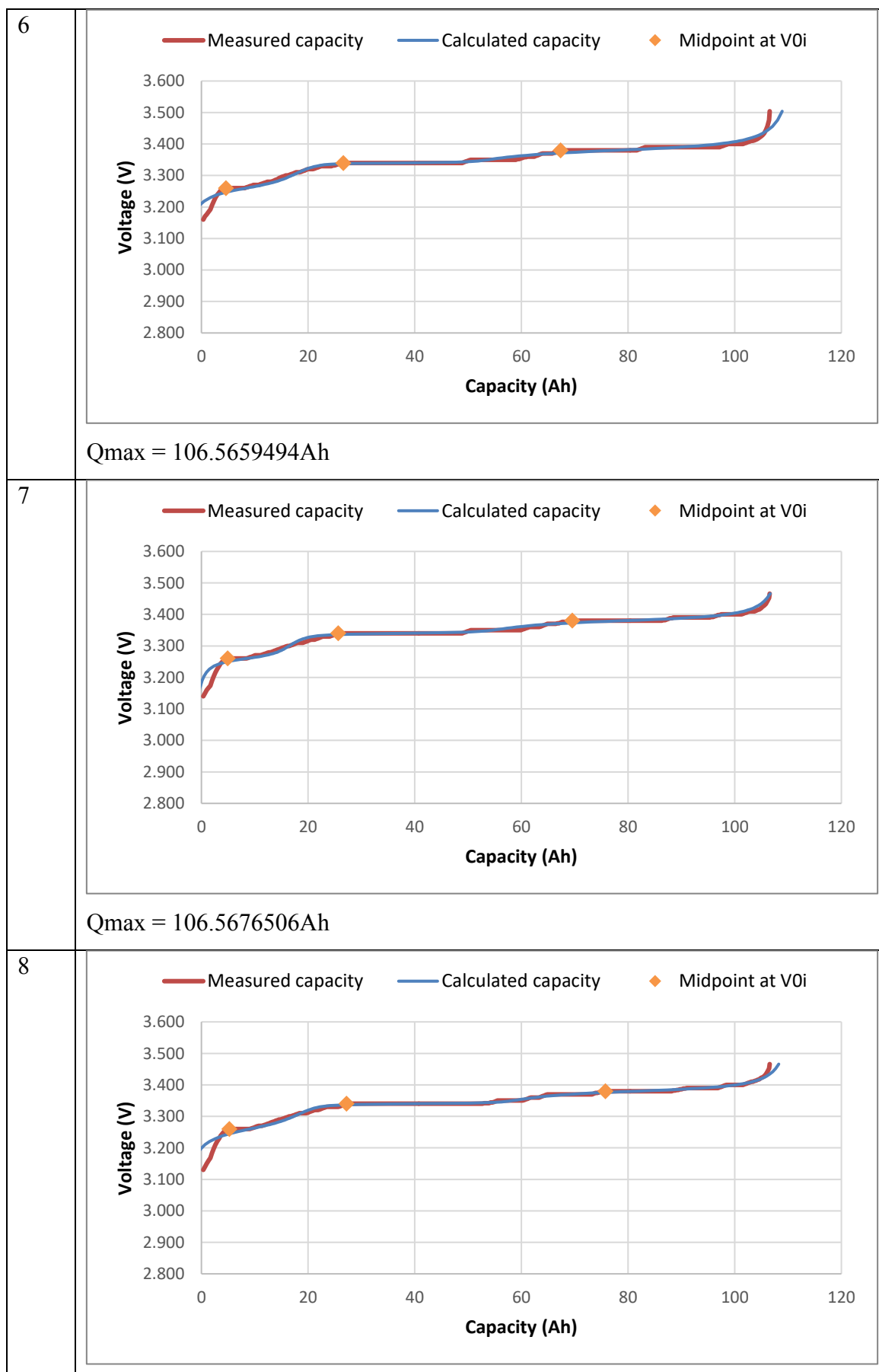
<p>11</p>	<p>— Measured capacity    — Calculated capacity    ◆ Midpoint at V0i</p> <p>Qmax = 107.3191875Ah</p>
<p>12</p>	<p>— Measured capacity    — Calculated capacity    ◆ Midpoint at V0i</p> <p>Qmax = 107.3191875Ah</p>
<p>13</p>	<p>— Measured capacity    — Calculated capacity    ◆ Midpoint at V0i</p>

	<p><math>Q_{max} = 107.3212833Ah</math></p>
<p>14</p>	<p><math>Q_{max} = 107.3191875Ah</math></p>
<p>15</p>	<p><math>Q_{max} = 107.3191875Ah</math></p>
<p>Average Maximum Capacity = 107.4223902Ah</p>	

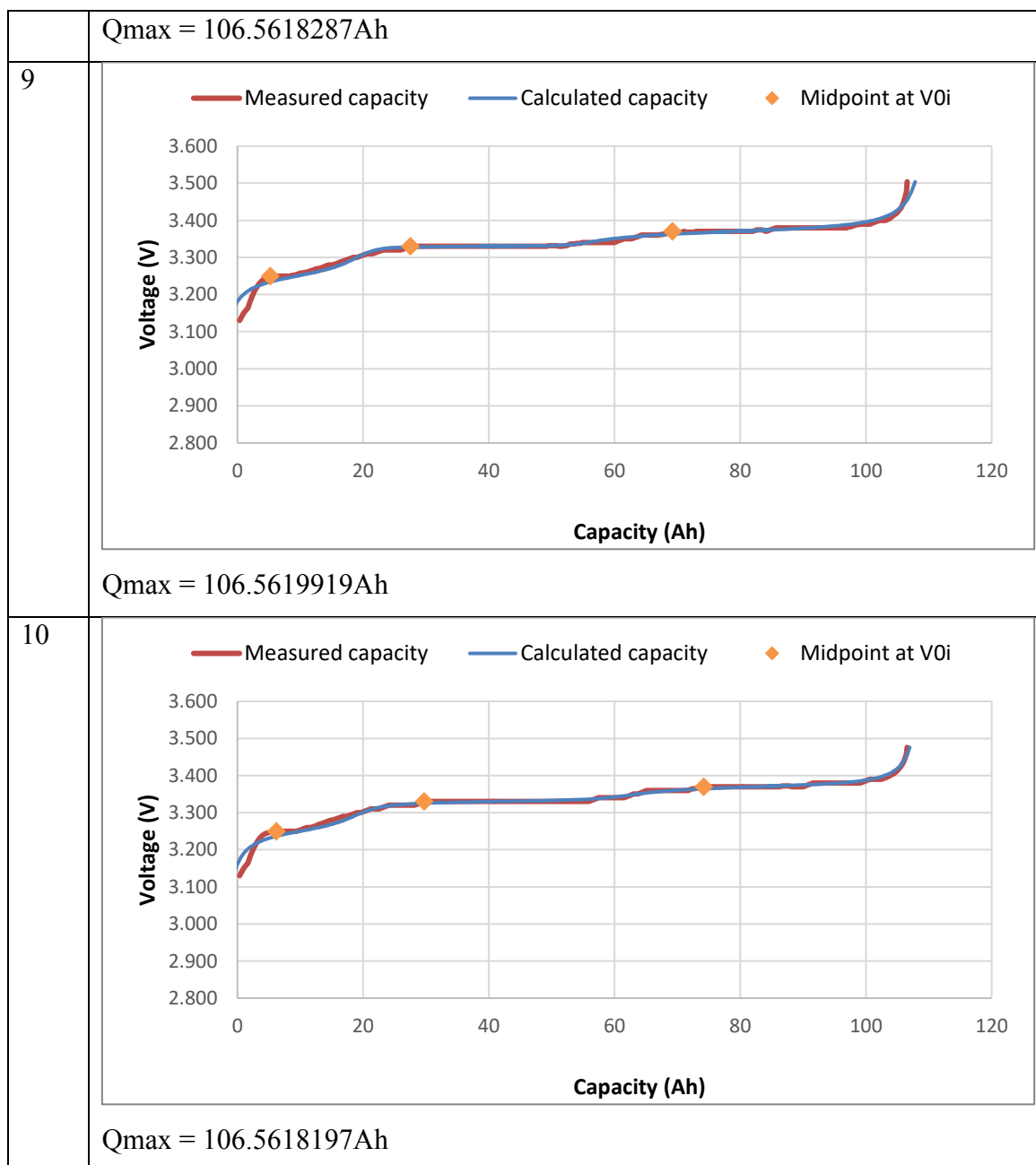
Table 0.12: Table of Voltage vs Capacity Curve with Calculated Maximum Capacity (2<sup>nd</sup> 1kW Charging)

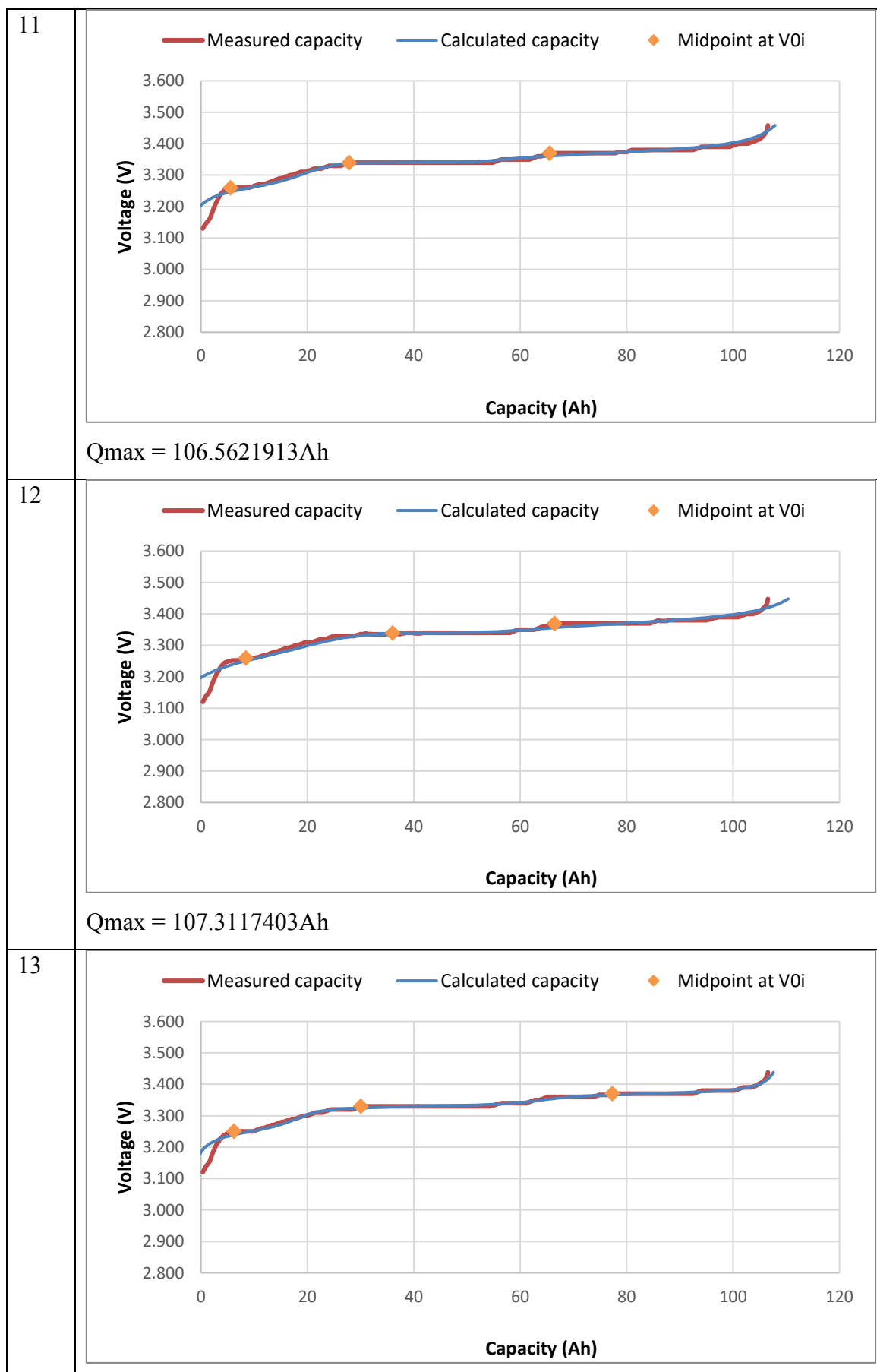
Cell	Graph of Voltage vs Measured and Calculated Capacity with the Maximum Capacity (Qmax) Value
1	 <p>Qmax = 106.9540381Ah</p>
2	 <p>Qmax = 107.0997146Ah</p>

<p>3</p>	 <p>Qmax = 107.0997146Ah</p>
<p>4</p>	 <p>Qmax = 113.2710747Ah</p>
<p>5</p>	 <p>Qmax = 106.9072072Ah</p>









	<p><math>Q_{max} = 107.2339435Ah</math></p>
<p>14</p>	<p><math>Q_{max} = 108.8267043Ah</math></p>
<p>15</p>	<p><math>Q_{max} = 106.5689004Ah</math></p>
<p>Average Maximum Capacity = 107.3409915Ah</p>	